AALBORG UNIVERSITY
INSTITUTE OF ELECTRONIC SYSTEMS

New Generation Metal Detector for Food

Frank Thornemann Hansen
Lars Vinding

APPLIED SIGNAL PROCESSING AND IMPLEMENTATION

MASTER THESIS

GROUP 1041

JUNE 2008

Aalborg University

Institute of Electronic Systems
Master Thesis - Applied Signal Processing and Implementation

TITLE:

Metal Detection in Food

PROJECT PERIOD:

September 1st, 2007 -
June 4th, 2008

PROJECT GROUP:

ASPI10 - group 1041

GROUP MEMBERS:

Frank Thornemann Hansen
Lars Vinding

SUPERVISORS:

Kjeld Hermansen
Anders Brødløs Olsen

NUMBER OF COPIES: 6

NUMBER OF PAGES

IN MAIN REPORT: 110

IN APPENDIX REPORT: 22

TOTAL NUMBER OF PAGES: 132

SYNOPSIS:

This thesis treats the development of a metal detector.

At first the transducer is threaded, together with the response of different materials. A series of tests is made to verify the model and it is reasonable accurate.

The next part of the thesis treats the extraction of features from the signals measured on the transducer and a classification based on these features. The features extracted are phase and gain for the transducer. Several methods for this feature extraction are found and thoroughly tested. The classification are made with a classic PCA.

The last part of the thesis treats the mapping of the feature extraction and the classification to a FPGA in a hardware/software co-design process. The mapping are done in to steps, where the first step treats the algorithm level and the second step threats the architecture level.

The system is finally tested and while it does not seem to give a significant improvement with the normal benchmark methods, where the tests are made with metal alone. It does give a significant improvement in the ability to detect metal that are mixed with a product.

Aalborg Universitet

TITEL:

Metal detection i fødevarer

PROJEKT PERIODE:

1. september, 2007 -
4. juni, 2008

PROJEKT GRUPPE:

ASPI10 - gruppe 1041

GRUPPEMEDLEMMER:

Frank Thornemann Hansen
Lars Vinding

VEJLEDERE:

Kjeld Hermansen
Anders Brødløs Olsen

ANTAL KOPIER: 6

ANTAL SIDER

I HOVEDRAPPORT: 110

I APPENDIX: 22

TOTALT ANTAL SIDER: 132

SYNOPSIS:

Dette speciale omhandler udviklingen af en metal detektor.

Først bliver transduceren analyseret, sammen med responset fra forskellige materialer i denne. En række tests bliver lavet for at verificere modellen og den viser sig at være tilstrækkelig god.

Den næste del af specialet omhandler estimeringen af features fra de målte signaler og den efterfølgende klassifiseringen på baggrund af disse. De features der bliver estimeret og benyttet er forstærkningen og fasedrejet i transduceren. Adskillige metoder til estimering af feature bliver opstillet og gennemtestet. Den efterfølgende klassificering bliver gjort med en klassisk PCA.

Den sidste del af specialet omhandler mapningen af denne feature estimering og den efterfølgende klassificering til en FPGA i en hardware/software co-design process. Mapningen sker i to steps, hvor det første step omhandler algoritme niveauet og det andet step omhandler arkitektur niveauet. Til sidst bliver det endelige system testet og det viser sig at det ikke giver nogen væsentlig forbedring i forhold til de benchmark metoder der bruges i dag, hvor detektorens evne til at detektere et metal testes uden at dette metal blandes med produktet. Dog viser det sig, at der er sket en signifikant forbedring i evnen til at detektere metaller, der kører igennem detektoren sammen med et produkt.

Preface

This thesis is carried out during the fall 2007 and the spring 2008 at the specialization: Applied Signal Processing and Implementation (ASPI). The thesis is based on the project proposal "New generation of metal detectors used in connection with article of food processing" by Kjeld Hermansen and Detectronic.

The documentation is split into two parts:

- **Main Report**

  The main report contains the main documentation of the project. That is the analysis of the detector head, feature extraction method and classification. From that algorithm and implementation is treated. Finally the system is tested and a conclusion is made based on the results of the project.

- **Appendix Report**

  The appendix report contains details about the analog hardware, which is used for the metal detector provided by Detectronic and interface for a measurement system. The appendix also includes measurement reports.

Reference throughout this report is made with syntax [author, yeah] and refer to identical marks in the bibliography in the back of the main report. Attached to the report is a CD-ROM which contain **FiXme**: *Hvad*

The group will finally extend their great appreciation to Detectronic which has provided a metal detector and sample board for measurements and contributed with experience within the area of Metal Detection. Special thanks are addressed to Lars Høyem which has been the contact person from Detectronic. Thanks are also addressed to group 08gr1040, which work with the same project, for cooperation and providing hardware for the system.

Aalborg, June 4th 2008

_____   _____

Frank Thornemann Hansen   Lars Vinding

Contents

Main Report

Appendix Report

Chapter 1
Problem statement

Metal detection in food is widely used in area where large amount of food is being processed and where metal objects are close to the food being processed. This can for example be in slaughterhouses where the workers which cut the meat have mail gloves to avoid cutting the hands. The small metal ring from the gloves might come off and fall into the meat. Another example is the parts of the machinery which might fall into the meat, this could be a screw, small metal splinter, etc. It is very important for a company that food never leaves the area with metal in it, since this could injure the consumer which would lead to bad publicity and in some case lawsuit. The companies test the metal detectors at regular basic, by testing that it find the expected metal in food. If it does not find the metal, the production line is shut down until the detector work again. It is therefore important with a reliable metal detector that can detect even small piece of metal. The main parameters when the customer buy metal detectors are the performance, the price is not important if it perform better.

The two major types of metal detection system are based on electromagnetic and x-ray. In this project the focus is the electromagnetic system.

The project proposal for this thesis, which originates from a company called Detectronic, was to examine the effect of increasing the operating frequency for the metal detector system and to change the domain from analog signal processing to digital signal processing. The company experienced that the competitors increased the operating frequency of their systems which makes them cable of detecting smaller objects of certain types, for example stainless steel, which Detectronic experiences problems detecting at 30 kHz.

When companies benchmark their metal detectors it is done based on the ability to identify metal objects, while there is nothing else in the metal detector. This kind of standardized test does however not show the performance for the detector when separating metal from food, which is the main challenge. The food is shown to be the greatest noise source and therefore the main challenge in this project is to find features which characterise the object passing through the detector head. Based on the features it should be stated if the object contains metal.

The structure of the work in this project is based on what is known as the A^3 model at Aalborg university, see figure 1.1. This model has three level of abstraction the application, algorithm and architecture. At the application level the functionality is described as mathematical functions. There may be more methods which implement the functionality and each has a one-to-many mapping into the algorithm domain. In this project it regards how features are extracted and how classification can be made. Based on simulation the best feature extractor and classifier is chosen. These will then be mapped into an algorithm domain as a one-to-many. The application can be implemented with various algorithms. When the algorithm is chosen they are mapped to the architecture level as a one-to-many. At the architecture level the platform for the algorithm is designed, the algorithm can be implemented on various architecture platforms, DSP, FGPA etc. and therefore the one to many mapping.

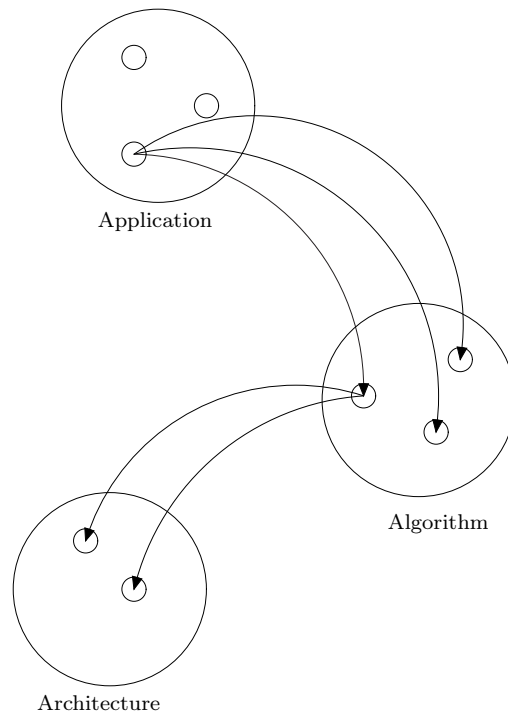This project is divided into several sub problems.

Figure 1.1: *The A^3*

- The first problem regards the hardware interface to the metal detector. High current is desired for the detector head since it gives strong magnetic field in the detector head, this is however difficult when the system operates at high frequencies. It is also desired to amplify the signal from the receiver coil much, but this is difficult due to unbalance in the system, these topic are evaluated in 2 and 3.

- The next sub problem is to extract features from the signals. The feature which has to be extracted is the phase and the amplitude as shown in chapter 2. A list of different methods for extraction of these two features has been examined and evaluated in chapter 3

- The next sub problem is to use these features to determine whether there is an object in the metal detector and to identify if the object is made of metal. The design of this classifier can be found in section 5

- The last sub problem is to get the feature and classier mapped onto an architecture

The basic system is shown in figure 1.2. The detector head which is provided by Detectronic need a signal generator and amplifiers.
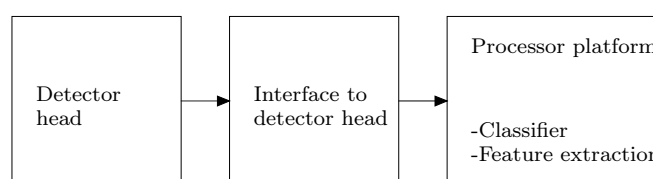

Figure 1.2: *This shows the block for the overall system*

1.1 Report structure

In this section the chapter for the report is outlined to give an overview of the report structure.

- Chapter 2 - Detector head analysis In this chapter the detector head is analysed and it is review what happen when an object pass though the detector head In this chapter the feature which should indicate if object are present is found to be phase and amplitude.

- Chapter 3 - Feature extraction: In this chapter the algorithm which estimate the amplitude and phase from the signal is review. Five different methods are evaluated and based on simulation one is chosen.

- Chapter 4 - Signal analysis: In this chapter measurements are analysed with the chosen feature extraction method. The characteristic of the feature is shown and balancing of the system evaluated. Test made on 30 kHz and 300 kHz is also evaluated.

- Chapter 5 - Classifier: In this chapter the classifier which should detect if metal are present in food are evaluated

- Chapter 6 - Algorithms: In this chapter the algorithms for the feature extraction and classifier is described.

- Chapter 7 - System design: In this chapter the overall system for implementation is described. The co design between hardware and software is made.

- Chapter 8 - Implementation: In this chapter the hardware and software implementation on the FPGA is described.

- Chapter 9 - System test: In this chapter the system is tested for how small metal object and type that can be detected.

- Chapter 10 - Conclusion: In this chapter the system is concluded and topics for further work is described

Chapter 2
Detector head Analysis

In this chapter the detector head will be analyzed, the purpose is to outline how the detector head works and what happens when an object passes through it. The chapter sets the basis for the signal processing part, since it identifies the signals to work with and how possible metal objects in food can be identified. The chapter is divided into five sections. The first section examines how the detector head works in basic, without any object. Then material properties are reviewed, which influence the response of a passing object has. When the basics of the detector head and materials are set, the passage of a metal object in the detector is described. From this a model is reviewed where the response of an object in a metal detector can be estimated. The chapter finishes with a section about food in the detector.

Before entering the sections a short introduction of the detector head will be outlined. The detector head consist of three coils placed next to each other as shown in figure 2.1. The coils are wrapped around a non-magnetic box, where the food to be checked for magnetic object can pass. The coil in the middle is the transmit coil. It is connected to a signal generator and when an electric signal is applied to the coil, a magnetic field is transmitted from the coil. The two adjacent coils are the receiver coils, which receive the magnetic field and convert it back to a voltage. The detector head can be seen as an antenna scenery. One antenna transmits a signal, and around the transmit antenna two receiver antennas are present, which receive the transmitted signal.
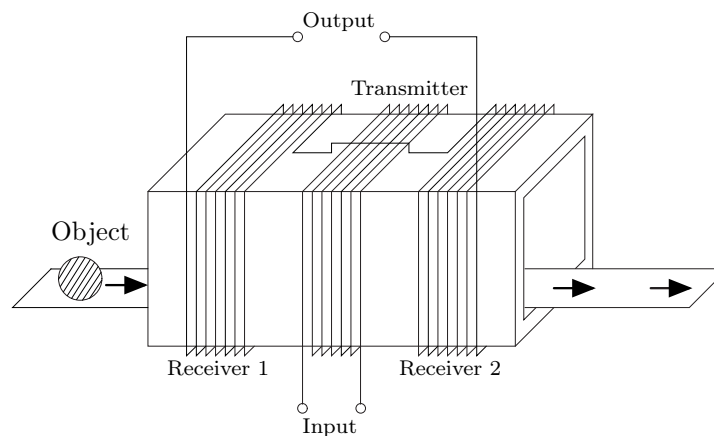
Figure 2.1: *Detector head model with one transmit coil and two receiver coils connected together*

The two receiver coils are wrapped opposite of each other and connected together as shown in figure 2.1. The voltage which is measured on the output is the differential voltage between the two receiver coils. If the receiver coils are placed at an equal distance from the transmit coil, see figure 2.2, the magnetic field radiating the coils are equal which yield zero differential voltage between the receiver coils. The fact that it is impossible to build the system to give an exact match difference will be present in the receiver coil. This problem will be treated later in section 4.1.

If an object with either electric or magnetic conducting properties enters the detector head a disturbance of the magnetic field appears. If for example an object passes through receiver 1

Figure 2.2: *Magnetic field distribution from transmit coil (Tx) into the two adjacent receiver coil (Rx$_1$ and Rx$_2$)*

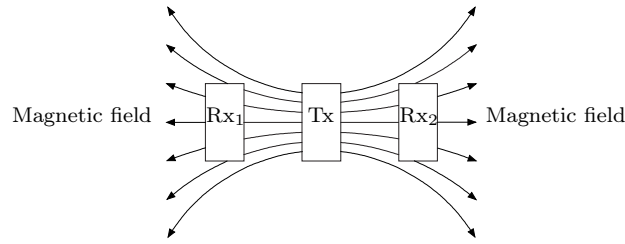the magnetic field in this coil will change, but the magnetic field in receiver 2 are unchanged, which means that the differential voltage is not zero anymore. It is this change in signal that should alert the system if metal is present, note however that food may also be able to conduct magnetic or electric signals and therefore give a similar differential signal.

2.1   Detector head

In this section the theory behind the detector head is described. The purpose is to describe the function of the detector head and what parameters that influences the performance. An exact calculation of the detector head is not in the scope of this project. The section starts with the generation of the magnetic field in the transmit coil and how this field is received at the receiver coils. Then the self-inductance of the coils and the minimization of this with a resonance circuit is reviewed. Last the interaction between the transmit coil and receiver coils are described.

Since the purpose of this section is to understand how the detector head works, and not to make an exact calculation on the detector head, some assumption are made to ensure a uniform magnetic field in the coils. The assumptions are [Demarest, 1998]:

- The coils are assumed to be solenoid, which means no corner exists where the magnetic field can build up, as for the rectangular detector head.

- The wire is assumed closely coiled, so the flux leakage between the turns are minimized.

- The length of the coil should be larger than the radius, since the magnetic field spread at the ends.

The three assumptions do not exactly comply with the detector head since there are some distances between the windings and the length of the coil is less than the radius of the opening, only seven windings are used. This cause the real detector head to have a non uniform magnetic field in the opening. The assumptions are however used since the principal are the same for the two setups. It makes it easier to describe the system and it is still possible to see what parameters influence the performance of the detector head.

2.1.1 Transmit signal

This subsection describes the generation of the magnetic field in the transmit coil. Ampere's law state that an electric signal give rise to a magnetic field. This means that when a current is applied to the transmit coil a magnetic field is produced. The relationship between the current and the magnetic field is stated in Ampere's law, as the line integral of the magnetic flux density B around any closed path C equal the product of the current I enclosed by the path times the permeability μ of the surroundings, see figure 2.3. Permeability is the ability for a material to be magnetized, which will be examined later. This means that when an electric signal is applied to the transmit coil, it produces a magnetic field around the wire. The signal which is applied to the transmit coil is sinusoidal, and so the magnetic field will also vary as a sinusoid. Ampere's law can be written as [Demarest, 1998]:

$$\oint_C B \bullet dl = \mu I \tag{2.1}$$

A note should be made to the equation above, since it only applies for steady current. Maxwell has modified the equation by adding a term called the displacement current which takes the time-varying electric field into account. The term can be neglected if the wires from which the coil are wrapped, are perfect conductors, which is assumed for the transmit coil.
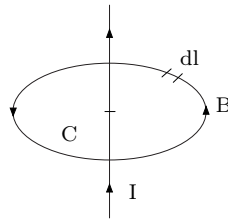

Figure 2.3: *Magnetic flux density B around a closed path C intersected with a conducting wire*

The magnetic flux density produced when a current is applied to the solenoid can be calculated as [Demarest, 1998]:

$$B = \mu \frac{NI}{T} \tag{2.2}$$

Where μ is the relative permeability, N is number of turn, I equals the current in the wire and T is the length of the solenoid.

To make a strong magnetic field in the transmit coil, many turns, high current or high permeability should be chosen. The permeability is fixed to μ_0, since it is the permeability of air. The length of the solenoid T should be kept small for a strong magnetic field.

The direction of the magnetic field from the transmit coil can be found by using the right hand rule. It states that if pointing the right hand thumb in the direction of the current then the magnetic field is in the direction of the fingers.

The generation of a magnetic field in the transmit coil has now been outlined and a strong magnetic field is obtained, when the current or the number of turns are kept high and the length of the solenoid are kept short. Next it will be described how the magnetic field from the transmit coil is converted back to an electric signal in the receiver coils.

2.1.2 Receive signal

Just as the time-varying electric field produces a magnetic field, the opposite is also true, namely a time-varying magnetic field produces an electric field. This means that when the magnetic field from the transmit coil intersect the two adjacent receiver coils an electric field is produced. A note should be made that the magnetic field should be time-varying, since the induced electric field is produced from the change in magnetic field. This is not the case for an electric current since a constant current will produce a constant magnetic field. The voltage induced in the receiver coil is called the electromotive force or emf and can be found based on Faraday's law as [Ida, 2004]:

$$emf = -N\frac{d}{dt}\int_S B \cdot ds = -N\frac{d\Phi}{dt} \qquad (2.3)$$

Where Φ is the flux through the loop and N is the number of loops.

It is desired to get a strong link between the transmit coil and receiver coil, and so it is desired to get a large voltage induced from the transmit signal. This can be done by increasing the number of turns in the coils or increase the change in the magnetic flux.

The polarity of the emf and thereby the direction of the current is such that the magnetic field which is produced by the induced current, opposes the change of the magnetic field from the transmit coil. In figure 2.4a the induced voltage is shown for increasing and decreasing magnetic field respectively. When the magnetic field B from the transmit coil increases, the direction of the magnetic field B_I from the induced current is downwards, since it opposes the change of the magnetic field. Based on the right hand rule the current is clockwise. When the magnetic field B decrease, the magnetic field from the induced current B_I changes direction to oppose the change. The direction of B_I is now the same as B and the current is counter clockwise. In figure 2.4b the magnetic field B versus the magnetic field from the induced current B_I is shown for a sinusoidal magnetic field. It can be seen that induced magnetic field B_I lag the radiated magnetic field B by 90°. The two situations from figure 2.4a with the increasing and decreasing magnetic field is shown as 1 and 2 respectively in figure 2.4b [Ulaby, 2005].

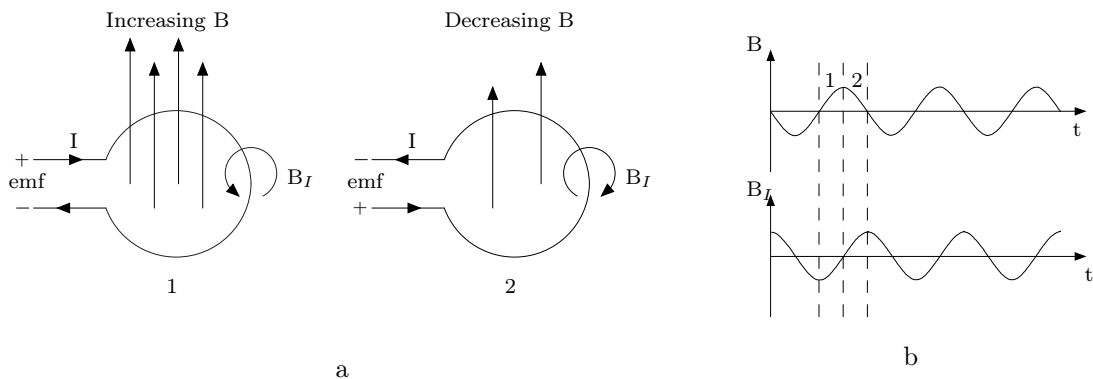**Figure 2.4:** *Figure a show the induced current for increasing and decreasing magnetic field. Figure b show a sinusoidal varying magnetic field B and the corresponding induced magnetic field B_I*

The generation of magnetic field in the transmit coil and the reception of this field in the receiver coils are described. Next the self-inductance is described, to see how this affect the receiver and transmit coil.

2.1.3   Self-inductance

When a time-varying current is applied to a coil of N loops a time-varying magnetic field is produced, as stated earlier. Each loop of the coil will produce a surrounding time-varying magnetic field, which will induce voltage in the adjacent loops. It is this effect which is known as self-inductance. The self-inductance is defined as the ratio of induced voltage versus the change in current producing it. The amount of induced voltage depends on the number of turns and changes of magnetic flux see equation (2.3). The magnetic flux Φ produced by the current I can be assumed to be proportional with a constant factor K, and so relation between the induced voltage and change in current can be written as [Schwarz, 1999]:

$$emf = -N\frac{d\Phi}{dt} = -NK\frac{dI}{dt} = -L\frac{dI}{dt} \tag{2.4}$$

where L is the self-inductance.

It can be seen from equation (2.4) that if the self-inductance L or the current I increase, the voltage across the coil also increase. It is desired to see which properties of the coil that has an influence on the self-inductance L. The magnetic flux Φ can be rewritten as flux density B times the area A of the solenoid. Using equation (2.2) the self-inductance L can be written as [Kraus & Fleisch, 1999]:

$$L = \frac{\Phi N}{I} = \frac{BAN}{I} = \frac{\mu N^2 A}{T} \tag{2.5}$$

From this equation it can be seen that an increase in number of turns N, permeability μ and area A will increase the interaction between change in current and induced voltage. The opposite is true for the length T.

The self-inductance of the transmit coil can be estimated based on equation (2.5). The cross-section area of the detector head cannot be measured exactly since the coil is not accessible, but the opening is 0.185 m times 0.36 m. The coil is probably 0.10 m longer, which yield 0.285 m times 0.46 m. The length of the coil cannot be measured either, but we know they make space between the windings, approximately 0.005 m plus the width of the wire 0.002 m, this yields approximately 0.05 m for 7 windings. The permeability of the coil equals air, which is μ_0 equal $4 \cdot \pi \cdot 10^{-7}$. The inductance of the coil can now be calculated as:

$$L = \frac{4 \cdot \pi \cdot 10^{-7} \cdot 7^2 \cdot 0.235 \cdot 0.41}{0.05} = 29.7\mu H \tag{2.6}$$

The coil is measured with an LCR meter to 27.3 μH. This yields an error of 8 % which also sound reasonable since the model is for a solenoid and the excact cross section area is unknown.

Equation (2.4) can also be rewritten as a phasor which makes it easier when analyzing it in an electric circuit. The term d/dt is replaced with $j\omega$ and from this the inductance can be written as [Demarest, 1998]:

$$v = L\frac{dI}{dt} \Leftrightarrow V = j\omega LI \Leftrightarrow \frac{V}{I} = j\omega L \tag{2.7}$$

The inductance L is the imaginary part of the impedance, also known as reactance. From equation (2.7) it can be seen that the reactance increases as frequency and inductance increase.

The reactance of the transmit coil is for 30 kHz and 300 kHz 5.1 Ω and 51 Ω respectively.

Since a large current is desired in the transmit coil, to get a strong magnetic field, the reactance should be kept low. Based on equation (2.7) the frequency or inductance should be kept low. From equation (2.5) it is shown that the inductance of the coil increases with a factor N^2, while it decreases the magnetic field produced by the transmit coil by a factor N, see equation (2.2) which is undesired. A decrease in frequency will also decrease the inductance, but it will also decreases the induced voltage. This is undesired since high voltage is desired in the receiver coil to make a good link between the transmit and receive coil.

It has now been shown that there are some contradiction between the inductance versus the magnetic field produced and the voltage induced. It is however possible to minimize the reactance by placing a capacitor in series, this makes a resonance circuit, which will be described in the following section.

2.1.4 Resonance

What happens in a resonance circuit is that at some frequency the inductance and capacitance becomes equal and therefore cancel each other This yield zero reactance for series connection and infinite for parallel connection. The reactance for series connection Z_s and parallel connection Z_p is [Johnson & Johnson, 1997]::

$$Z_s = j2\pi fL + \frac{1}{j2\pi fC} = j\left(2\pi fL - \frac{1}{2\pi fC}\right) \tag{2.8}$$

$$Z_p = \frac{\frac{1}{j2\pi fL}j2\pi f}{\frac{1}{j2\pi fL} + j2\pi fC} = \frac{1}{j\left(-\frac{1}{2\pi fL} + 2\pi fC\right)} \tag{2.9}$$

The resonance frequency for which the inductance and capacitance is equal is:

$$f = \frac{1}{2\pi\sqrt{LC}} \tag{2.10}$$

It is possible to calculate the capacitance which minimizes the impedance and thereby maximize the current, since the frequency and the inductance is known:

$$C = \frac{1}{L \cdot (2 \cdot \pi \cdot f_r)^2} \tag{2.11}$$

It is desired to measure the current in the transmit coil since it is proportional to the magnetic field with some constant. The current is measured by connecting a resistor in series with the transmit coil and then measure the voltage across the resistor. The resistor influences the resonance filter since it controls the gain of the peak as G=1/R and the bandwidth of the peak as BW=R/(L $\cdot$ 2). This means that the resistor should be chosen small, since a high current is desired. This makes the peak more narrow, and influences from variation in the inductance and capacitance increase. For example inaccuracy in the capacitor changes the current more around a narrow peak. For the inductance which is given in equation (2.5), it can seen that the permeability

have an influence, and so when an object with permeability above one enters the detector head, it changes the inductance of the coil. If for example iron, which has permeability of 1000, is filling the opening of the transmit coil, the inductance will increase a factor 1000, and move the peak to another resonance frequency. Note however that the opening is often much bigger than the objects which should be detected, and so it will not change the inductance significant. Food which enter the detector fill out the opening more, since the detector head is designed to fit the food with some margin. The permeability of food is however often approximately one, and so it does not change the permeability much. Simulation has been made for an RLC circuit with resonance frequency 30 kHz. The resistor is set to 1 Ω and the capacitor is chosen 948 nF. The inductor is set equal to the transmit coil which is 29.7 μH for permeability one. A second simulation is made with an inductor of 59.3 μH, which equals permeability of 2. The result is shown in figure 2.5 on the left figure. The blue line is inducatance of 29.7 μH equal relative permeability one and the red line is 59.3 μH equal relative permeability of two. It can be seen that when the relative permeability of the coil opening change from one to two, the current decrease about 15 dB. The right figure in 2.5 compares the current with and without resonance circuit, for μ equal 2. It is shown that the current is approximately 6 dB higher for the resonance circuit so there are still advantage in using the resonance circuit, even though the peak is off.
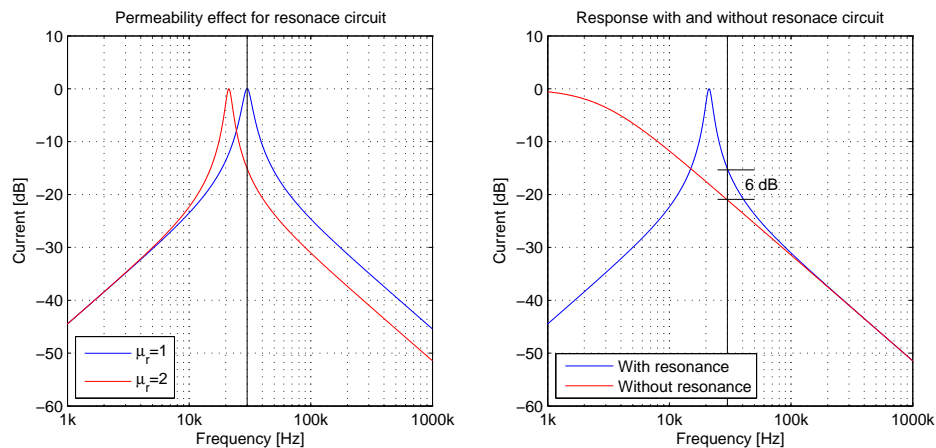

Figure 2.5: *Permeability influence on resonance frequency (left) and response with and without resonance circuit (right).*

Test has been made on the transmit coil where a metal object with high permeability is placed in the transmit coil, but the inductance did not change. This is due to the opening being much larger.

It has now been shown how the undesired self-inductance can be minimized and simulation shows that the resonance circuit has the highest current even though the peak is off. In the next section the interaction between the transmit coil and receiver coils are described and how it relate to mutual inductance.

2.1.5   Interaction between receiver and transmit coils

The interaction between the receiver coil and transmit coil was introduced shortly in the beginning of this chapter. The detector head has three coils, a transmit coil and two adjacent receiver coils. When the transmit coil emits a time varying magnetic field, a voltage will be

induced in the two adjacent coils. The two receiver coils are connected together, but they can be seen as two separated coils, with induced voltage V_1 and V_2, as shown in figure 2.6. The differential voltage V_{diff}, which is measured between the two receiver coils are:

$$V_{diff} = V_1 - V_2 \tag{2.12}$$

In figure 2.6 the induced voltage for increasing (a) and decreasing (b) magnetic field is shown. The current induced in the receiver coil will create a magnetic field, which oppose the increasing or decreasing magnetic flux B, as stated earlier by Lenz Law. Since the coils are coiled opposite, the direction of the current in the two coils I_1 and I_2 are opposite. With equal distance and thereby equal magnetic flux radiating the coils, the total current in the coils is zero, since the two currents I_1 and I_2 cancels each other.

For increasing magnetic field, see figure 2.6a, the voltage V_1 and V_2 is positive, and with equal distance the differential voltage is zero, see equation (2.12). In practice it is not possible to get 100 % equal distance and so the differential voltage will never be completely zero. When the magnetic field decrease, see figure 2.6b, the currents I_1 and I_2 change direction, to oppose the decreasing effect. The voltage V_1 and V_2 is now negative, but the differential voltage is still zero.
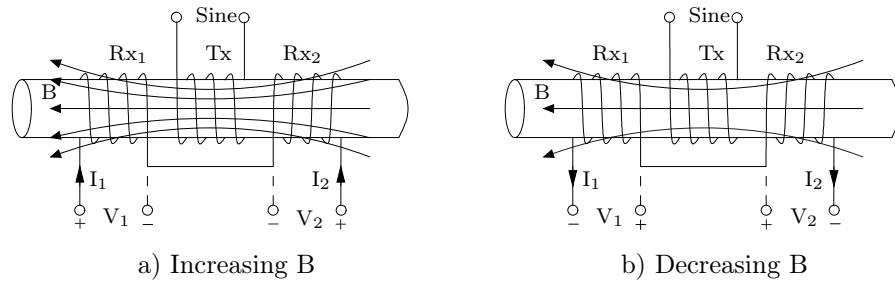

a) Increasing B   b) Decreasing B

Figure 2.6: *Induced voltages in receiver coils due to increasing (a) and decreasing (b) magnetic flux density B*

A way to describe the link between the transmit coil and receiver coil is by mutual inductance. Just like the self inductance describes the ratio between the induced voltages in the coil to the change in current in the coil, the mutual inductance is the ratio between the induced voltage in the coil and the change of current in a neighboring coil. The induced voltage in one of the receive coil can be written as:

$$v_{Rx} = L_{rx}\frac{\partial}{\partial t}i_{rx} + N_{rx}\frac{\partial}{\partial t}\Phi_{rx,tx} \tag{2.13}$$

where L_{rx},i_{rx} and N_{rx} is the inductance, current and number of turn in the receiver coil. $\Phi_{rx,tx}$ is the magnetic flux in the receiver coil caused by the transmit coil. Just like the self-inductance, the magnetic flux is assumed to be proportional with a constant $K_{rx,tx}$ to the current in the transmit coil. Equation (2.13) can be written as:

$$v_{rx} = L_{rx}\frac{\partial}{\partial t}i_{rx} + K_{rx,tx}N_{rx}\frac{\partial}{\partial t}i_{tx} \Leftrightarrow \tag{2.14}$$

$$v_{rx} = L\frac{\partial}{\partial t}i_{rx} + M_{rx,tx}\frac{\partial}{\partial t}i_{tx} \tag{2.15}$$

where $M_{rx,tx}$ describes the flux linkage $N_{rx}\Phi_{rx,tx}$ between the transmit and receive coil to the current i_{tx} in the transmit coil [Schwarz, 1999].

The mutual inductance M can be written in term of properties of the coil based on equation (2.5):

$$M_{rx,tx} = \frac{N_{rx}\Phi_{rx,tx}}{i_{tx}} = \frac{N_{rx}N_{tx}A\mu}{T} \tag{2.16}$$

where A is the cross section area of the detector head, T is the length of the coils, μ is the magnetic permeability between the coils and N_{rx} and N_{tx} is the number of turn in the receiver coil and transmit coil respectively. From this equation it can be seen that the interaction between the transmit coil and one of the receiver coil increases as the number of turns, the cross section area or the permeability increase. The opposite apply for the length of the coils. It can be seen that when an object with permeability above one pass through the detector head, the mutual inductance will change which causes a change in the induced voltage at the receiver coil.

The function of the detector head has now been analyzed and the parameters which influence the performance have been found. It was shown that to get a strong magnetic field the current, number of turns or permeability should be high in the transmit coil, the opposite apply for the length. To get a strong signal at the receiver the number of turns or change of magnetic field should be high. It was shown that a low self-inductance was desired for the transmit coil since increase in self-inductance decrease the current in the coil. The self-inductance could be minimized by decreasing the permeability, number of turns, cross section of the coil or the frequency, the opposite apply for the length. If the frequency, number of turns, or cross section area is increased, it decreases the performance of the receiver and transmitter. The permeability cannot be changed since it equal that of air. A method to minimize the inductance is to make a resonance circuit with a capacitor. Last the interaction between the transmitter and receiver was modeled with mutual inductance.

2.2 Physical properties of materials

In this section the physical properties of materials will be outlined. The focus is on permeability and conductivity, since they have an influence on the response of the object in the metal detector. The section will describe the two quantities and list sub category for each.

2.2.1 Permeability

Permeability indicates how easy a magnetic dipole is formed in an object when a magnetic field is present. Often a unit less quantity called relative permeability μ_r is used. It is relative to the permeability of vacuum ($\mu_0 = 4\pi X10^{-7}$), which means the total permeability of the object is, $\mu = \mu_r\mu_0$. Permeability link the magnetic flux density B and the magnetic field strength H together as, $B = \mu H$.

Materials can be classified according to their response of a magnetic field. The main classes are diamagnetic, paramagnetic, ferromagnetic and ferrimagnetic.

Diamagnetic materials have no magnetic moment, when no magnetic field is applied. When a magnetic field is applied, a small anti parallel magnetic moment occurs, which oppose the

magnetic field. The object is repelled by either pole of a permanent magnet, but only a small repulsive force. The magnetic field in the material is less than the surrounding magnetic field, and so μ_r is less than 1. Typical diamagnetic materials are copper, gold, silicon, etc.

Paramagnetic materials have an average moment of zero when the magnetic field is absent. When a magnetic field is applied slightly more than half of the magnetic moment is parallel to the applied field and the last is anti parallel, this result in a net magnetic moment parallel to the applied field. For paramagnetic materials μ_r is slightly bigger than one, and they are attracted to permanent magnets with a small force. Typical materials are air, tungsten, aluminum etc.

Ferromagnetic material can be divided into magnetic domains. When a magnetic field is applied some of the domains turn parallel to the applied magnetic field, depending on the strength of the magnetic field. At some point all the domains is parallel and so further increase in magnetic field, will not increase the magnetic moment of the object. Ferromagnetic materials have the ability to maintain some of the magnetic moment, when the external magnetic field is removed. A note should however be made that if the material exceed a curtain temperature called the Currie temperature, it acts as a paramagnetic material. In figure 2.7 the relationship between magnetic flux density B and magnetic field strength H is shown. At first the ferromagnetic materials is demagnetized which is shown at point 1. When the magnetic field strength H increases so does the magnetic field B, untill it reaches saturation at point 2. This is where all the ferromagnetic domains are aligned with the magnetic field, and the magnetic flux density is saturation B_s. When H decreases, so does B, but it will not return to origo. When H return to zero, some of the domains keep their magnetic flux density, which is B_r, the remnant magnetic flux density. To get the flux density back to zero a magnetic field strength of H_c is required, the coercive field strength. The flux density B now become negative and decrease until saturation point 5. When H increases again it ends at point 2 without intersect origo. The intersection B_r is equal the permanent magnetic effect of the material [Demarest, 1998].
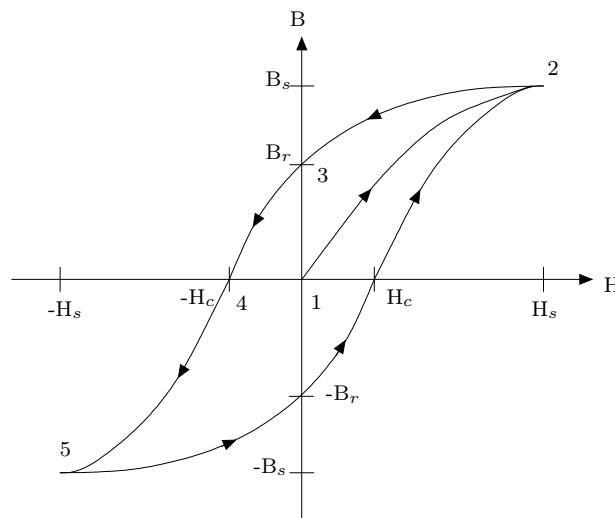

Figure 2.7: *Hysterese loop for B versus H*

The form of the hysteresis loop depends on the permeability of the material. It can be seen that the permeability is not constant as the magnetic field strength H change, since it would yield a straight line intersecting in origo, and with slope equal to the permeability. The permeability from point 1 to 2 is shown in figure 2.8. It can be seen that the permeability start at an initial value and then peak at μ_{max} from where it decreases to saturation μ_{sat}, which is equal to μ_0.

Typical ferromagnetic materials are iron, steel and nickel. The range of relative permeability is often between 100-20,000 and is a function of frequency and magnetic field strength. Often the relative permeability is one above a few tens of kilohertz.
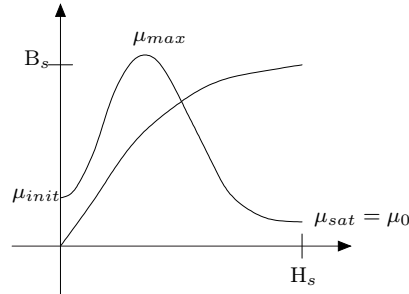

Figure 2.8: *Relative permeability versus the initial magnetization*

In ferrimagnetic the adjacent magnetic moment align opposite of each other, the magnetic moment are however not equal, so there are a net magnetic moment parallel to the applied field. The net magnetic moment is less than for ferromagnetic. Iron oxide and nickel-zinc belong to ferrite. The relative permeability is in the order 1,500, and the permeability is high for high frequencies, nickel-zinc has permeability in the order 100 at 100 MHZ.

2.2.2 Conductivity

Conductivity is an indication of how easy the charges can be moved in a material, when an electric field is applied. An equation relating the current density J and the electric field E is:

$$J = \sigma E \tag{2.17}$$

where σ is the conductivity measured in Siemens per meter [S/m]. The connection between the electrical resistance R of a material and the conductivity is:

$$\sigma = \frac{1}{RA} \tag{2.18}$$

Materials can be divided into three categories regarding conductivity that is: dielectrics, conductors and semiconductors. The conductivity of a material depends on temperature and composition of the materiel.

The conductivity for dielectric material, also known as isolator is very low and so the charges cannot move from atom to atom, which means approximately no current can run in the material. Glass and ferrite are examples of dielectric materials with conductivity 10^{-17} S/m and 10^{-3} S/m respectively [Ida, 2004].

Conductors have a high conductivity which means charges can move easy from atom to atom. It is the electron of the atom which moves in conductors and the conductivities is determined by the charge density of the electrons ρ_e and the electron mobility μ_e:

$$\sigma = -\rho_e \mu_e \tag{2.19}$$

The minus sign is due to the electrons movement in the opposite direction of the applied electric field. Examples of conductors are aluminum and iron with conductivity of $3.5 \cdot 10^7$ S/m and

$1.0 \cdot 10^6$ S/m respectively. Note that an increase in temperature decreases the conductivity [Ulaby, 2005].

Semiconductors have conductivity in between the dielectrics and conductors. Just like conductors electron can move between atoms, but an addition charge carrier exist for semiconductors. This charge carrier are known as holes, which can be seen as a positive-charge carrier, moving in the same direction as the applied electric field. The conductivities are now determined by additionally the charge density of the holes ρ_h and mobility of the holes μ_h:

$$\sigma = -\rho_e \mu_e + \rho_h \mu_h \tag{2.20}$$

Examples of semiconductors is germanium and silicon with conductivities $4.4 \cdot 10^{-4}$ S/m and 2.2 S/m respectively [Ulaby, 2005]. The conductivity increase when the temperature increases [Kraus & Fleisch, 1999].

Permeability and conductivity are now outlined, and they will be shown to have great influence on the response of the material in the metal detector.

2.3 Metal objects in detector head

In this section it is described what happens when a metal object is present in the detector head and the response when it passes through the detector.

Basically what happens is that the magnetic field in the coils changes when a metal object is present in the coil. There are two properties which can change the magnetic field in the coils, that is the magnetic permeability and the electrical conductivity, as described in section 2.2.

When a conducting material is present in the detector head, the time-varying magnetic field from the transmit coil, which is called primary, penetrate the material and eddy currents are induced in the material, as shown in figure 2.9. The eddy currents circulate around the primary magnetic field line, and the currents produce a secondary magnetic field. This means that net magnetic field is less than the primary magnetic field.
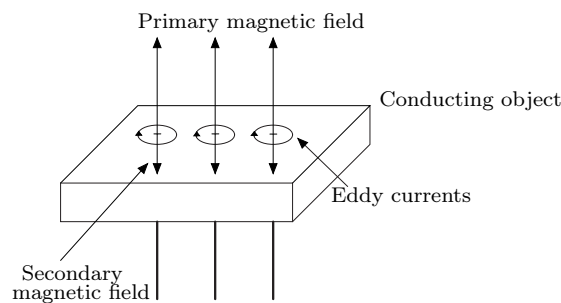

Figure 2.9: *Magnetic field induces eddy current in conducting object*

When a magnetic object is present in the detector head the magnetic field line is redistributed, and the magnetic field in the material is enhanced, this means the net magnetic field in the detector head is increased.

When no metal object is present in the detector head, the voltage difference between the two receiver coils should be zero. If a conducting material enters one of the receiver coils, the magnetic

field will decrease, which means the voltage of this coil also decrease and the difference between the two receiver coils is no longer zero. If a magnetic material enters the receiver coil instead the magnetic field increase, which means the voltage increase in and the difference is no longer zero.

It will now be described what happens when a magnetic object passes through the detector head, see figure 2.10. The figure show the amplitude and phase, when a magnetic object pass the detector head. The object enters the first receiver Rx_1 and the voltage of this receiver will increase until the object is in the middle of the receiver coil. The phase reaches a steady value which depends on the different parameters, which will be shown later. The object continue to the transmit coil, and the voltage of Rx_1 decrease. When the object is in the middle of the transmit coil, the voltage is equal for both receiver coil. The phase now switch 180°, since the voltage of Rx_2 increase. The voltage of Rx_2 increase until the object is in the middle of Rx_2. Afterwards the voltage decrease until the object is no longer near the detector head and the voltage for the two receiver coil is equal and the difference signal is zero.
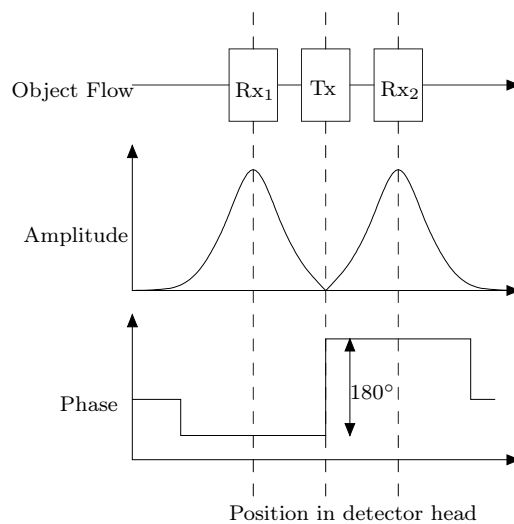

Figure 2.10: *A metal object passage in detector head*

The differential signal from the receiver can be seen as an amplitude modulation. The carrier equals the transmitted signal and the information signal is the signal from the passing object. The equation for the modulation can be written as:

$$s(t) = A_c \cdot sin(2 \cdot \pi \cdot f_c \cdot t) \cdot A_i \cdot sin(2 \cdot \pi \cdot f_i \cdot t) \qquad (2.21)$$

where A_c and f_c are the amplitude and frequency of the carrier respectively. A_i and f_i is the amplitude and frequency of the information signal respectively.

In figure 2.11 the AM modulation is shown for a metal object passing through the detector head. The information signal is zero when no object is near the detector head, and so is the AM modulated signal, with the assumption that the coil setup is perfectly balanced. When the object passes through the detector head an approximately sinus shape signal is modulating the carrier signal. Note that the information signal is not the sinusoid shown in figure 2.11. In addition to the amplitude modulation the signal is also phase modulated, since it change phase when an object passes through the detector head.
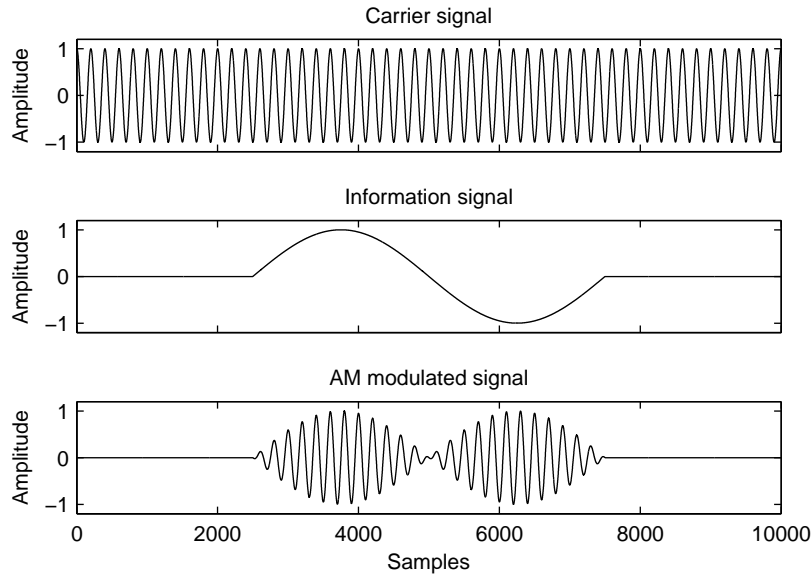
Figure 2.11: *AM modulation for object passing through detector head*

It has been now shown what happens when a metal object is passing through the detector head and how the parameters, conductivity and permeability, cause the response from the object. In the next section a model which calculate the response is reviewed.

2.4   Model for a metal sphere in a metal detector

In the previous section it was stated that a phase lag occur when an object passes through the detector head and that this phase lag depends on different material parameters. In this section a model from the paper [Bruschini et. al., 2000] is reviewed, which estimate the response of a metal object. The motivation behind the paper is in mine detection, but the setup is approximately the same. The mine detector has a transmitter and a receiver coil and so the response in the receiver is estimated when a sphere object is present near the mine detector. In our setup there are two receivers but one can be neglected, since it is only a matter of not getting the differential voltage. Another deviation from the model is that the objects do not pass through the mine detector, but approximations are made in the paper where the response does not depend on the position of the sphere. The purpose of this section is to verify if the model comply with real measurement and find the parameters which influence the response of the metal object. The derivation of the equation given by the paper will not be done in this report as the calculations are extensive and out of the scope of this project. Instead the model will be simulated in matlab and compared with real measurements to see if they comply.

The equation for the approximated response function is given in the paper as:

$$X_n(ka) + iY_n(ka) \quad = \quad \frac{(2\mu_r + 1)ka\ cosh(ka) - (2\mu_r + 1 + k^2 a^2)sinh(ka)}{(\mu_r - 1)ka\ cosh(ka) + (-\mu_r + 1 + k^2 a^2)sinh(ka)} \quad \text{(2.22)}$$

where $k^2 a^2 = i\sigma\mu\omega a^2$ is the response parameters. It can be seen that the response function depends on the conductivity σ, permeability μ, frequency ω and the radius of the sphere a. Note that the radius is squared which means it has greater influence. The output of the response

function yields a real and imaginary part. The phase can be calculated as the angle between the two and taking the absolute value yields the magnitude. To get the phase between the transmitter and receiver, the complex number should be multiplied with i to add the initial phaselag of 90° between the transmitter and receiver, as stated in section 2.1.

2.4.1 Model verification

The model will now be simulated in matlab and tested with real measurements to verify if the model complies.

Measurement will be made on a miniature model of the detector head as that in figure 2.1, except that a cylinder is used instead of a box. Five comparisons are made, that is for Brass, Aluminum, Stainless Steel, Ferrite and Iron, see measurement report B.1. The object is not sphere as in the model, but cylindrical rods. The reason for this is that no big sphere were available. The model should also approximately work for non-sphere object. The tests are made with a sweep in frequency, to see the progress of the phase. The results are shown in figure 2.12, except for ferrit which is a stright line.
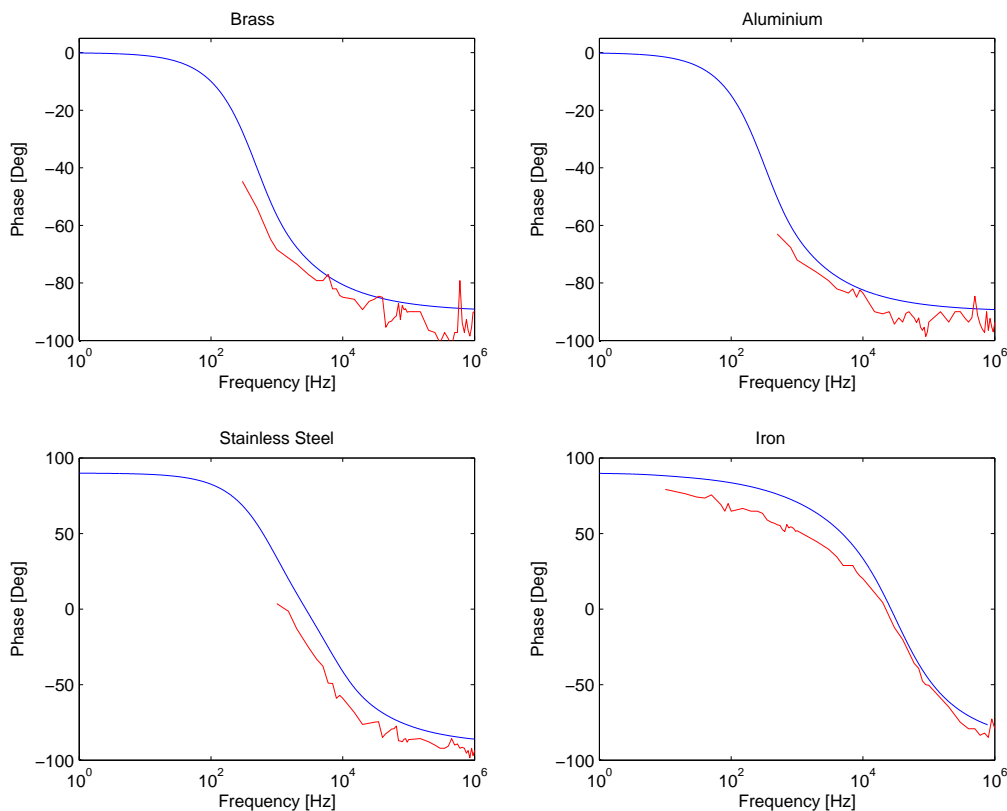

Figure 2.12: *This figure compare model and measurement*

Brass and Aluminum are non-magnetic with conductivity $1.5x10^7$ and $3.54x10^7$ respectively [Ida, 2004]. The phase lag, according to the model should be between -90° to 0°. Unfortunately measurements were only possible down to about 500 Hz, since the signal was too weak below. The progress of the measurement follow the simulation, the two lines are however not exactly on top of each other.

Stainless steel is generally close to non-magnetic $\mu_r = 1$, it however depends on the processing of the material [ASSDA, 2007]. The conductivity is set equal $0.14x10^7$ [ECT, 2007] and relative permeability is chosen 1.1. From the measurement it shows that the phase is above 0° and therefore it is assumed to have some magnetic properties. The simulation and measurement show similarity, there are however some uncertainty since the exact type of stainless steel is unknown.

Iron which are magnetic, has a simulated phase lag between -90° to 90°. Conductivity is set equal $1x10^7$ [Ida, 2004] and permeability is set equal 100. Similarity can be seen between simulation and measurement, it is however not reliable, since the graph are adjusted with the permeability to make it fit the measurement. It is not possible to find a fixed permeability in tables, since iron can vary and the exact kind of iron is unknown. The permeability would be expected higher since the permeability is above 1000 for iron in tables [Ida, 2004]. The reason can be that the permeability varies with frequency and strength of the magnetic field as shown in 2.2.1.

In figure 2.13 the measurement for the five metal type is plotted. It can be seen that ferrit is an approametly stright line, which also comply with the theory in section 2.2 where it was stated that the permeability of ferrite was high for frequencies above 1 MHz. The measurements for Brass and Aluminum are close to each other which is because the conductivities are close to each $1.5x10^7$ and $3.54x10^7$. Aluminum and Brass are conductive material where iron and ferrite are magnetic material. Stainless steel has lower conductivity than aluminum and brass, namely $0.14x10^7$, and looks like there could be some mild magnetic properties, since the phase are above one.
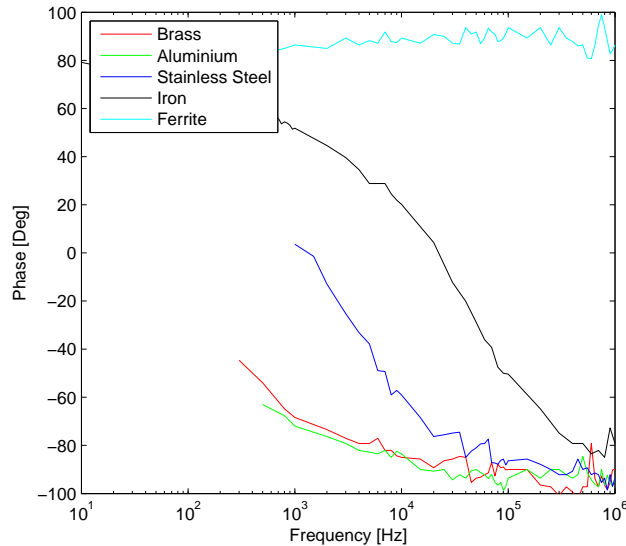

Figure 2.13: *This figure compare the measurements for different metal*

It is shown from the comparison that the model complies with real measurements with some deviation. The reason for the deviation could be that the model is an estimate for a sphere where cylindrical rods are used. The model also assumes the object to be much smaller than the opening, where the radius of the opening is only three times bigger than the rod. There is also uncertainty regarding the exact conductivity and permeability of the objects.

2.4.2 Simulation

The model has been tested to see if it complies with real measurements, in this section simulations will be made based on the response function from equation (2.22). The purpose of the simulations is to see how the four parameters: permeability, conductivity, size and frequency effect the phase and amplitude.

The first simulation will be carried out for three different conductivities σ: $0.1x10^7$, $1x10^7$ and $10x10^7$. Simulation for each conductivity will be made, with a sweep in frequency from 0 Hz to 1 MHz. The permeability μ_r is set equal 1 which means non-magnetic. In figure 2.14 the phase and absolute value for the response function are plotted.
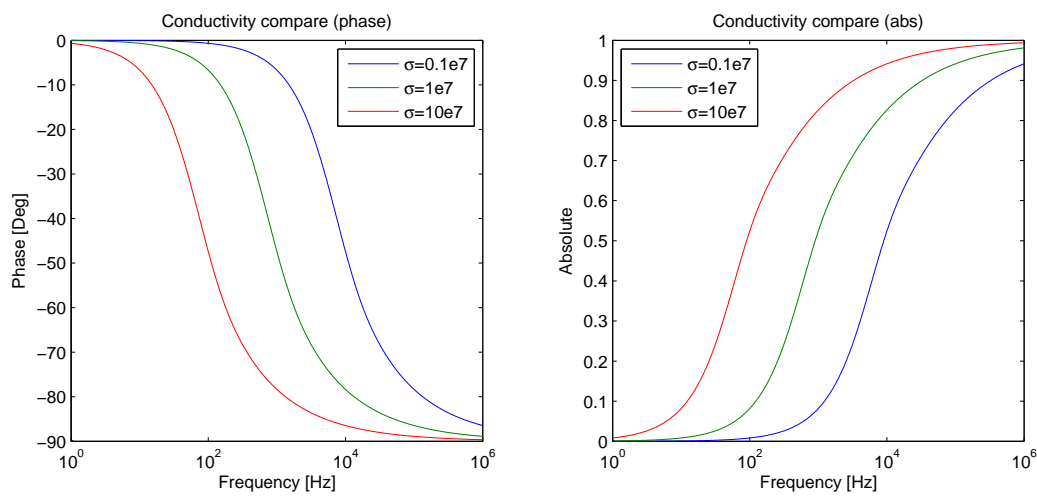

Figure 2.14: *This figure compare the phase and absolute value for different conductivity*

From the phase plot one can see that phase saturate for low frequency at $0°$ and for high frequency it saturate at $-90°$. It is also noted that the shape of the graphs for different conductivity are the same but the graphs are shifted. For low conductivity the graph is shifted up in frequencies and vice verse, this means that metal with low conductivity has less phase lag than metal with high conductivity at a given frequency. The graphs for amplitude are also shifted according to conductivity, but they have the same shape. From the figure it is shown that the absolute values converge to zero for low frequencies and converge to 1 for high frequencies. This means that it is favored to use higher frequencies, since the response is bigger.

The second simulation is made with different relative permeability μ_r: 1, 10, 100 and 1000. Again a sweep is made from 0 Hz to 1 MHz and conductivity is chosen $1x10^7$. In figure 2.15 the simulation for phase and absolute value of the response function is shown.

The figure for the phase shows that the phase converges to $+90°$ for low frequencies and $-90°$ at high frequencies. It can be seen that only metal with permeability above one has positive phase lag. Notice that for $\mu_r = 100$ and $\mu_r = 1000$ the graph is not shown up to 1 MHz. This is because sinh and cosh get too big in the equation for the model. The figure for the absolute value show that metal with permeability above 1, converge to a positive value above 1 for low frequencies and converge to 1 for high frequencies. It is therefore desired to operate at a low frequency, when detecting magnetic objects, because of the bigger response.
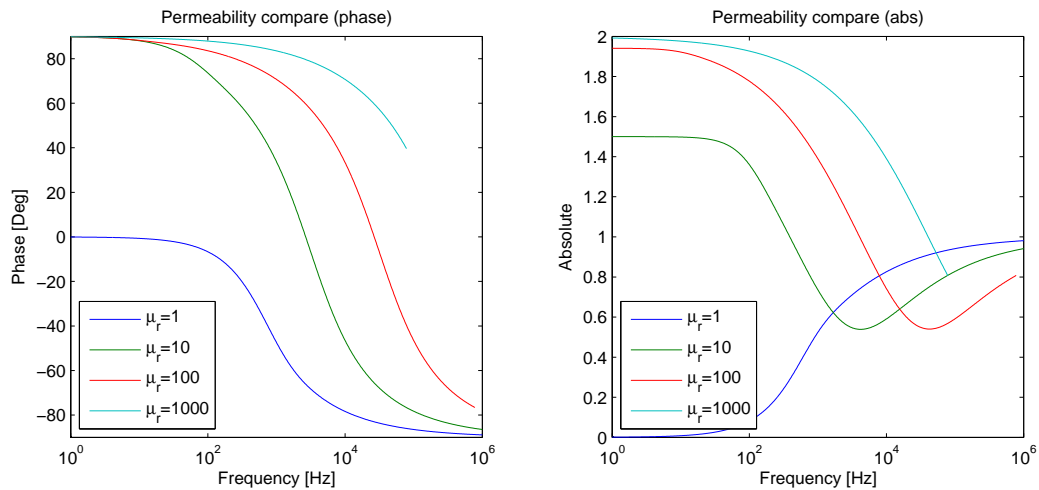
Figure 2.15: *This figure compare the phase and absolute value for different permeability*

The last simulation is made with different radius of the object: 0.1 cm, 1 cm and 10 cm. Permeability is chosen to 1 and conductivity is chosen $1x10^7$. The plot for the phase and absolute value are shown in figure 2.16.
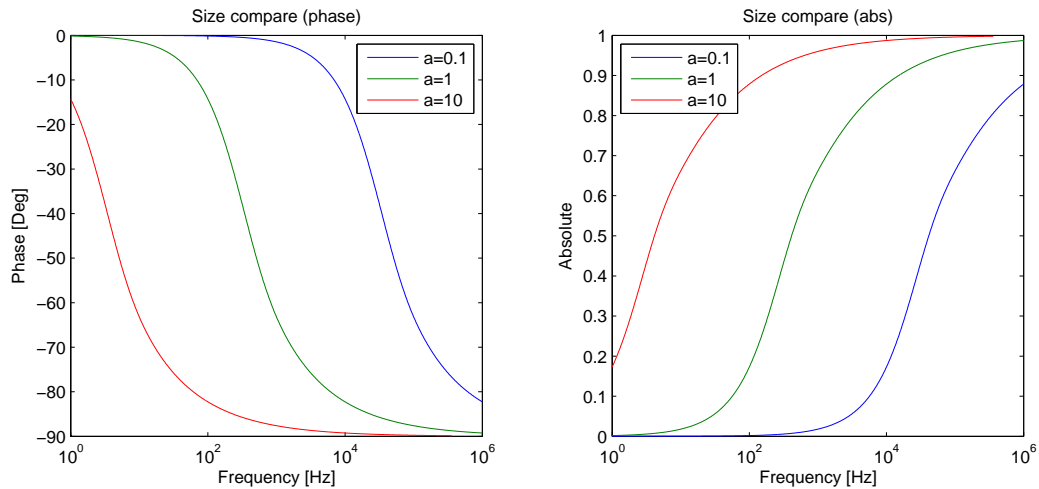

Figure 2.16: *This figure compare the phase and absolute value for different radius*

Here more deviation are noticed, when increasing radius with a factor 10, this is due to a^2 as input to the response function. This shows that the size of the metal object has a great influence on the response function. This is not desired since the size of the object for the metal detector is unknown.

Now to sum up this simulation, for a specific frequency, less conductivity, permeability and smaller object yields less phase lag. It is also noted that the range of phase lag for non-magnetic object is -90° to 0° and for magnetic object the range is -90° to 90°. The absolute value for non-magnetic object is maximized at high frequencies and for magnetic object it is at low frequencies, which means that high frequency is desired for detecting conducting metal and low frequencies are desired for detecting magnetic object. It is also noted that change in size of object has the greatest influence. The conclusion is that it is difficult to divide material into class according

to type of metal, since there are four factors which change the response. Especially the size is difficult to handle, because the size of the objects in metal detection are unknown.

2.5   Food in the detector

It has now been described what happens when a metal object passes through the metal detector and what parameters affect the response of the object. In this section it is review what happens when food passes through the metal detector.

It was stated in section 2.4 that four parameters influence the response of an object passing through the metal detector that is permeability, conductivity, frequency and size. The problem with food is that only one parameter is known that is the frequency. It is not possible to find the exact conductivity and permeability for food in tables, often the product also consist of more than one material. For example a chicken contains bones, meat, blood, tendon, skin and fat all of which has different permeability and conductivity. Bread is also build of different substances, crust, seed and flour with different permeability and conductivity. The size of the object, shape and orientation when is passes through the detector head can also vary. So it is not possible to estimate an exact phase and amplitude for a given food product.

It has been possible to find some approximated conductivity value for biological materials see table 2.1. Permeability has however not been possible. From the table it can be seen that in general food are expected to have low conductivity. It is assumed that the permeability is approximately one. The conductivity value is much lower than metal, but the size of the food is also much bigger, than the expected metal objects. For example a sphere of 2 mm has a cross section area of 12 mm^2 where a rye bread with dimension 100 mm times 300 mm equal 30000 mm^2 when passing the detector across. This yields a difference of 2500 times and the size parameter is squared in the response function. In the example only the cross section area is used, the volume is however also of influence. From table 2.1 it can be seen that the conductivity is 10^6-10^7 times lower than aluminum of $3.54x10^7$ [Kraus & Fleisch, 1999]. So even though the size of the food is much greater the response will often be much lower.

Animal fat	Animal body average	Blood	Body tissue	Sea water	Distilled water
0.04	0.2	0.7	0.01	4	0.0001

Table 2.1: *Conductivity for biological materials [Ida, 2004] [Kraus & Fleisch, 1999]*

Notice the big difference between the sea water and distilled water. The reason for this is that sea water contain more salt, which is electric conducting.

In figure 2.17 the response for an aluminum sphere of 2 mm and the response for average animal body of 20 cm is compared, the conductivity is set to $3.5 \cdot 10^7$ and 0.3 respectively. There are two plots for the animal body where the permeability is one and two. This is due to the unknown permeability. The result should not be emphasized too much, since the model assumes the object to be much smaller than the opening of the coils, which does not comply for food. The phase and amplitude graph for food are expected to be more to the left. It can be seen, when comparing aluminum and food with μ_r equal one, that the phase of the food are higher then aluminum and there are no phase variation at low frequency. The magnitude is lower for food. This makes it

easier to detects metal object in food, since they are expected to yield higher magnitude and the phase are different from zero. When comparing with food of permeability two, the phase increases 90° but it is still constant. The magnitude is higher than the aluminum sphere for frequencies below 10 kHz. Based on this it would be desired to operate at higher frequencies, so the magnitude of the sphere do exceed food, and the phase of the aluminum sphere is different from 90°.

It is shown that the magnitude decrease for conducting materials at low frequencies, this is a problem with for example stainless steel, since it has low conductivity $1 \cdot 10^6$ and low permeability approximately one. This implies that high frequencies are preferred to be able to detect small conducting spheres. If the frequency is increased too much, the magnitude of the food will be high and it can be harder to detect smaller spheres.
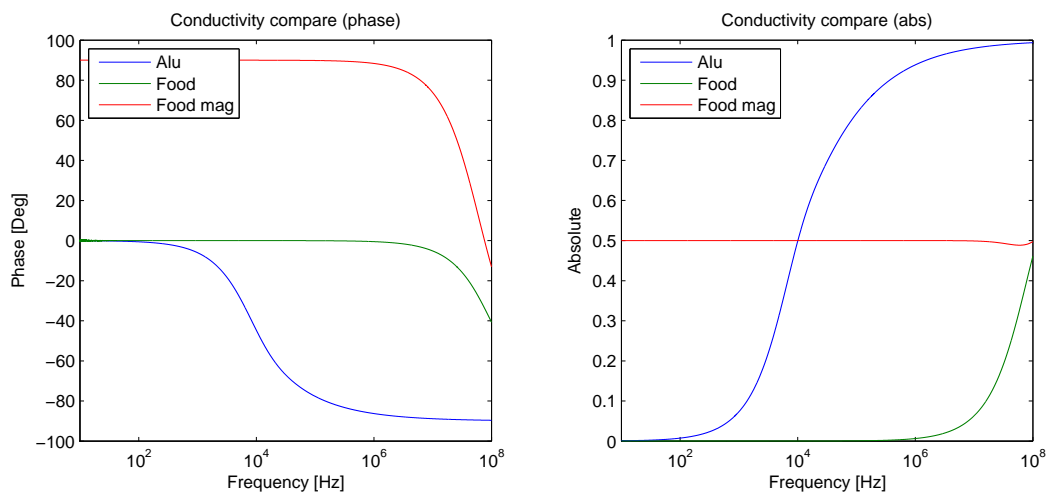

Figure 2.17: *This figure compare the phase and absolute value for aluminium of 2 mm and food with permeability one and two.*

The conclusion of this section is that it is difficult to make an exact estimate of the food, since the relative permeability is unknown. The product consists of varies material types with different properties and the form and size of the product may also vary in some cases. It is shown that conductivity are much smaller than metal, but the size of the food is also greater than the metal objects that needs to be found. The magnitudes of non magnetic food are small for low frequencies which are desired. The problem are however that small metal spheres with low conductivity yields a small response at low frequencies and therefore the frequency should not be too low.

2.6 Conclusion

In this chapter the detector head has been analysed, first the structure of the detector head was described and the parameters which influence the performance were described. It was shown that the generation of magnetic increased when the number of turn, permeability and current increase and decreased when the length of the coil increased. The amount of induced voltage in the receiver increased when the number of turn or rate of change for the magnetic field increase. It was then shown that the impedance of the coil increased as the number of turn, area or

permeability increased and decreased for increasing length of the coil. This work against the generation of magnetic field and induction in the receiver coils. A solution to minimize the impedance is to put an capacitor in series with the coil and then at the resonance frequency the impedance is approximately zero.

The two properties conductivity and permeability was also describe since they influence the response from the metal object passing though the detector head. Sub group was list for the two properties and parameters which influence the properties was described.

It was shown that the passage of en metal object could be seen as an AM and PM modulation.

A model which estimate the response from a metal sphere when present near a transmit and receiver coil was tested. The measurements did correlate with the model but they where not identical, this was due to some approximation. The model stated that the phase and amplitude of a given metal object was controlled by the size, frequency, permeability and conductivity, where the area was squared. This means that it is difficult to predict wanted and unwanted phase and amplitude for at given system.

Based on the model it was shown that the response from the conducting metal increase as the frequency increased and for magnetic material the response decreased. The phase for conducting material were within 0 and -90∘ and for magnetic the phase was within 90∘ and -90∘.

Based on the model it was concluded that for magnetic food product it would be desired to operate at high frequency since the response decreased and so does the permeability. This makes it easy to see metal with conducting properties it however reduce the sensitivity for magnetic metal object. This would also make it easier to estimate stainless steal, which has been shown to be difficult, since the conductivity and permeability are low. If the food instead were conducting it would be desired to use low frequency but than stainless steel can be difficult to estimate.

In figure 2.18 the system for the metal detector is shown. The detectorhead is interfaced with hardware from the transmit and receive coil is passes to an processing unit which calculate the phase and gain between the two signal. The phase and amplitude is then passed to a new processing unit which should estimate if metal is present based on the phase and gain sequence.
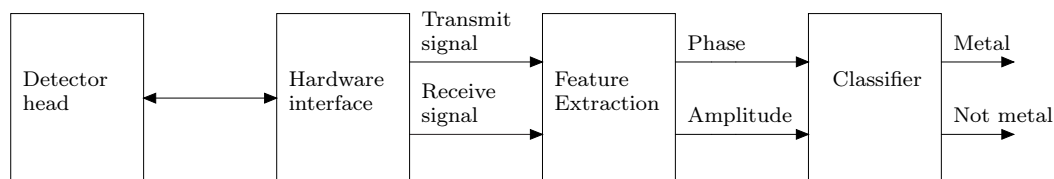

Figure 2.18: *This figure show the balancing setup for the system*

Chapter 3
Feature Extraction

3.1 Methods for Phaselag and Amplitude Detection

The purpose of this section is to list a variety of methods for phaselag detection, and gain estimation. These features are significant because they represent the transfer function value of the applied signal frequency in the transducer. This transfer function changes, when an object is moved through the metal detector. The characteristic transfer function to a given time is defined by the materials inside the detector head. A good extraction of these features which are able to suppress noise artifacts will make the following classification easier. This is due to a reduced spreading from the noise artifacts. The methods in this chapter will focus in a suppression of Gaussian noise artifacts, which can be expected to be substantial as the signals from the transducer are small and radiated noise components are amplified with the signal.
The methods will be tested qualitative to find the best method before a specific method is chosen for the final implementation. The methods described in this document are all based on the assumption that the received signal can be seen as a signal with the same frequency as the transmitted signal over a short period of time, because the modulating signal has a frequency which is significantly slower than the transmitted signal, see section 2.3.

3.1.1 Cross Correlation Method

This method is used to find the phaselag. The idea is to use the fact that the highest output of the cross correlation has its maximum at the point where to signals are closest to being identical. The cross correlation has the advantage that Gaussian noise components in the two signals are - in principle - eliminated because the Gaussian noise in the two sequences are uncorrelated.

The cross correlation method uses a cross correlation to find the lag which gives the highest degree of correlation between the reference signal Tx and the received signal Rx. The lag with the highest correlation denotes the lag in samples. It is easy to calculate the phaselag from the lag given by the cross correlation, when the signal frequency and the sample frequency is known. The disadvantage with this method is the resolution, which is determined by the oversampling rate of the signal. The resolution in the found phaselag is 360 degrees divided by the amount of samples for each period of the signal frequency. This means that it will be necessary to have a dramatic oversampling to obtain a reasonable phase resolution.

A closer examination of the Cross correlation shows that two sine's with different phase will give a sine function with a phase offset relative to lag zero as seen in equation (3.1)

$$xfc(n) = \sum^{m} A \cdot sin(\omega \cdot m + n) \cdot B \cdot sin(\omega \cdot m + n + \Theta)$$

$$xfc(n) = \sum^{m} A \cdot B \cdot cos(n + \Theta)/2 - \sum^{m} A \cdot B \cdot cos(2 \cdot \omega \cdot m + n)/2$$

$$xfc(n) \approx \sum^{m} A \cdot B \cdot cos(n + \Theta)/2 \qquad (3.1)$$

where

xfc is the cross correlation function

$\omega = 2 \cdot \pi \cdot f / fs$

θ is the phaselag between the Tx and Rx signal

The amplitude can be eliminated by a normalization using the autocorrelation function of each of the signals. The normalization factor C is defined as.

$$Rxx(\tau) = \sum^{m} A \cdot sin(\omega \cdot m) A sin(\omega \cdot m + \tau)$$

$$Rxx(\tau) = \frac{m \cdot A^2 \cdot sin(\tau)}{2}$$

$$Ryy(\tau) = \sum^{m} B \cdot sin(\omega \cdot m + \Theta) \cdot B \cdot sin(\omega \cdot m + \Theta + \tau)$$

$$Ryy(\tau) = \frac{m \cdot B^2 \cdot sin(\tau)}{2}$$

$$C = \frac{1}{\sqrt{Rxx(\tau) \cdot Ryy(\tau)}}$$

$$C = \frac{2}{A \cdot B} \tag{3.2}$$

Where

Rxx is the autocorrelation function for Tx

Ryy is the autocorrelation function for Rx

This normalization does however have a disadvantage because a high amount of Gaussian noise in the signal will push the normalization factor towards zero, because it increases the value of the autocorrelation. This problem can be solved by calculating the autocorrelations for the lag placed one period later were the periodic signal has the same contribution but the Gaussian noise are uncorrelated and has an expected contribution of zero outside lag zero. Non Gaussian noise artifacts are removed by a narrowband bandpass filter.

The normalization does also have the advantage that it gives a good estimate of the amplitude as a ratio between Rxx and Ryy.

The interval of the phase given by this method is only 0 to pi. An increase of the range to all four quadrants can be made by calculation of two points in the cross correlation function. The Phase difference between this new point in the autocorrelation function and lag zero can be found with by a small manipulation of equation(3.1). The rest of the expansion can be done by a few logic statements.

3.1.2   Addition Formula Method

The use of the addition formulas to create a method which are able to find the phaselag between two signals are an attempt to create a model based method, where the a priori knowledge of the signals are used to create the model. The later tests of this method showed that it was vulnerable to bad estimations of the ratio between A and B. The bad estimations may both occur due to

noise or non stationarity of the real signals. This ended up with a breakdown of the method with relatively small noise contributions.

The addition formulas uses that the two signals can be written as:

$$Tx(t) = Asin(2\pi ft)$$

$$Rx(t) = Bsin(2\pi ft + \theta)$$

It is possible to find the amplitude of the two signals for a short interval by estimating the highest absolute value. Dividing by this value normalizes the Tx and Rx signals. Doing this normalization followed by a differentiation gives the following

$$T(t) = sin(2\pi ft)$$

$$R(t) = sin(2\pi ft + \theta)$$

$$T'(t) = 2\pi fcos(2\pi ft)$$

$$R'(t) = 2\pi fcos(2\pi ft + \theta)$$

The differentiated signals can be normalized by the same method as the original signal. The concluding step is to apply the following addition formula

$$cos(x \pm y) = cos(x)cos(y) \mp sin(x)sin(y) \tag{3.3}$$

where
x=2πft+θ
y=2πft
This gives

$$cos(\theta) = cos(2\pi ft + \theta \pm 2\pi ft) \tag{3.4}$$

Test has shown that especially the normalizations are prone to add errors to the signals. The cosines could be found by applying an allpass filter which gives a group delay corresponding to a phase shift of 90 degrees. However a small error is still introduced by the first normalization.

The allpass filters used are on the form:

$$H(z) = \frac{z - \lambda}{1 - \lambda \cdot z} \tag{3.5}$$

The phase shift is controlled by adjusting lambda in the interval from -1 to 1. Several of these allpass blocks are used in cascade to give a phase shift of 90 degrees when the limitation of the phase shift created by the filter is a problem. This problem is demonstrated in figure 3.1.

The final method with the allpass filters can be seen in figure 3.2 where the boxes with the |X| are an amplitude estimation. The method are quite good as long as there are no noise and the amplitude estimations are fixed, however the method does not rely enough on statistics and does not take bad estimations into account which makes the phaselag estimation fail when a signal that are just close to a real signal are applied. The methods are therefore not going to be used and will not even be a part of the evaluation.
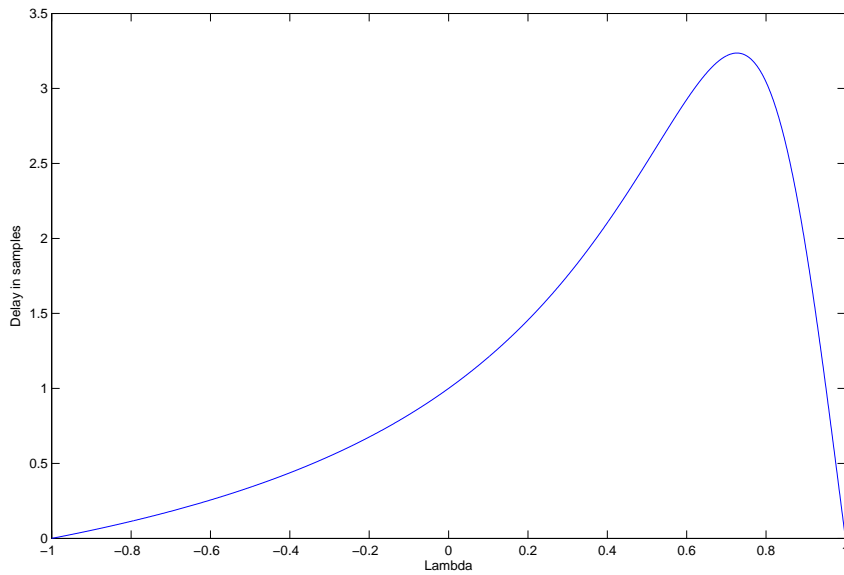
Figure 3.1: *Displays the delay of an allpass filter stage in samples as a function of the lambda value in the filter. The oversampling rate is 10 times*
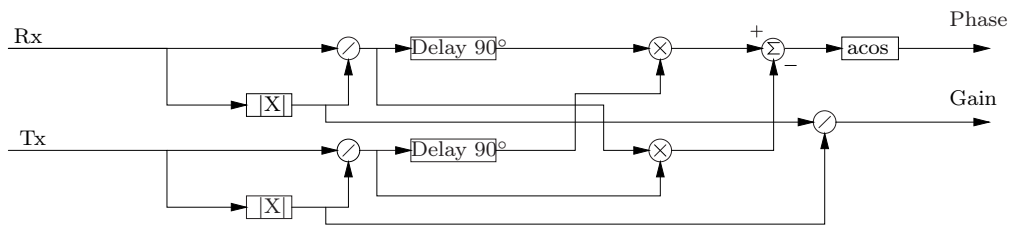

Figure 3.2: *This shows the addition formula based method for phaselag and amplitude estimation.*

3.1.3   DFT

The use of a DFT to calculate the amplitude of the two signals Tx and Rx is quite easy. It is known that everything in the two signals that are different from one specific frequency is noise. This means that it is only necessary to calculate a single frequency point in the DFT of the signals. The rejection of the noise in the other signals is given by the choice of window. The two main parameters are the type of window and the length of the window. When choosing the window it is desired that the main loop is as narrow as possible. The window that gives the narrowest main loop is the rectangular window. This window has a second feature because it saves one multiplication for each sample. The width of the main loop is inverse proportional to the length of the window, meaning that the noise rejection in the system increases as the length of the windows is increased. This means that it is desired to choose a window which are as long as possible. The limit to this is that the signal should be stationary within the window. The quasi stationarity of the system are defined by the speed of the conveyor, because it controls the frequency of the underlying signal which needs to be determined.

When the amplitude of the two signals has been found the gain is given as the ratio between Tx and Rx. This is given by the ratio between the amplitudes of Rx and Tx. The feature of the phase information in the DFT can be found be examining the equation for the DFT, which is

defined as: [Oppenheim & Schafer, 1999]

$$X[k] = \sum_{n=0}^{N-1} x[n] e^{-j\frac{2\pi}{N} k \cdot n} \tag{3.6}$$

In this case it will only be necessary to calculate one point of the DFT because the signal consists of one frequency. Writing $x[n]$ as this signal and setting k equal to the matching frequency while rewriting the complex sine to a sine and cosine sum yields the following equation.

$$X[k] = \sum_{n=0}^{N-1} A \cdot sin(2\pi k/N + \Psi)(cos(\frac{2\pi}{N}k \cdot n) - jsin(\frac{2\pi}{N}k \cdot n))$$

$$X[k] = \sum_{n=0}^{N-1} \frac{A}{2}(sin(4\pi k/N + \Psi) + sin(\Psi)j \cdot cos(4\pi k/N + \Psi) - j \cdot cos(\Psi)) \tag{3.7}$$

When the sum is long it will eliminate the sine and cosine functions dependent on n which reduces the equation to the following.

$$X[k] = \sum_{n=0} N - 1 - \frac{A}{2}(sin(Psi) + j \cdot cos(\Psi))X[k] = \frac{N \cdot A}{2}(sin(Psi) + j \cdot cos(\Psi))$$

Doing this for $Rx = A \cdot sin(2\pi k/N + \Psi)$ and $Tx = B \cdot sin(2\pi k/N + \Theta)$ yields two complex numbers with the amplitude estimates $\frac{N \cdot A}{2}$ and $\frac{N \cdot B}{2}$ and phases Ψ and Θ. A division of the amplitudes clearly ends up as a ratio between A and B, and therefore giving the gain, while a subtraction of the two phases yields the phaselag. However this phaselag does need a phase wrapping to ensure the phase lies between $\pm\pi$. This is due to the fact that the angular representation does not cover several turns on the unit circle but resets itself. The simple solution is to subtract or add 2π respectively when the absolute value is greater than π. The DFT implementation except the phase wrapping can be seen figure 3.3
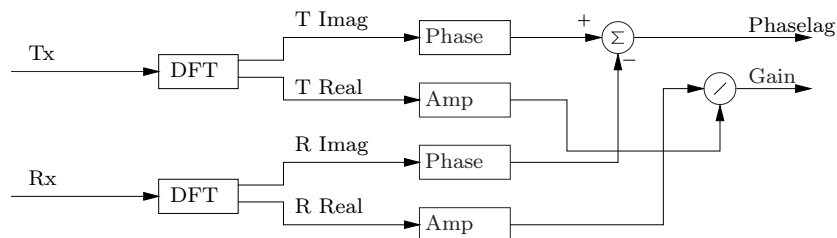

Figure 3.3: *This figure shows the main lines of the DFT implementation of the DFT method, where each of the DFT blocks represent a single point dft placed at the signal frequency*

3.1.4   Adaptive Allpass Filter Method

The idea of this is to use an adaptive filter, which moves the phase of the Tx signal so it is in phase with the Rx signal. The phaselag between the two signals are given from the parameters of the allpass filter. This means that the problem is reduced to three sub problems. The first sub problem is to find an error estimation method which can be used as a measurement for the phase error, where the phase error is seen as the phase difference between the Tx signal after it has passed the allpass filters and the Rx signal. This estimate does not need to give a phaselag, but it must go towards zero when the phaselag approaches zero.

The second problem is to use the phase error to control the allpass filters. The problem is that the allpass filters has a peak in group delay as a function of λ which is the parameter used to control the group delay for the allpass filter as seen in figure 3.1. The second problem in this controller is to make it sufficiently fast to track the quasi stationary signals, while averaging over as much data as possible to obtain the best possible phase error estimate, and thereby minimizing the noise effects.

The third problem is to find the group delay of the allpass filter. This sub problem can be solved independently in time from the other two sub problems. This gives the possibility to do this in parallel if necessary. The only disadvantage of this is that it may introduce a small delay before the detection of an object which does not matter in the final system, because the only effect is that the object will move a little further on the conveyor belt.

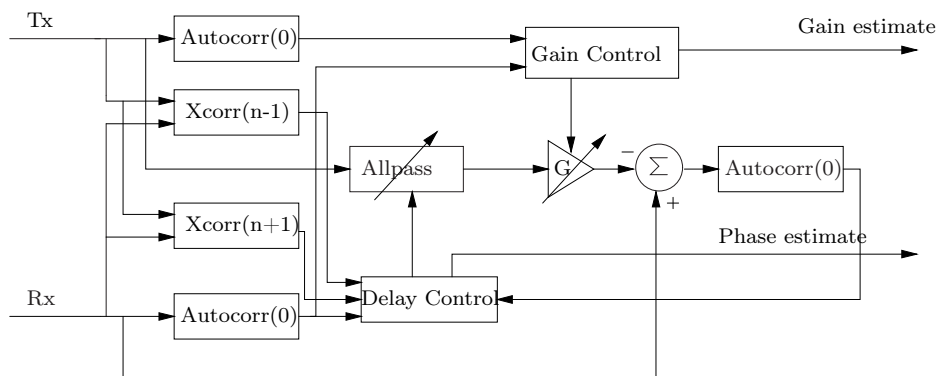The schematics for the tracking algorithm can be seen in figure 3.4

Figure 3.4: *This figure shows the schematic of adaptive allpass filter estimation method.*

The gain G is controlled to ensure that the energy of the signals T and Rx are identical. The gain is controlled by calculation of the a single point in the autocorrelation functions of Rx and Tx. The gain G are given by the point from the autocorrelation of Rx and by the point from the autocorrelation Tx. The points in the autocorrelation functions has to be off the same lag, however it will be an advantage to chose a lag that are different from zero because this means that Gaussian contributions are ignored.

The nonlinear relationship of the group delay in the allpass filter blocks versus the λ parameter of the filter are dealt with by increasing the number of allpass filters and operate them in a small section of the possible range of λ. This will linearize the function. The objective is then to chose an attack point in the function because the necessity is to be able to control the group delay to vary by a whole period, but it is not serious a problem with a constant delay of several periods. This is shown in figure 3.5. The maximum difference between the best fit and the delay

function corresponds to 3.0 degrees. This is sufficiently good to create a controller that uses this. The number of delay function elements could be reduced even further with a variable delay line which reduces the delay which has to be created by IIR filters to less than one sample. This does have the problem that the controller will be more complex and the advantage in calculations is reduced when the oversampling rate is increased. This is due to the fact that the group delay of the IIR delay element is increased with the samplerate while the delay elements in the delay line does not. This means that the IIR implementation is more adaptable, which makes it easier to construct a good controller, even though it may not be the most cost effective method in all cases. Based on this, the clean IIR implementation is chosen.
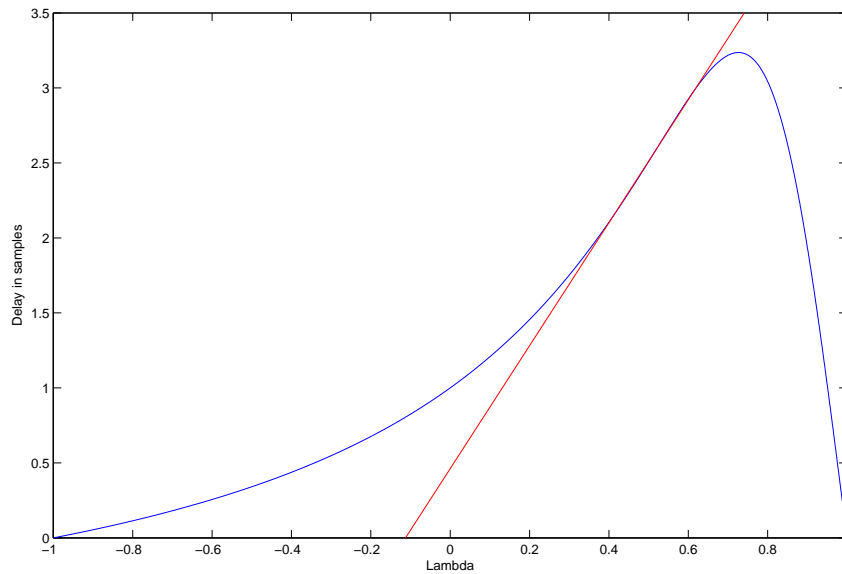

Figure 3.5: *This figure shows a section of the delay function figure. All values has been multiplied by 13 to illustrate the effect of cascading 13 allpass filters. The red line shows the best fit of a straight line to the delay of the allpass filters.*

The controller for the allpass filters are divided into two sections. The first part is to ensure a quick upstart. This upstart ensures that the error on the phase are less than 60 degrees inside the first three updates. This is done with a simple check to see if the error is less than 60 degrees and if the error is greater than 60 degrees the allpass filters will be changed 90 degrees.

The first adjustment which has to be made by the controller is to set the gain so the statement $G \cdot |Tx| = |Rx|$ As the figure shows $T = G \cdot |Tx| \angle \Psi$ where the angle Ψ is the angle created by the filter. The goal is to control the filters to ensure that the difference between Ψ and Θ is minimized. It is easy to see that $D = Rx - G \cdot Tx$, by looking at figure 3.4. Using the cosine relation from trigonometry the relation can be calculated:

$$|D|^2 = |Rx|^2 + |T|^2 - 2 \cdot |T| \cdot |Rx|\cos(\Theta - \Psi) \tag{3.8}$$

Using the comparison in equation (3.9). From this point it is easy to show that the comparison is only true if $|\Theta - \Psi| < 60°$ which can be seen in equation (3.10)

$$0 > |D|^2 - |Rx|^2 \tag{3.9}$$

$$0 > |T|^2 - 2 \cdot |T| \cdot |Rx|\cos(\Theta - \Psi)$$

Inserting $|Rx| = |T|$ gives the following

$$|T|^2 < 2 \cdot |T|^2\cos(\Theta - \Psi)$$

$$\frac{1}{2} < \cos(\Theta - \Psi) \tag{3.10}$$

When the error is less than 60 degrees a PI regulator takes over to minimize the error. It has been attempted to add a differential element, but the effect was depending on the gain of this element, either very small or destructive because it had a tendency to give oscillations at the output in steady state.

The PI regulator has a problem which is the reaction time on the step that will occur when a 180 degrees phase shift are applied. This phase shift can be handled by a check that are similar to the check made for the initiation procedure. If there are a sudden shift in phase so the error is greater than 60 degrees a phase shift of 180 degrees are automatically applied to the filters because it is likely that an object is passing through the metal detector and thus applying a 180 degrees phase shift, when passing the middle of the metal detector.

The solution of the last of the three problems is (3.11)

$$T = -\frac{d}{d\omega} \angle \left[H\left(e^{j\omega}\right) \right] \tag{3.11}$$

Where T is the group delay in samples.

Applying this formula for a first order allpass filter gives the following

$$T = -\frac{d}{d\omega} \angle \left[\frac{e^{-j\omega} - a*}{1 - ae^{-j\omega}} \right]$$

The complex number a is switched with $re^{j\Theta}$

$$T = -\frac{d}{d\omega} \left[\frac{e^{-j\omega} - re^{-j\Theta}}{1 - re^{-j\Theta}e^{-j\omega}} \right]$$

The next step uses the fact that only real values are used for coefficients and changes the representation to Euclidian coordinates. This means that $e^{\pm j\Theta} = 1$

$$T = -\frac{d}{d\omega} \left(-\omega - 2 \cdot \tan^{-}1\left(\frac{r \cdot \sin(\omega)}{1 - r \cdot \cos(\omega)} \right) \right)$$

Performing the differentiation of this equation yields:

$$T = 1 + 2 \cdot \frac{1}{1 + \left(\frac{r \cdot \sin(\omega)}{1 - r \cdot \cos}\right)^2} \frac{-r^2 \cdot \cos(\omega) - r^2 \cdot \sin(\omega) + r \cdot \cos(\omega)}{(1 - r \cdot \cos(\omega))^2}$$

$$= \frac{1 - r^2}{1 + r^2 - 2 \cdot r \cdot \cos}$$

With this last step it is now possible to calculate the phaselag between the two signals and the gain can be found in the same fashion as it was in the improved cross correlation method.

3.1.5 I/Q Expansion

The idea of this method is to make an expansion of the input signal into two signals representing the real and the imaginary part of the input signal, and at the same time removes the carrier frequency of the signal. This is done by multiplying the input signal with a sine and a cosine for each of the two expansion signals which gives two new signals, one at and one at the double frequency. Lowpass filtering these signals gives the DC components which is still able to represent the entire signal.

$$Rx(n) = A \cdot sin\left(\omega \cdot n + \theta\right)$$
$$Ir(n) = cos\left(\omega \cdot n\right) \cdot Rx(n)$$
$$Ir(n) = fracA2 \cdot \left(sin\left(\theta\right) + sin\left(2 \cdot \omega \cdot n + \theta\right)\right) \tag{3.12}$$
$$Qr(n) = sin\left(\omega \cdot n\right) \cdot Rx(n)$$
$$Qr(n) = cos\left(\omega \cdot n - \frac{pi}{2}\right) \cdot Rx(n) Qr(n) = fracA2 \cdot \left(sin\left(\theta + \frac{pi}{2}\right) + sin\left(2 \cdot \omega \cdot n + \theta - \frac{pi}{2}\right)\right) \tag{3.13}$$

Lowpass filtering of the Ir and Qr signals yields two signals that are 90 degrees out of phase and are representing the original signal

$$Ir(n) = \frac{A}{2} \cdot \left(sin\left(\theta\right)\right)$$
$$Qr(n) = \frac{A}{2} \cdot \left(sin\left(\theta + \frac{pi}{2}\right)\right)$$

The amplitude can be written as:

$$\text{AmpR}(n) = \sqrt{Ir\left(n\right)^2 + Qr\left(n\right)^2}$$
$$\text{AmpR}(n) = \sqrt{\frac{A^2}{2^2}} = \frac{A}{2}$$

and the phase can be written as:

$$\text{PhaseR}(n) = \text{atan}\left(\frac{Qr(n)}{Ir(n)}\right)$$

$$\text{PhaseR}(n) = \text{atan}\left(\frac{\frac{A}{2}\cdot\left(sin\left(\theta+\frac{\pi}{2}\right)\right)}{\frac{A}{2}\cdot(sin\left(\theta\right))}\right)$$

$$\text{PhaseR}(n) = \text{atan}\left(\frac{cos\left(\theta\right)}{sin\left(\theta\right)}\right)$$

$$\text{PhaseR}(n) = \text{atan}\left(cot\left(\theta\right)\right)$$

$$\text{PhaseR}(n) = \text{atan}\left(-tan\left(\theta-\frac{\pi}{2}\right)\right)$$

$$\text{PhaseR}(n) = -\theta + \frac{\pi}{2}$$

The I and Q signals for Tx defined as $Tx = B\cdot sin\left(\omega\cdot n+\psi\right)$ are shown in equation: 3.14

$$It(n) = \frac{B}{2}\cdot(sin\left(\psi\right)) \tag{3.14}$$

$$Qt(n) = \frac{B}{2}\cdot\left(sin\left(\psi+\frac{\pi}{2}\right)\right)$$

$$\text{AmpT}(n) = \frac{B}{2}$$

$$\text{PhaseT}(n) = -\psi + \frac{\pi}{2}$$

The Ratio between the two amplitudes shows to be the ratio that gives the gain between the Tx and Rx signal while the difference between the phases gives the phase shift between the signals. This was required for the estimation.

3.1.6   Method evaluation

The purpose of this method evaluation is to provide an analysis of the performance for the methods. The measurement of performance is both made on the quality of the feature estimates based on various parameters and on the computational complexity for each method. The results of this evaluation are going to be the basis for the choice of method for the final implementation. The addition formula method will not take part in this evaluation because tests has shown that it cannot handle any degree of noise.

The evaluation of the quality of the feature estimates is done by using a measurement of the variance from the feature, when it has reach a steady state. The variance are plotted as a function of the input parameters, but because the variance has a tendency of growing exponentially in some cases it will be plotted as $20\cdot log(var(x))$ where x is the variance from a dataset of the estimate of a feature. The variance is generally calculated using the correct value as the expected value of the feature which is being evaluated. This has the advantage that offset errors will give an increased variance and thus be a part of the evaluation.

Output Variance vs Input Noise

This subsection contains the results for the tests made for each of the feature extraction algorithms where the input noise levels are varied. The purpose of this is to see how sensitive the different methods are to an increase in input noise.

The general tendency for these tests are that each of the method has an error that are not related to the noise levels and that this error is dominant when the noise levels on the input signals are low. The variance on the output signal increases linearly with the increase in noise at the input levels when the variance from this part becomes dominant on the signals. The improved cross correlation method and the adaptive filter method has a certain point where they break down completely on the phase estimates. The only effect on the other methods are that the noise on the output are increased to a certain point where it seems like a random output.

The settings for this test are listed below

- Blocklength = 100 periods

- Oversamplingsrate = 10 samples pr period

- Phaselag = 45 degrees

- Gain = 1
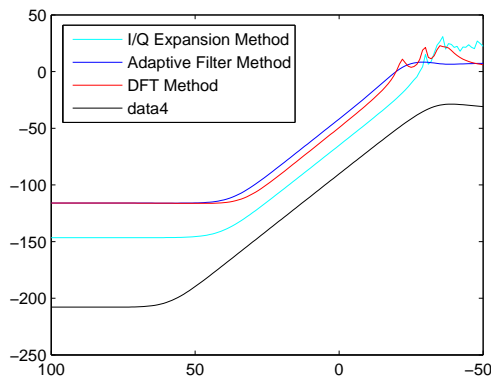
Figure 3.6: *This figure shows the quality of the gain feature as a function of the input SNR. The variance are plotted on a logarithmic scale on the y-axis, while the input snr are given in db on the x-axis*
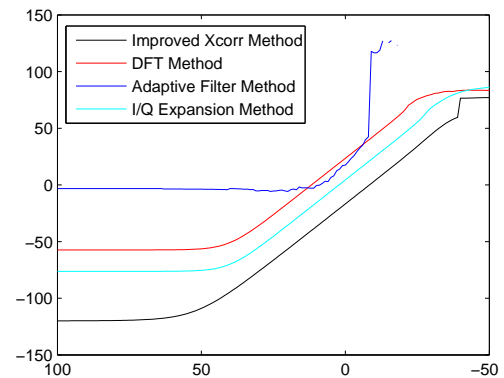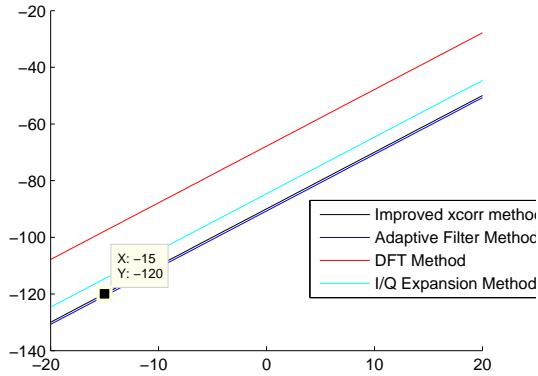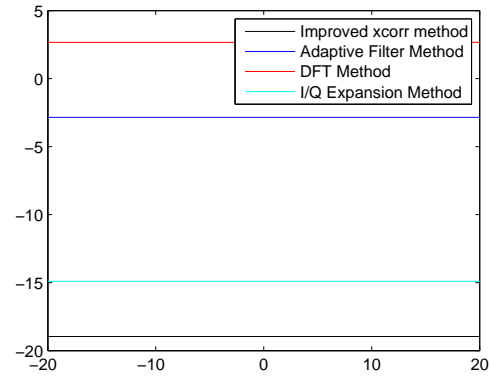
Figure 3.7: *This figure shows the quality of the phase feature as a function of the input SNR. The variance are plotted on a logarithmic scale on the y-axis, while the input snr are given in db on the x-axis*

Output Variance vs Gain

This test of the methods is made to see how the different methods are affected by a varying gain in the coil system. As The variance are not normalized compared to the total value it is expected that the variance will increase linearly with the gain. This can also be seen in figure 3.8

The settings for this test are listed below

- Blocklength = 100 periods

- Oversamplingsrate = 10 samples pr period

- Phaselag = 45 degrees

- SNR = 20 db

Figure 3.8: *This figure shows the quality of the gain feature as a function of the input gain. The variance are plotted on a logarithmic scale on the y-axis, while the input gain are given in db on the x-axis*

Figure 3.9: *This figure shows the quality of the phase feature as a function of the input gain. The variance are plotted on a logarithmic scale on the y-axis, while the input gain are given in db on the x-axis*

Output Variance vs Phaselag

This test of the methods is made to see how the different methods are affected by a varying phase in the coil system. This test differs from the other test because it will have some point where it is expected to perform badly. This is due to the fact that the methods have a point where they are doing a phase wrapping so the total phase range is 360 degrees. This means that small errors will be seen as errors close to 360 degrees and thereby result in a large contribution to the phase variance.

The settings for this test are listed below

- Blocklength = 100 periods

- Oversamplingsrate = 10 samples pr period
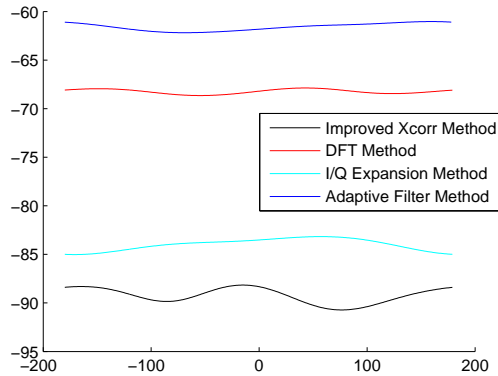
- Gain = 1

- SNR = 20 db

Figure 3.10: *This figure shows the quality of the gain feature as a function of the input phase. The variance are plotted on a logarithmic scale on the y-axis, while the input phase are given in degree on the x-axis*
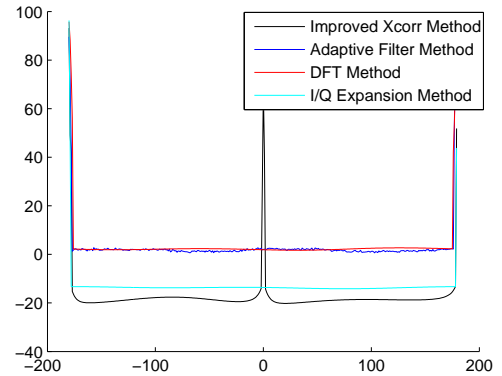

Figure 3.11: *This figure shows the quality of the phase feature as a function of the input phase. The variance are plotted on a logarithmic scale on the y-axis, while the input phase are given in degree on the x-axis*

Output Variance vs Block Length

The methods are tested with varying input SNR and block length, where the blocklength is measured as whole periods of the signal. This test is not performed for the I/Q expansion because the I/Q expansion is a method that are made sample by sample instead of block based calculation. As the figures show there is a clear gain when the block length is increased. The maximum blocklength is defined by the ratio between the carrier signal frequency of the system and the frequency of signal from a passing object, because the signals are downsampled by the block length. The figures show that both the improved cross correlation and the FFT based method gives an improvement when the block length are increased. Using a logarithmic scale for the axis with the block length shows a linear improvement on the output noise levels which are also plotted on a logarithmic scale. This means that there is a significant gain by using a window that is as large as possible, which was actually what was expected. Each of the following figures shows the output variance of the phase and the gain features as a function of the blocklength and the input SNR. The oversamplingsrate and the gain are kept constant at 10 times oversampling and unity gain in these evaluations.

The settings for this test are listed below

- Oversamplingsrate = 10 samples pr period

- Gain = 1

- Phase = 45 degrees

Improved crosscorrelation   The figures from these measurements show that it is significantly easier to find the gain than the phaselag. The tendency is that the noise suppression is significantly greater when the blocklength is increased. The tendency is that the decrease in variance is linear with the increase in blocklength as both are plotted on a logarithmic scale and

still has a linear relationship with each other. This was also expected because the noise should be suppressed by the length of the windows because it should be zero on average and redundancy of the signal is increased with an increasing number of replicas of the same signal as it is periodic. The figure also shows that there are no significant change in the amount of noise that will inflict a breakdown of the algorithm as this point is constant at a SNR of approximately -15db SNR. The algorithm has a small error which cannot be traced back to the noise on the input which could be seen as a constant value when the SNR was low in the test of output variance vs input noise. This error seems to be suppressed by an increase of the blocklength.
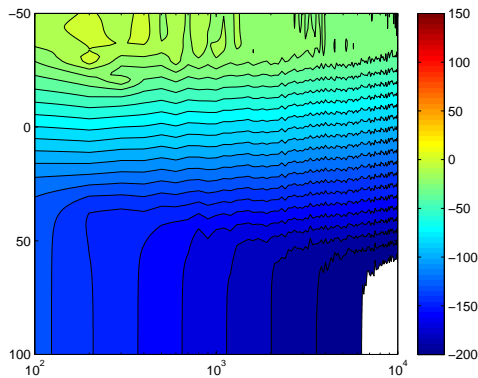
Figure 3.12: *This figure, for the improved cross correlation, shows the variance on the gain estimate, as a function of the noise on the input and the blocklength measured in whole periods shown on the x-axis. The input noise levels are shown on the y-axis on a db scale. The color levels represent the variance on the output.*
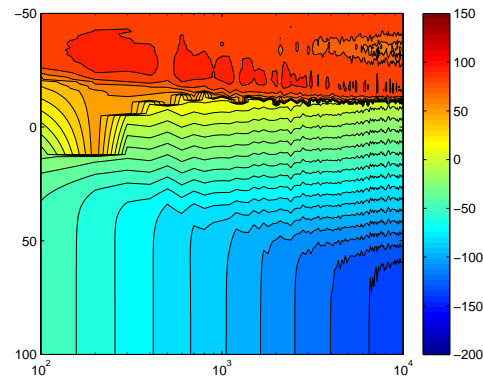

Figure 3.13: *This figure, for the improved cross correltion, shows the variance on the phase estimate, as a function of the noise on the input and the blocklength measured in whole periods shown on the x-axis. The input noise levels are shown on the y-axis on a db scale. The color levels represent the variance on the output.*

DFT   The DFT shows some similar properties as the improved cross correlation. The main differences on these two sets are that the DFT does not break down when the noise levels are high and the improvement when increasing the blocklength on the DFT are higher, which can be seen from the slopes on the contour plots.

Adaptive Allpass   The adaptive does improve with an improved blocklength as the other methods, The method does have a breakdown point beyond which it will not be able to find the phase and amplitude.

Output Variance vs Oversamplingsrate

The tests in this section are similar to the test with the block length, only this time the tests are made on varying oversamplingsrate, to uncover whether there is a gain in increasing or decreasing the samplerate for the different methods. The settings for these tests are:
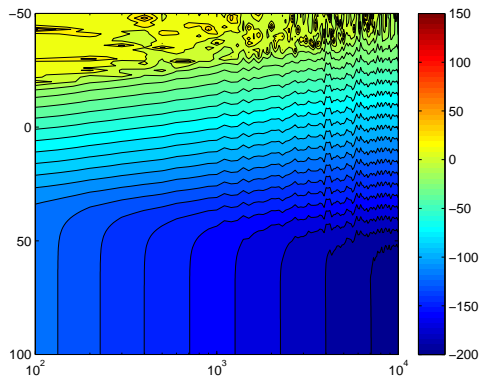
- Blocklength = 100 periods

Figure 3.14: *This figure, for the DFT, shows the variance on the gain estimate, as a function of the noise on the input and the blocklength measured in whole periods shown on the x-axis. The input noise levels are shown on the y-axis on a db scale. The color levels represent the variance on the output.*
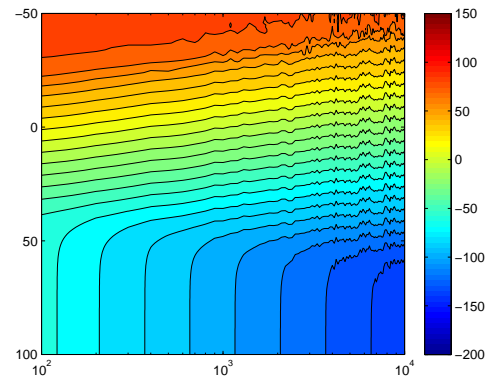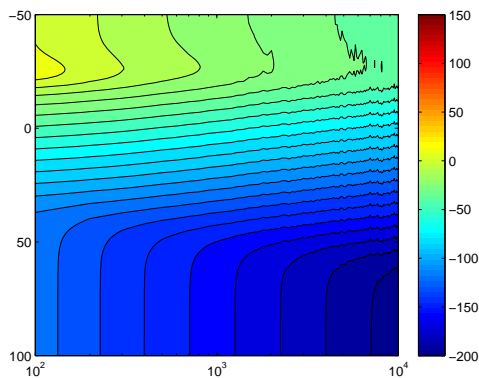

Figure 3.15: *This figure, for the DFT, shows the variance on the phase estimate, as a function of the noise on the input and the blocklength measured in whole periods shown on the x-axis. The input noise levels are shown on the y-axis on a db scale. The color levels represent the variance on the output.*

Figure 3.16: *This figure, for the adaptive allpass, shows the variance on the gain estimate, as a function of the noise on the input and the blocklength measured in whole periods shown on the x-axis. The input noise levels are shown on the y-axis on a db scale. The color levels represent the variance on the output.*
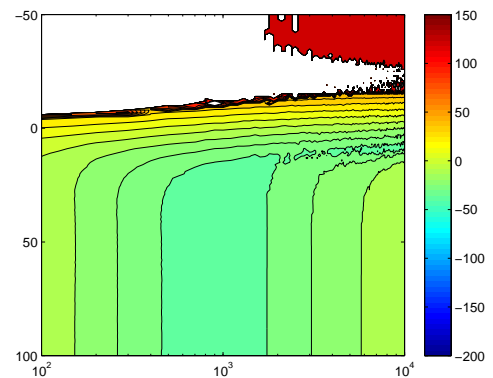

Figure 3.17: *This figure, for the adaptive allpass, shows the variance on the phase estimate, as a function of the noise on the input and the blocklength measured in whole periods shown on the x-axis. The input noise levels are shown on the y-axis on a dB scale. The color levels represent the variance on the output.*

- Oversamplingsrate = 10 samples pr. period

- Gain = 1

- SNR = 20 dB

Improved crosscorrelation   The improved cross correlation does not seem to be improved by an increase in oversamplingsrate. On the contrary it seems that the minimum fault is greater

when the oversamplingsrate is increased, which suggests that a high samplerate is undesirable. This can be seen in figure 3.18 and figure 3.19
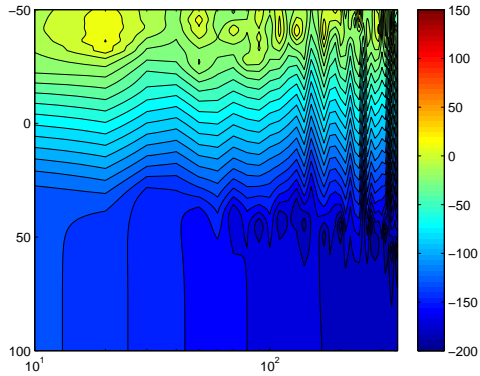

Figure 3.18: *This figure shows the variance on the gain estimate, as a function of the noise on the input and the oversamplingsrate on the input signal on the x-axis for the improved cross correlation method. The input noise levels are shown on the y-axis on a dB scale. The color levels represent the variance on the output.*
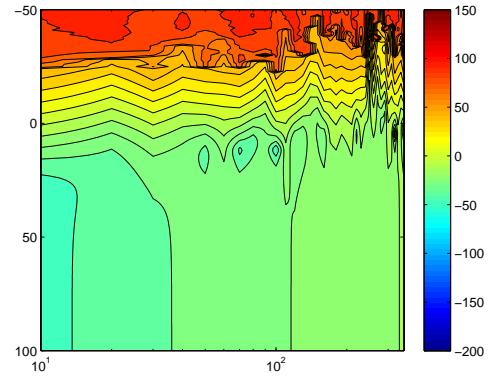

Figure 3.19: *This figure shows the variance on the phase estimate, as a function of the noise on the oversamplingsrate on the input signal on the x-axis for the improved cross correlation method. The input noise levels are shown on the y-axis on a dB scale. The color levels represent the variance on the output.*

DFT The DFT has the same characteristic in relation to the sample rate. The minimum fault seems to increase with the sample rate and an increase has no advantages in any way. This can be seen in figure 3.20 and figure 3.21
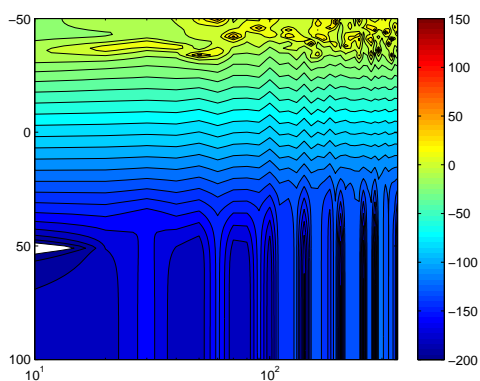

Figure 3.20: *This figure shows the variance on the gain estimate, as a function of the noise on the input and the oversamplingsrate on the input signal on the x-axis for the DFT method. The input noise levels are shown on the y-axis on a dB scale. The color levels represent the variance on the output.*

Figure 3.21: *This figure shows the variance on the phase estimate, as a function of the noise on the oversamplingsrate on the input signal on the x-axis for the DFT method. The input noise levels are shown on the y-axis on a dB scale. The color levels represent the variance on the output.*
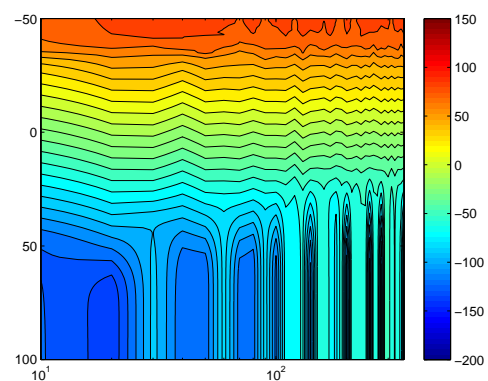
Adaptive Allpass   The following tests shows that the adaptive allpass filter are very sensitive when it comes to samplerate, see figure 3.22 and 3.23. This may be due to the fact that there are several design parameters that has to be designed for a specific degree of oversampling. An example of this is the linearization of the delay function in the allpass filters.
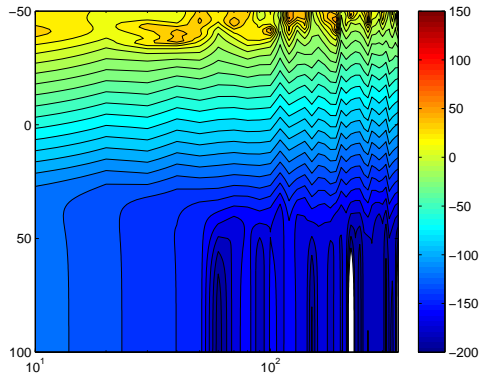

Figure 3.22: *This figure shows the variance on the gain estimate, as a function of the noise on the input and the oversamplingsrate on the input signal on the x-axis for the adaptive filter method. The input noise levels are shown on the y-axis on a dB scale. The color levels represent the variance on the output.*

Figure 3.23: *This figure shows the variance on the phase estimate, as a function of the noise on the oversamplingsrate on the input signal on the x-axis for the adaptive filter method. The input noise levels are shown on the y-axis on a dB scale. The color levels represent the variance on the output.*
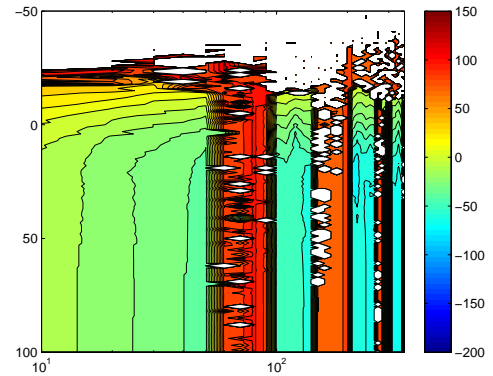
I/Q Expansion   The tests of the I/Q expansion shows that the minimum variance increases with the oversamplerate, while the contributions from input noise are unchanged. This can be seen in figure 3.24 and 3.25

Computational complexity

The computational complexity off the different algorithms will be evaluated in this section. Generally it is not a problem if the computational complexity of an algorithm is high because the sales price of the metal detector is insignificant relatively to the quality of the overall system.

Improved cross correlation method   This method is divided into three sequential blocks. Each of the blocks will be evaluated separately. These three blocks are the peak filters, the correlations and the calculation of features based on the correlations.

- The peak filters has a constant number of calculations for each sample and a therefore represented by a constant. This is however for a fixed samplerate. If the samplerate increases so does the amount of computations in this block linearly with the sample rate. What makes matters even worse is that an increase in oversampling will give a higher demand for the word length of internal variables and coefficients in the filter.
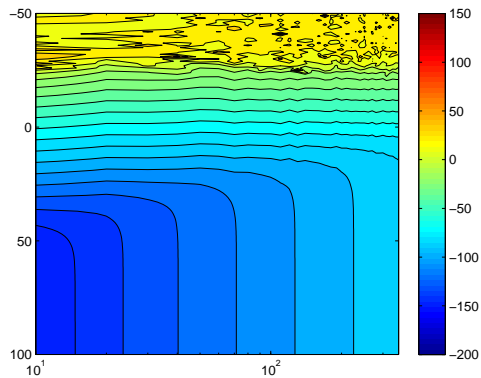
Figure 3.24: *This figure shows the variance on the gain estimate, as a function of the noise on the input and the oversamplingsrate on the input signal on the x-axis for the I/Q expansion method. The input noise levels are shown on the y-axis on a dB scale. The color levels represent the variance on the output.*

Figure 3.25: *This figure shows the variance on the phase estimate, as a function of the noise on the oversamplingsrate on the input signal on the x-axis for the I/Q expansion method. The input noise levels are shown on the y-axis on a dB scale. The color levels represent the variance on the output.*
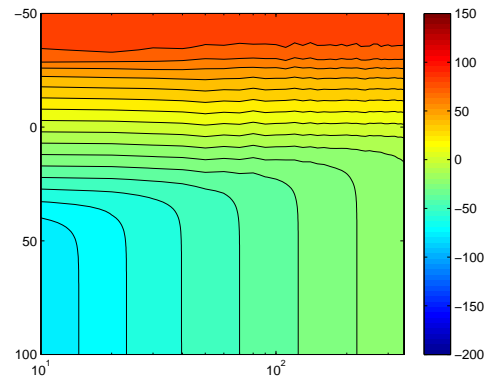
- The correlation blocks covers both the autocorrelations and the cross correlations. Both of these correlations has a memory dependency that are relative to the degree of oversampling, because this defines how many samples it needs to save in order to create the delay, if the delays are not made using IIR All-pass filters. This does not change the number of computations for this method are constant for each of the correlations for each sample. Looking on the system as a whole the amount of computations will also increase linearly with an increase in samplerate.

- Calculation of features based on the correlations are constant. The amount of calculations in this part is not dependent on the same sample frequency as the first two blocks. This is due to the indirect downsampling that are made from the calculation of the correlation functions which are done in windows. The new sample frequency is based on the bandwidth of the feature signal, which again is controlled by the speed of the conveyor belt. As these calculations are based on a much lower constant they are seen as insignificant.

To summarize this, there is only one significant source which can increase the cost of this method which is the samplerate of the system. And the cost of the calculations increases linearly with the samplerate.

DFT The calculation of the computational complexity of a single point DFT is quite simple because the calculations can be based on two multiply accumulate functions, one for the real part of the twiddle factors and one for the imaginary parts. This is of course doubled because it is necessary to calculate one DFT for each channel. Because the calculations are done in windows it will only increase linearly in computational complexity when the samplerate are increased and otherwise be constant. The method does however need some memory for the twiddle factors, were the amount will increase linearly with the length of the windows used for the DFT.

To summarize this, the costs for the DFT are similar in computational complexity to that of the improved crosscorrelation method however it has a greater need for memory due to the twiddle factors which needs to be saved.

Adaptive Allpass Filter Method   This method has some similarities to the improved crosscorrelation method as it uses autocorrelations and crosscorrelations to control the allpass filters. The Allpass filters are IIR filters, which has the same computational complexity as the peaking filters. The rest of the method is the control of the allpass filters and the calculation of the phaselag in this filter, which are at the low sample frequency controlled by the speed of the conveyor belt and is therefore insignificant.

To summarize this, the adaptive allpass filter method has two major blocks that have a linear increase in computational complexity with an increase in samplerate.

I/Q Expansion method   This method has a similar need of saving some coefficients for the signals used in the conversion or. The expansion itself is two multiplications for each sample meaning that the complexity increase linearly with the samplerate. The final signal needs to be lowpass filtered before it is down converted. Doing this with an IIR filter may require a high wordlength in the filter due the fact that the sample rate is still very high compared to the cut-off frequency for the filter. An FIR filter will on the other hand require many tabs because of the low frequency. A multirate filter implementation may help on the implementation of this filter, but will be challenging to implement. Even though this last filter will be challenging for a good implementation it will not have a computational complexity that reaches a linear increase with the sample rate because it can be implemented in several steps where each step is combined with a downsampling.

3.2   Conclusion on Feature Extraction

A variety of different methods for phase and gain estimation has been examined in this section. These methods cover both frequency and time based methods, where some of the methods are known and others has been constructed for the purpose. The different methods that were examined had no significant difference in computation complexity as they all ended up with an O-notation as a constant. The methods have been thoroughly tested on a variety off parameters. These tests did not reveal any unsuspected tendencies, as the variance did increase in the cases where it was expected (Increased noise and increased gain). The methods did in general have one or two phase wrapping points where there was a great increase in variance on the phase parameter, which was expected. The methods did not improve by an increase in sample frequency, which was as expected as no new information was given by this, but they did improve by an increase of the number of whole periods used in the estimation. Looking at the scheme from a windowing perspective the DFT does also reveal that this does decrease the width of the main loop and therefore it is not a surprise that it does give an improvement in this method. However the extra redundancy from the extra methods did also improve the adaptive filter method and the improved cross correlation method. The adaptive filter method that was developed is clearly not the best method, but the work done on this method has given inspiration to the solution of the balancing problem. This is discussed in section 4.1. The method itself may give an adaptive solution to

the balance problem if it is implemented with a DAC and a partial analog implementation. This means that it can be possible to use this method to both eliminate the balance problem and obtain the feature signals, if it is not a problem that the feature noise suppression on the feature signals are a little lower than it is in some of the other methods.

The improved cross correlation methods are clearly the best in the tests, with the minor exception that it does have some difficulties in phase estimation around zero degrees. The choice to continue with the improved cross correlation, for the final system is therefore chosen based on this.

Chapter 4
Signal analysis

In this chapter measurements from the real system is being analysed with the feature extraction algorithm, Improved cross correlation, which was chosen in chapter 3. The purpose of this chapter is to outline the feature for the classifier and state the problems. First the overall system for the feature extraction is set, and then a comparison will be made for the system working at 30 kHz and 300 kHz, which are the frequencies used at Detectronic. After choosing the frequency, characteristic of the metal and food are stated and the variance of the feature is examined.

A real detector head is supplied by Detectronic and it consists of seven windings for the transmit coil and seven winding for each of the receiver head. The detector head is used for 30 kHz. The conveyor belt for the detector head is also supplied. To supply sufficient current to the transmit coil an class AB power amplifier is made, see section A.1, since the signal generator available at AAU could not supply the sufficient current. To minimize the impedance of the transmit coil, a capacitor is set in series with the transmit coil to make a resonance frequency, this was described in section 2.1. A resistor is set in series with the capacitor to measure the current in the coil. The signal is passed though an instrumentation amplifier to amplify the signal. The differential voltage for the two receiver coils is low and therefore two instrumentation amplifier was setup to amplify the signal sufficient A.2. A capacitor was set in parallel with the coil to filter possible noise. The analog signal is converted to digital and the two signals are process on a computer to give the phase and amplitude feature. One of the problem setting up the system, was that the system was not balanced, which means the magnetic field from the transmit coil is not equal for the adjacent receiver coil and therefore signals are present at the output of the receiver when no object are in the detector head. This degrades the amount of amplification for the received signal. To minimize the "noise" signal due to the imbalance signal several thing has been made.

4.1 Balancing

In this section the balancing of the system is described. Two methods have been used to balance the system. In the beginning of the project the balancing was performed by placing different metal object in the metal detector until the received signal was minimal. This method is also used on the detector head from Detectronic where they weld metal piece in the detector head, and that it is not able to readjust if someone places a large metal object close to the detector. The problem with this method is that it takes time to adjust the detector head. In this project the metal piece was only fixed with tape and so the metal piece could move over time, due to vibration in the system. It is also difficult to place the metal object, since the hand yields a response on the receiver coil, this is particularly a problem when the frequency are increased, since the response of the hand increase, due to the conducting properties, see section 2.4.

To improve the balancing process a circuit consisting of three variable Allpass filter followed by a voltage divider is made [linkwitzlab Aktive Filters , 2008]. The circuit can adjust the phase and amplitude of a signal, the reason for three allpass filter is because each filter has a maximum phase shift 180° and it is undesired to reach the limitation, so to make 360°, three blocks are needed. The signal from the transmit coil is applied to the circuit and then the output is applied

to the second instrumentation amplifier for the received signal, see figure 4.1. The purpose is to match the signal from the receiver coils when no object is present in the detector head. When the two signals match the output of the instrumentation amplifier should be zero, and thereby the unbalance component is zero. It is not possible to match the signal completely and therefore signal will be present on the output of the second instrumentation amplifier, but it is reduced significant. A comparison has been made which shown that the electronic balancing do match the balancing of the metal. It is difficult to state which minimize the signal most, since both can be tuned. The allpass filter method is faster and no metal object is placed in the detector head to interface with the magnetic field.
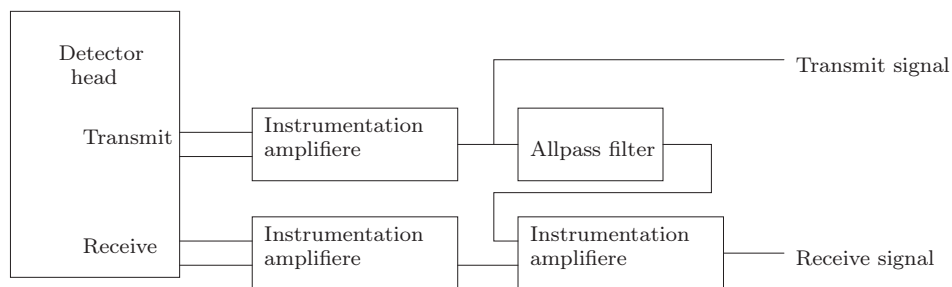

Figure 4.1: *This figure show the balancing setup for the system*

In figure 4.2 and 4.3 the gain and phase for AISI 3 mm passing though the detector head is shown. It can be seen that the gain and phase do not comply with figure 2.10, which is the theoretical expected. The reason for this is that the signal is not balanced completely. An offset is present which cause the signal never to be zero and the phase never flip 180°.
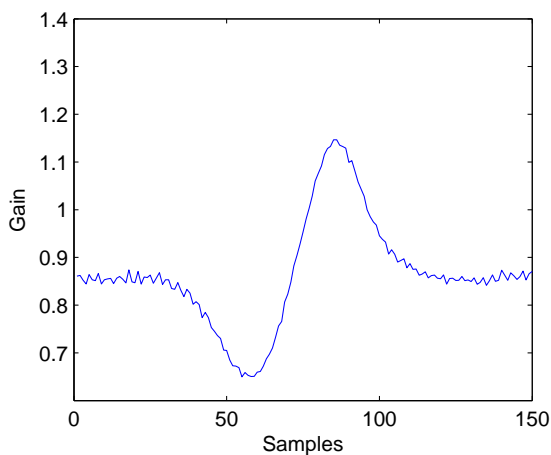

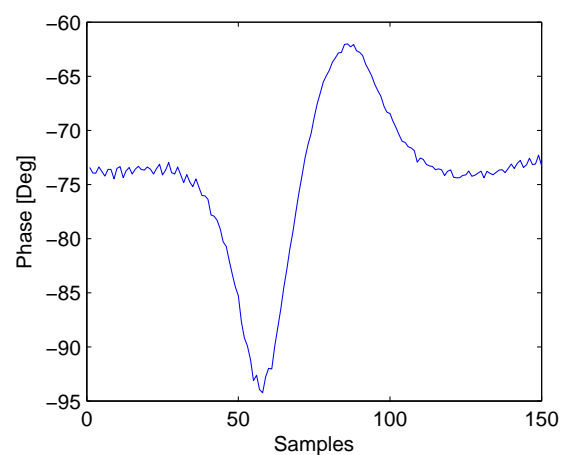**Figure 4.2:** *The gain sequence for AISI 3 mm passing through the detector head.*

Figure 4.3: *The phase sequence for AISI 3mm passing through the detector head.*

To remove the last of the unbalance, the feature is converted to a complex representation. Phase and amplitude can be converted into a complex number consisting of a real and imaginary number. The gain is $\sqrt{x^2 + y^2}$ and the phase is $arctan(y/x)$ where x and y are the real and imaginary number respectively. In figure 4.3 the two sequence for the real and imaginary part is shown when the AISI 3 mm passes though the detector. It can be seen that an offset is present, and it is this offset which should be removed. In figure 4.5 the complex representation
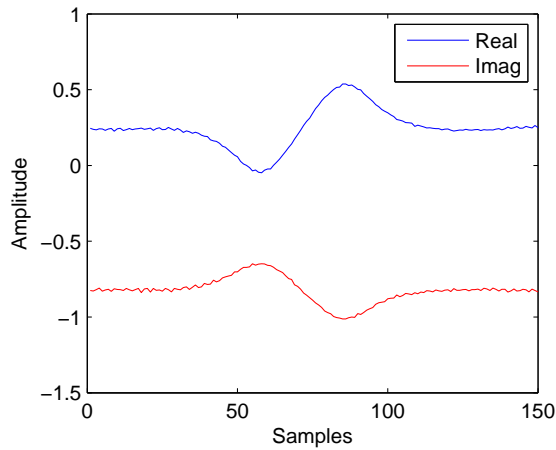
Figure 4.4: *The real and imaginary sequence of the complex representation for AISI 3 mm passing through the detector head.*
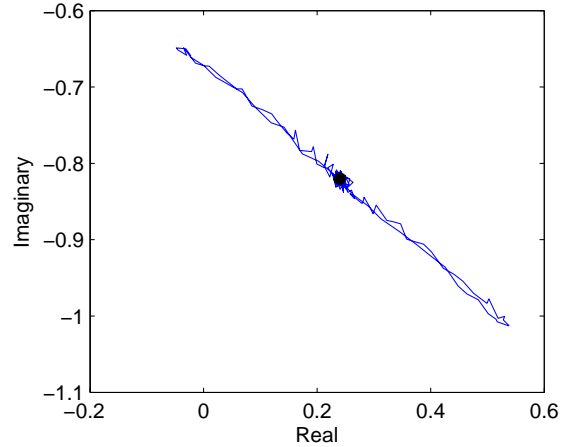
Figure 4.5: *The complex representation for AISI 3 mm passing through the detector head.*

is shown. The black dot should be zero when the system is balanced. The coordinate of the circle correspond to the offset in figure 4.3 for the two sequence. The offset can be removed by estimating the offset for the real and imaginary part, when no object is present in the detector head and then subtract it. A highpass filter could also be applied to the real and imaginary part. In figure 4.6 the complex representation is shown with and without filtering. It can be seen that the offset is removed.
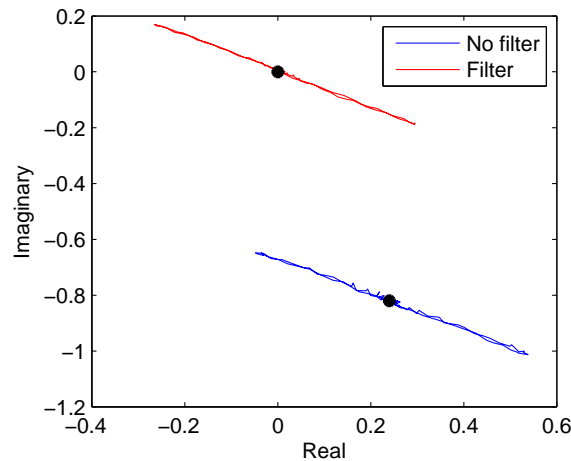

Figure 4.6: *Complex representation of AISI 3mm with and without filtering the real and imaginary part*

In figure 4.7 and 4.8 the gain and phase is shown after the filtering, the figures now approximately correspond to the figure in section 2.3. The gain plot get two peak as expected, they are not exactly equal because the system is still not 100% in balance. The phase sequence show a phase shift of 180° when the object pass the middle of the detector head and is fixed when it pass through one of the receive coil. The phase when no object is present is undefined, because of the noise. The complex signal varies around origin, and the signal moves between the four quadrants which yield large phase shift.
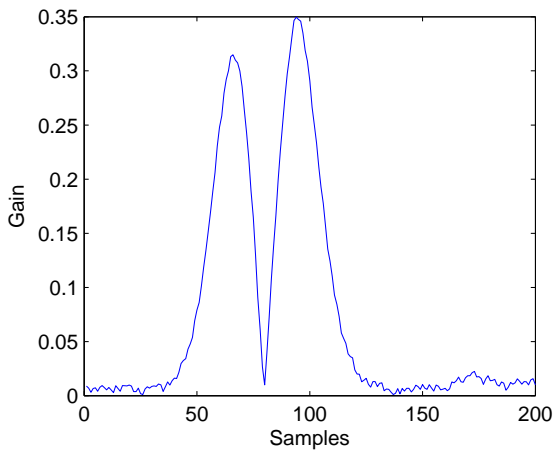
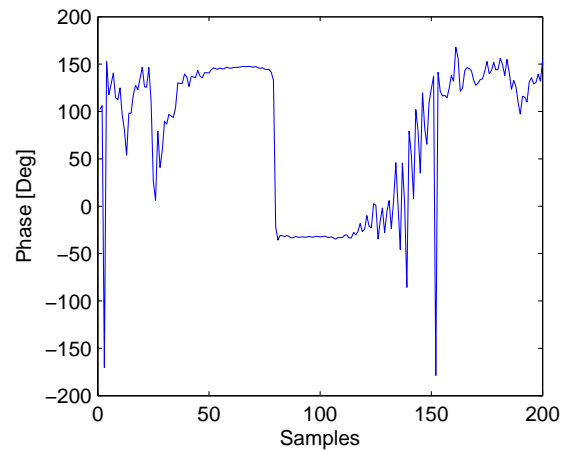**Figure 4.7:** *The gain sequence for AISI 3 mm passing through the detector head.*

Figure 4.8: *The phase sequence for AISI 3mm passing through the detector head*

4.2   Feature analysis

With the balancing problem minimized, the features will be examined further. In section 2.4 it was described that the sensitivity of metal vary depending on type of metal and what frequency that was used. It was described that magnetic object reduced the sensitivity when the frequency increased and the opposite is true for conductivity. This means that if food has permeability above 1, high frequency is desired to reduce the amplitude. The opposite is true for conductive food. At Detectronic two frequencies are used 30 kHz and 300 kHz. Measurements is made on the system with frequency 30 kHz and 300 kHz to determine the best frequency, the measurements are described in B.2. The measurement showed that the performance of the analog hardware, which means the signal amplifier for the transmit coil and the instrumentation amplifier for the transmit and receive coil decreased for 300 kHz. It was not possible to get the same amount of current through the transmit coil and the gain for the instrumentation amplifier was decreased. Another problem was the balancing, since metal object was used at that time and it was difficult to place the metal objects in the detector head, since the hand interfered much more. The problem with the balancing is solved with the electronic balancing, but the amplifiers need to be improved for higher frequencies. Since the main focus of this project is on signal processing and implementation, it is chosen not to make new hardware for the high frequency. It is therefore chosen to use 30 kHz for this project. It was noted that the sensitivity did increase for conducting material, which also was predicted in 2.4.

In figure 4.9 the complex representation of six different metal objects is shown. The figure shows that the phase and amplitude is depending on type and size, which was stated in section 2.4. Comparing aluminum 2 mm with aluminum 3 mm it can be seen that the amplitude increase with the size and the phase change. The same apply for iron 1 mm and iron 2 mm. It is also shown that aluminum and bronze are in the same quadrants, this is because both of the metal are conductive and non magnetic. Iron and AISI are in the two other quadrants. Iron has magnetic properties and some AISI do also have magnetic properties depending on the structure of the metal, but the permeability is low compared to iron. The gain of the AISI is low compared to the other material, this is because the conductivity and permeability is low. AISI 2 mm and

bronze 2 mm was also tested, but they were difficult to see. Experience from Detectronic also
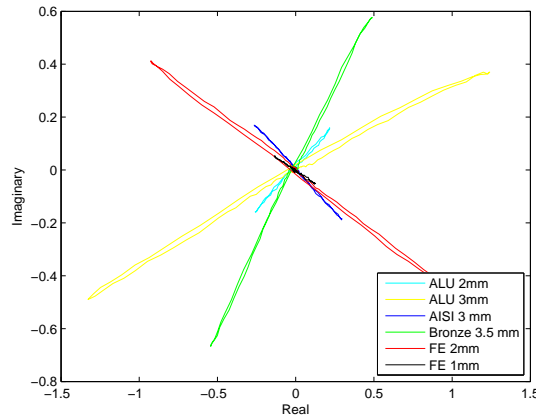state that AISI is difficult to detect.

Figure 4.9: *Complex representation of feature for six different metal objects*

The features for food has been measured for various food products raisin, breed, candy, chips and
microwave unpop-popcorn. The product with the highest gain was popcorn and it is therefore
chosen to use popcorn as the food product for which metal should be separated from. The gain
and phase for popcorn is shown in figure 4.10 and 4.11 respectively. It is shown that there
are four peaks, where only two were expected. The reason for this can be that the products
consists of different materials with different properties, but nothing has been validated. The
phenomenon was detected for all the food products which were tested, but none of the metal
object had four peaks. It can be seen that for each valley a phase shift of approximately $180°$
occur which is because the polarization of the signal change at the receiver. A phase shift of $360°$
occur at sample 50, this is because the method only map the phase between $±180°$. In figure
4.12 the sequence of the real and imaginary part of the complex representation is shown and
the complex representation is shown in figure 4.13. It can be seen that the real and imaginary
part are more stable features, than using the phase, which vary when no object is present. The
complex representations do not correlate as close to a straight line as the metal do.
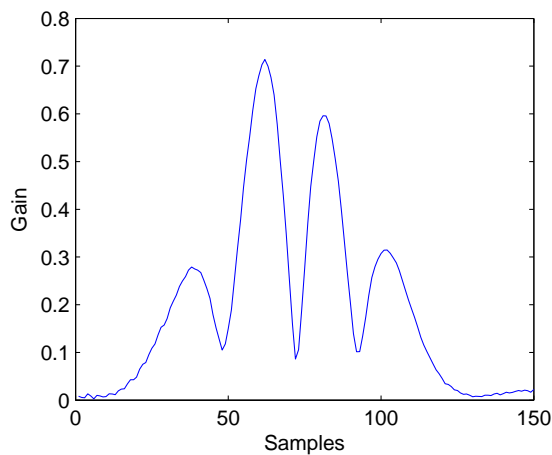

Figure 4.10: *The gain sequence for popcorn passing through the detector head.*
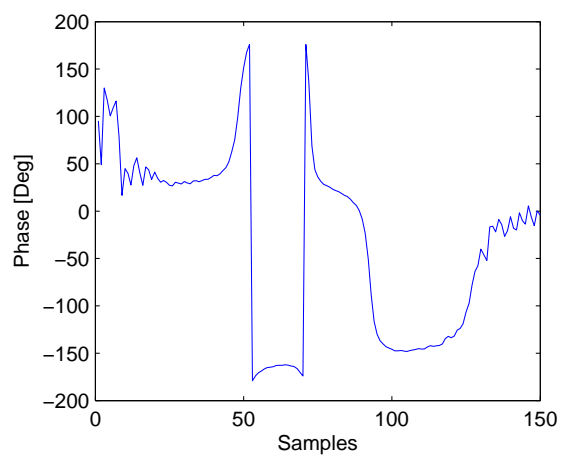

Figure 4.11: *The phase sequence for popcorn passing through the detector head.*
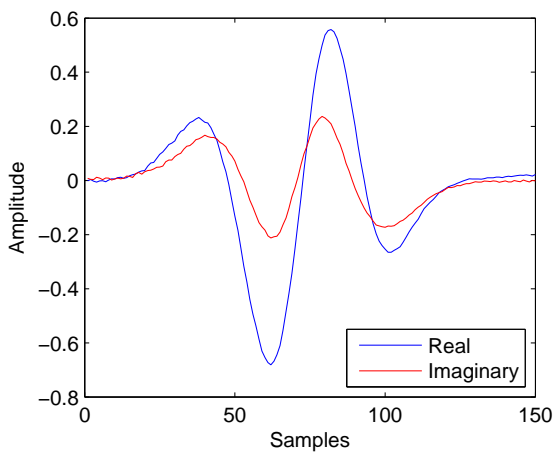
Figure 4.12: *The real and imaginary sequence of the complex representation for popcorn passing through the detector head.*
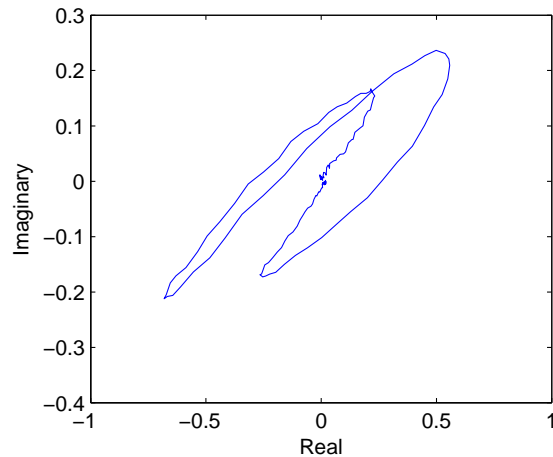
Figure 4.13: *The complex representation for popcorn passing through the detector head.*

Measurements have also been tested to check the variance for a given metal object passing through the detector head at different position on the conveyor belt. Six measurements for left, right and centre are performed for aluminum 2mm and the complex representations of the feature are plotted in 4.14. From the plot it can be seen that the gain is highest when the object is placed at the left or right position on the conveyor belt. This is due to the magnetic field being stronger at the outer of the opening in the detector head. The slope of the sequence is approximately the same, which means the phase is the same.
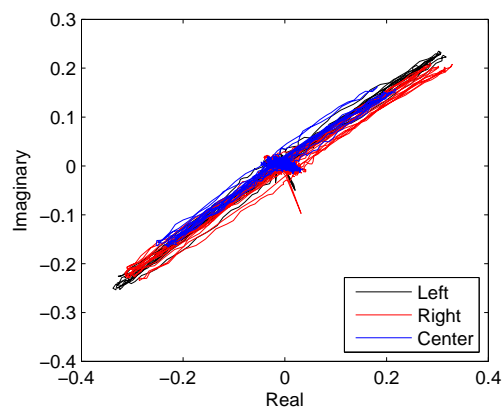
Figure 4.14: *Complex representation of the feature of aluminum 2 mm placed at left, right and centre at the conveyor belt. Six measurements are plotted for each position.*

If two objects are present in the detector head at the same time, the resulting contribution can be seen as a summation of the two individual contributions. In figure 4.15 and 4.16 the real and imaginary part of the complex representation is shown for AISI 3 mm, aluminum 2 mm and for the two object mixed together. It can be seen that the summation of the two individual objects will approximately give the same as the measured mix between the objects. In figure 4.17 the complex representation of the feature is shown where it can be seen that taking the vector for each of the individual product and add them together gives approximately the vector for the

mix.
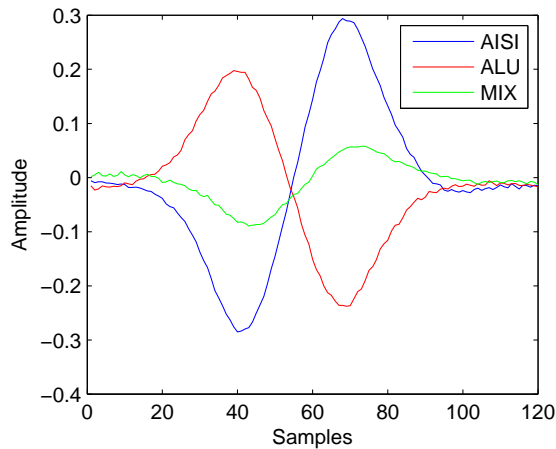
Figure 4.15: *The real sequence of the complex representation for AISI 3mm and aluminum 2 mm and the two mixed together*
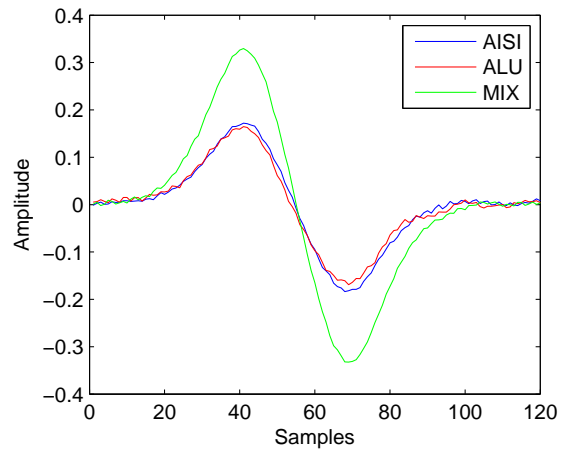
Figure 4.16: *The real sequence of the complex representation for AISI 3mm and aluminum 2 mm and the two mixed together*
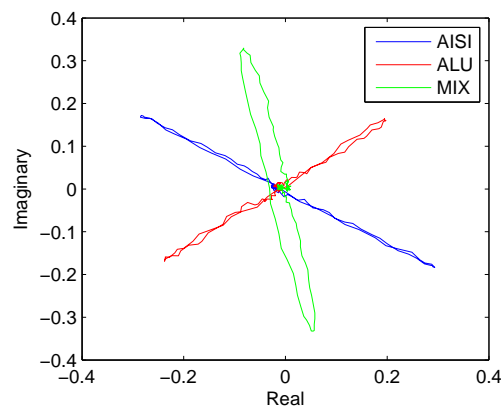
Figure 4.17: *Complex representation of the feature for AISI 3mm, ALU 2 mm and the mix between them.*

To check the noise a frequency response is made on the real and imaginary part see figure 4.18 and 4.19. The frequency response is made where the offset of the real and imaginary part is subtracted, no filtering is made. The frequency contend of the object is below 10 Hz. A peak is present at approximately 32 Hz and it is present for all the measurement performed, also measurement made without the conveyor belt moving. No noise source has been found for the peak.

4.3 Conclusion on signal analysis

It was stated in this chapter that effect should be made to remove the unbalance component. This can be made mechanically by inserting different type of metal object. The disadvantage of this method is that it is time consuming and when the frequency increases so does the response of the hand which makes it difficult to place the object right. Another solution is to estimate
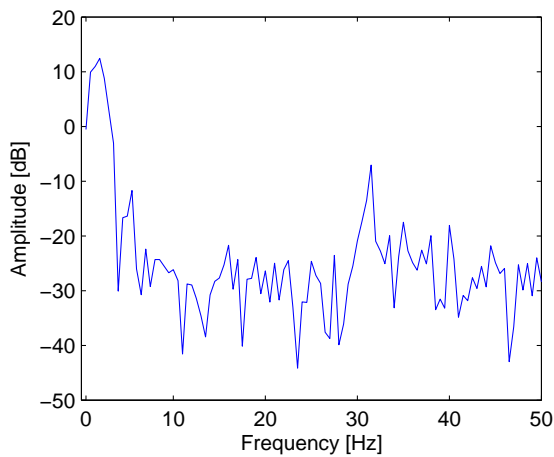
Figure 4.18: *The frequency response for the real part when an object passes through the detector head.*
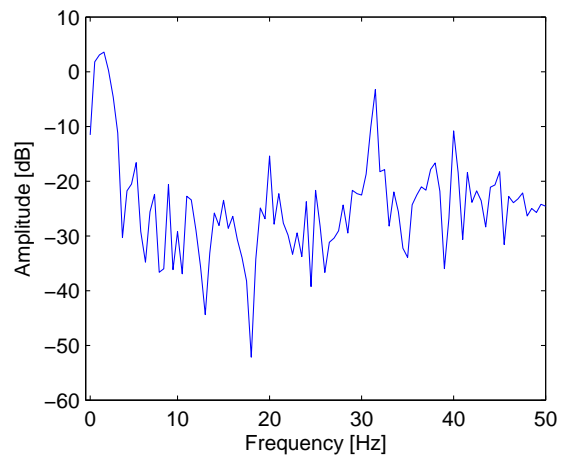
Figure 4.19: *Frequency response for the imaginary part when an object passes through the detector head*

the unbalance signal and the subtract it. This has been made with variable allpass filters and a voltage divider to adjust the amplitude. The signal from the allpass filter and the receiver signal are then mixed together in an instrumentation amplifier. It is not possible to remove the balance component completely, therefore a digital balancing system is made which filter the real and imaginary part, to remove the offset caused by the unbalance.

Measurement has been made on both 30 kHz and 300 kHz to find the frequency which makes the best separation between food and metal. It was shown that the analog hardware which was made decreased the performance when the frequency increases to 300 kHz. For that reason 30 kHz was chosen since the analog hardware is not the main focus of this project. It was noted that conducting products did increase in sensitivity when the frequency increased.

Measurement performed on the different metal shown that the phase and amplitude change, which were expected. It was also shown that the amplitude increased when an object were placed away from the centre of the conveyor belt. The features for food showed that they have four peaks where only two were expected. Reasons for that could be the product consisting of more than one material.

Chapter 5
Classifier

The classification of the objects passing through the detector head, based on the features which are extracted, are the last step towards a final system. The signal to noise ratio and the degree of correlation between the features of the different objects in the previous section are a limiting factor for the quality of a classifier. In some cases a classifier will have to distinguish between some known cases, however this does not apply to this case because all different metal types of different size may enter the metal detector, which in other terms reduces the classification to a distinction between the product and everything else. Another problem in the classification is that it is unknown if there is anything inside the detector head meaning that it must be able to distinguish noise artifacts from a signal generated by an object inside the detector head. This gives the following cases which the classifier has to be able to handle.

- Nothing in the detector head all features are noise.

- Product in the detector head. Features are a sum of noise and product

- More than one product in the detector head. In some cases this may be an unwanted situation, because it may result in more than one product in a package while it may be something that the system should ignore in other situations because the customer does not want to separate the items at this time in the process.

- A foreign object in the detector head.

- Product and a foreign object in the detector head at the same time.

The following sections will list a set of schemes for the handling of these different situations in the classifier. The optimal solution are of course to be able to handle all types of problems, however if it will give an improvement to the system it may be an advantage to use more than one of the following classification schemes in the final classifier. Even heavy calculations are not a problem because the feature extraction has the ability to downsample the frequency to a few hundred Hz.

5.1 Orthogonal classifier

The principle of this is to detect the parts of the signal that are orthogonal to the direction in which the product vector points. This means that it - in principle - should be possible to use this as a filter which removes the product. The obvious disadvantages of this is that the product cannot be removed completely because of the variations in this signal and that the metal object will be damped as well if the feature vector of the metal object are not orthogonal to the feature vector from the product.

The learning process of this algorithm is primarily to find the mean direction of the product. The general solution is then to use a simple projection of the input data vectors to this line. The simple classification based on this is a level detector for the absolute value of the projection.
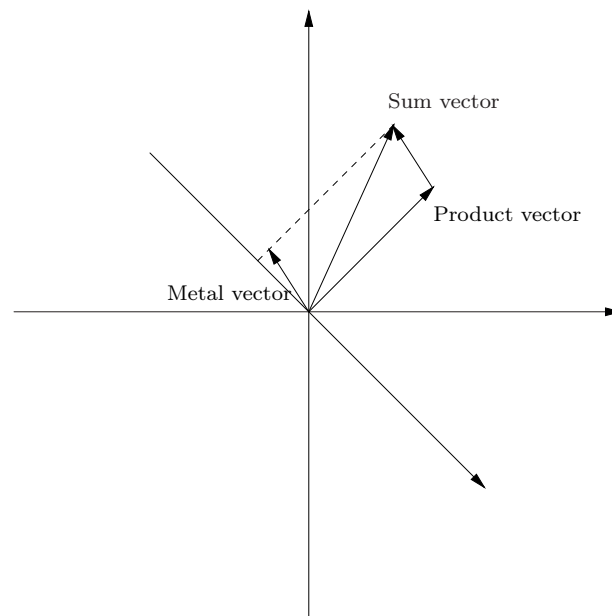
Figure 5.1: *This figure shows the principle of the orthogonal classifier where it can be seen that the classifier maps the sum of the two vectors to the same position on the line orthogonal line as it does with the metal vector. The product vector maps to zero on the orthogonal line*

Various methods can be used to increase the signal to noise ratio on this output. A simple way is to use a crosscorrelation with the amplitude function of a product to reduce the effect of Gaussian noise. This does however introduce a new problem because a signal from a product that has a variation in angle from the mean, will have a high correlation with the signal on the projection. This case may be possible to detect because there are a high degree of correlation with the projection along the line which are parallel with standard product vector. This does also apply to a product however the ratio between the amplitudes on the two projections is relative to the gain of the filter defined by the projection. This gain should be significantly smaller for a product than for a metal object.

5.2 Principal component analysis classifier

The principal component analysis classifier is build upon the classic principal component analysis method. The first part of the classification is to determine if there is anything to classify based on the data received from the feature extraction. At the same time the data are aligned so the shift in phase lays in the center of the signal to further aid the principal component analysis.
The principal components for the system are made based on a large quantity of samples with the product in the detector.
The detection are based on a likelihood of being a product. If the sample are too far away from one of the sample clusters, the product is classified as a foreign object.

5.2.1 Alignment of Data

The Alignment of data is the first part of the classifier. It uses a "V" shape signal to correlate with the amplitude signal and a Step to correlate with the phase signal. The two correlation

signals are normalized. The signal is detected as the centre of a symbol from an object, if the sum of the two correlation signals are above a threshold value. This method ensures that the signals are aligned while it effectively filters out the signals where no object is passing through the metal detector.

A number of samples around the alignment point are used for further classification. The number of points is chosen to give a maximum number of points inside the symbol without using data points that are outside the symbol range. Obviously this number of samples will change if the speed of the conveyor belt is changed because this changes the symbol length.

5.2.2 Principal Component Analysis

The principal component analysis uses the method described by [Duda, Hart & Stork, 2001, p. 115-117]. The transformation matrix is found by eigenvector decomposition of the Scatter matrix . The eigenvalues shows that the two most significant dimensions are much more significant, than any of the others and thus a transformation matrix which transforms the system to a two dimensional system. The eigenvalues are plotted in figure 5.2
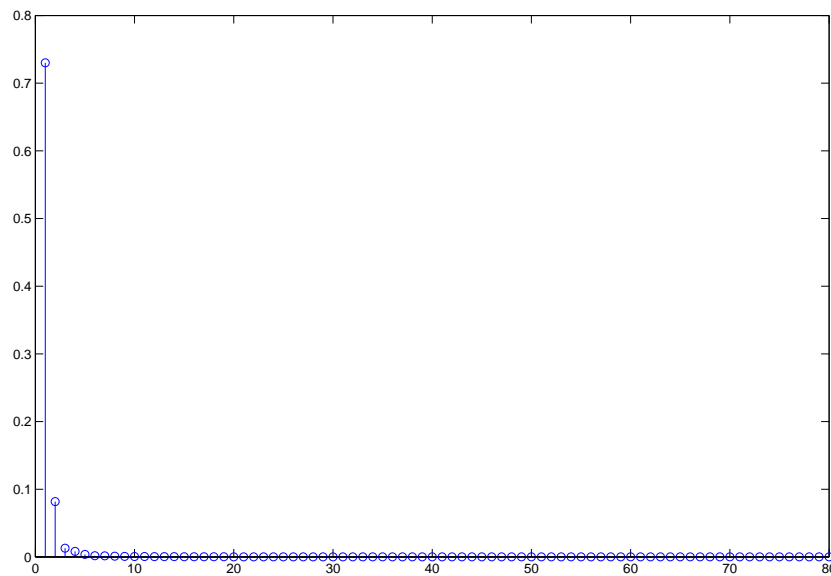
Figure 5.2: *This figure shows the eigenvalues which were obtained in the training of the PCA. It is clear that the 2 first values are much greater than the rest, but it the 3rd and 4th value may also have a small amount of information as they are slightly greater than the rest of the values.*

The data points show a tendency to gather in three different clusters for the product, which can be seen in figure 5.3. This is as expected because three different alignment points are found for each product passing through the metal detector. A second training set has been made where the product was placed at the same way on the conveyor belt each time to see how much of the variation that was due to the product. The scatter plot of this can be seen in figure 5.4. The variance is clearly smaller in this plot due to the minimized variation of the product. It does also show that there is little reason to try to improve the feature extraction further because the main contributor to the variance are the product itself, and thereby the product sets a limit for further improvement of the system.

Figure 5.3: *This scatter plot shows the training data for random placed popcorn packages on the conveyor belt. each packages gives three data points, one in each of the clusters seen on the scatter plot. The red circles are the centers of the classes and the cyan ellipses are the decision boundaries*

Figure 5.4: *This plot shows how the training data falls out when the popcorn are placed in the center of the conveyor belt and turning the same wa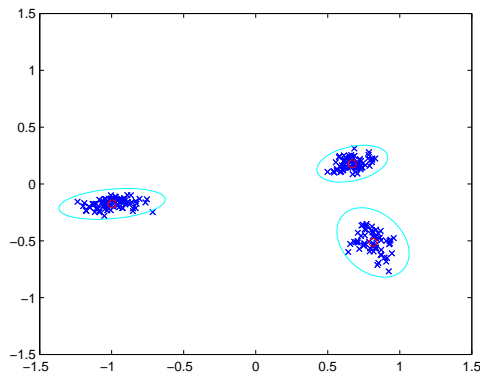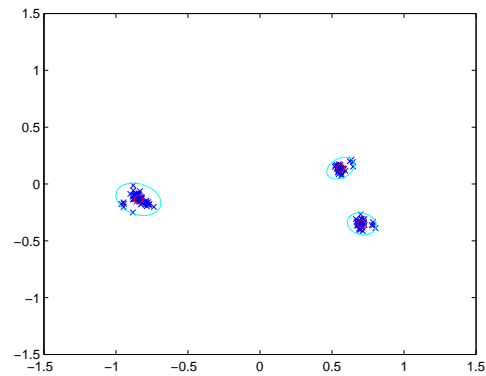y each time. It is clear that this reduces the variance of the dataset significantly, which greatly improves the chances of finding metal.*

5.2.3 Distance Classification

The last objective is to determine whether a dataset from an object belongs to one of the three clusters. This is done by calculating the distance to the centre of each of the clusters and comparing the distance with a threshold value for each of the clusters. This threshold value is predetermined from an assumption that the clusters have a normal distribution which makes it possible to set a threshold value. Test has shown that the normal distribution is multivariate, meaning that the variance is not the same in all directions. A linear transformation can transform distribution from a multivariate to a univariate distribution. This transformation is found by the use of the eigenvalue decomposition. The transformation A is given as. [Duda, Hart & Stork, 2001, eq 44]

$$A = \Phi \Lambda^{-1/2}$$

Where Φ are the orthonormal eigenvectors of the covariance matrix and Λ are the corresponding eigenvectors. Using a circular decision boundary in the new domain which the transformation gives corresponds to an elliptic decision boundary in the old domain. This gives them a decision boundary that is significantly better than a circular boundary in the old domain. The data can be seen in the domain before the linear transformation in figure 5.5 and in the new domain in fig:5.6

The Threshold value is determined by, the acceptable amount of products, which are thrown away due to erroneous classification as a foreign object. This is a compromise because an increase of the threshold value will decrease the number of erroneous discarded products but also increase the number of foreign objects that are not detected by the system.
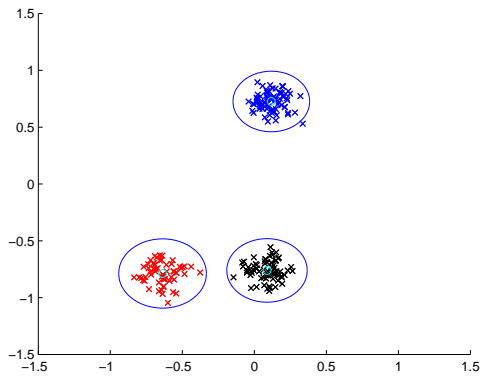
Figure 5.5: *This scatter plot shows the training data for random placed popcorn packages on the conveyor belt after the linear conversion.*
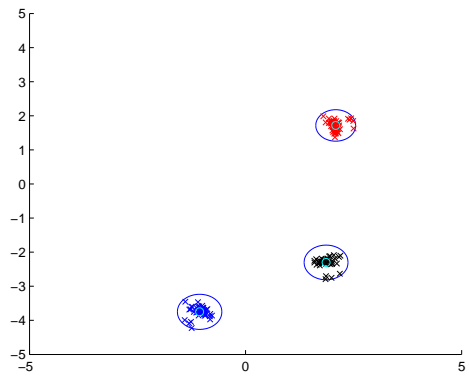
Figure 5.6: *This figure shows the effect of a similar linear transformation. The 3 classes end at some different locations which have made it necessary to change the scaling on the axis for this figure*

5.3 Evaluation of classifiers

The orthogonal classifier has the problem that the phase does not reach a constant value for the product as anticipated. This means that it is impossible to eliminate the product from the signal and thereby reduce the signal to noise and foreign objects. The method may work in some cases, but in general it does not. The principal component analysis does give a somewhat good, but not perfect classification. This classifier can be improved by improving the signal to noise ratio on the features, because this will give a lower variance on the clusters for the product, which will make it possible to detect smaller objects in a product as a small contribution will have a tendency to give a small change in the placement of the data points. It is sufficient that the contribution is greater than the spreading of the data points from a product. This can easily be seen in figure 5.7 where product and 2mm aluminum objects are mixed. The principal component analysis is good in cases where the characteristics of the foreign objects which are to be found are unknown. It should be possible to improve the classification by using methods that are able to use a priori knowledge of the characteristic of a certain foreign object in a case were this is known.
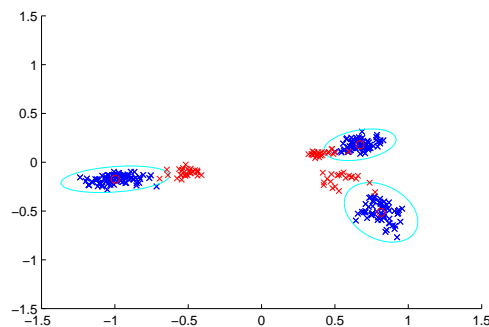
Figure 5.7: *The figure is a scatter plot where the blue markers represent the training data of popcorn. The red circles are the class centers. The purple ellipses are the decision boundaries and the red 'x' markers are the markers from the combination of 2mm aluminum and popcorn*

5.4   Conclusion on Classifier analysis

This chapter has analyzed two different kinds of classifiers. The first classifier tried to remove contributions that pointed in the same direction as the product. This method was discarded because the popcorn product, which was used in this analysis seemed to have more than one contributor to the transfer function of the coil system. The different characteristics of these made to much fluctuation in the phase to effectively remove the product impossible. The second method uses a classic PCA analysis to determine if a hypothesis which states that an object that passes through the metal detector is a product. A product with a metal object does not have the same characteristics as a product without a metal object in it. This method stops working when the signal from the metal object becomes so small that the contribution from it cannot be recognized from the variations in the product itself. The method gives some good results and is therefore chosen for implementation. Further studies of this method does also show that there only be a little gain by improving the feature extraction from the current implementation because the largest contributor to the variance of the clusters are the variation from the location of the product on the conveyor belt and the variations in the product itself.

Chapter 6
Algorithm Design

In this chapter the algorithms for features extraction and classifier is described. It was chosen in chapter 3, that the feature extraction to implement should be the improved cross correlation. The classifier chosen in chapter 5 was principal component analysis. A detailed description of the algorithms is made, to prepare them for implementation on a given platform. The overall diagram for the algorithms is shown in figure 6.1.
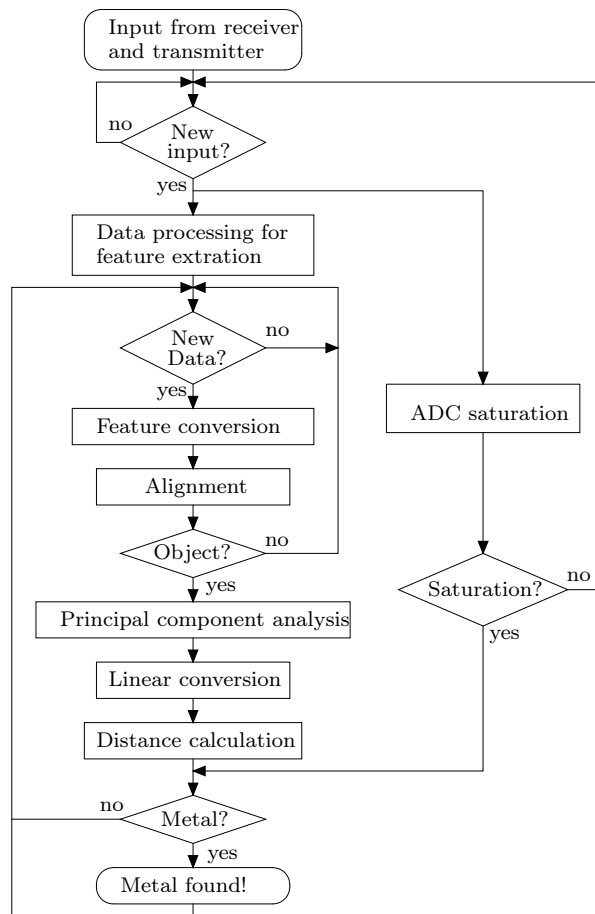
Figure 6.1: *Flow diagram for the algorithms*

First the input signal is being processed for the feature conversion. The processing includes peak filter for the input and four correlation functions where three of the signal needs to be delayed. The four output samples from the correlation functions are converted to phase, amplitude, real and imaginary part. Note that the sample rate decrease after the correlation functions, depending on the number of samples for the correlation functions. The next step is the alignment algorithm, which tries to find the three V-shape and the three phase shift, which is characteristic for food and then align around the three point. If no phase shift or V-shape is found, no object is assumed to be in the detector head and the classifier stop. If there are found a phase shift and V-shape the PCA is calculated for the samples around them, which gives a point in the two dimensional plan for each V-shape point. Next linear conversion is made on the PCA points to get circular

decision boundary. Last the distance is calculated to see if the points are within the decision boundary for food. If there is not a point within each of the three boundaries for the food, it is assumed that there are metal in the detector and the system should alert.

The overall algorithm design has now been described, in the following sections a more detailed description of the algorithms is described.

6.1 Feature extraction

In this section the algorithm for feature extraction is described. The structure of the feature extraction is shown in figure 6.2. It can be seen as mentioned earlier that a down conversion is made after the correlation functions. The samplerate in the peak filter and correlation function equal that of the input signal and then a down conversion is made which is equal to the number of samples processed in the correlation function. The section is divided into two subsection the first section describes the algorithm running at fast sample rate and the second section describes the feature conversion running at low sample rate.
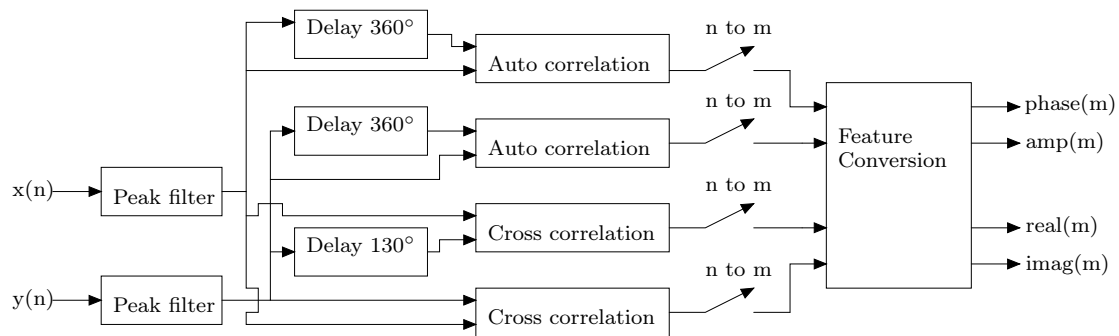
Figure 6.2: *Block diagram for the feature algorithms*

6.1.1 High samplerate processing

The two input signal is first filter to remove noise outside the modulated frequency around the transmit frequency. Then four correlation function is made where one of the input for each of the autocorrelation is delayed 360°, due to avoid white noise in the correlation. In one of the cross correlation the input is delayed 130° which is used for calculating the phase all around the 360°. The three blocks, peak filter, delay and correlation function will now be examined.

The peak filter is designed as a second order IIR filter with the Matlab commando `iirpeak`. The equation for a second order IIR filter is:

$$y(n) = x(n) \cdot b_0 + x(n-1) \cdot b_1 + x(n-2) \cdot b_2 - y(n-1) \cdot a_1 - y(n-2) \cdot a_2 \qquad (6.1)$$

From the equation it can be seen that five multiplications and four add/sub is required. The equation can be reduced since the b_1 coefficient is zero and b_0=-b_2 for the peak filter. This reduces the equation to:

$$y(n) = (x(n) - x(n-2)) \cdot b \cdot -y(n-1) \cdot a_1 - y(n-2) \cdot a_2 \qquad (6.2)$$
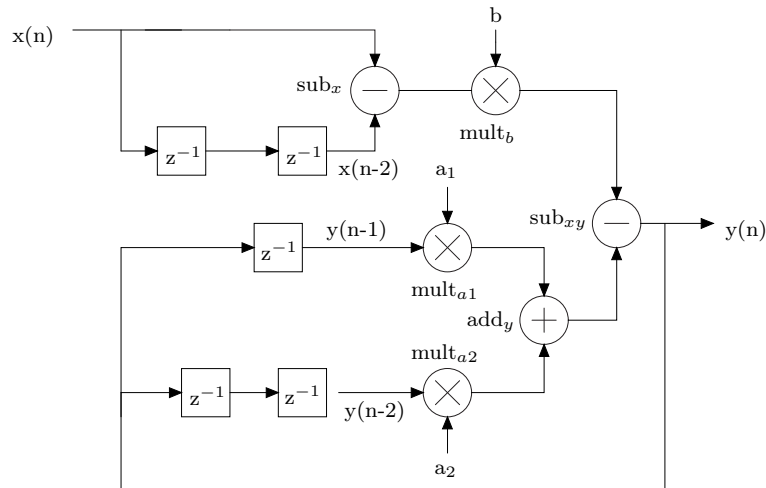
Figure 6.3: *Block diagram for the peak filter*

This equation requires three multiplications and three sub/add, a reduction of two multipliers and one add/sub. The block diagram for the peak filter is shown in figure 6.3

The delay of 130° and 360° can be implemented in different ways. The simple solution is to insert delay elements corresponding to the phaselag. This requires a high oversample to get an accurate phaselag and with high oversample many delay elements are required. Variation within some degree is allowed for the phaselag. Another method for making a phaselag is to use an allpass filter. This method can make an accurate phaselag without the high oversample, and it do not require many delay element, it need however some arithmetic units.

The equation for the allpass filter is [Karjalainen et. al., 2000]:

$$y(n) = (x(n) - y(n-1)) \cdot \lambda + x(n-1) \tag{6.3}$$

It can be seen that the algorithm require two add/sub and one multiplication. One allpass filter can only make a phaselag below 180°, so for the phaselag of 360° three allpass filter is needed. The block diagram for one allpass filter is shown in figure 6.4. It has been chosen to used the allpass filter method since it make a more accurate phaselag and reduce the amount of delay elements. It does however cost some arithmetic elements.

Figure 6.4: *Block diagram for the allpass filter*

The last four block is the correlation function, which can be seen as one Multiply accumulate (MAC), since the correlation is only calculated for one lag. Two signal of a given length is multiplied together sample by sample, and then the products are summed together:

$$y(m) = \sum_{n=1}^{T} x_1(n) \cdot x_2(n) \tag{6.4}$$

The index n corresponds to the sample frequency of the input signal and the index m indicates the new down sampled index. The factor between the n and m index is controlled by T, which state the number of samples of the two input signals being correlated.
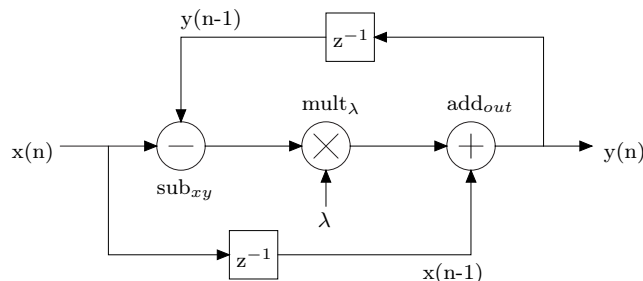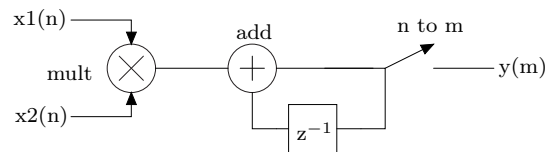

Figure 6.5: *Block diagram for MAC*

The functions for the high sample rate have been described, as it can be seen the functions are rather simple and ideal for basic arithmetic units. The total arithmetic units are 14 multiplication and 18 addition/subtraction.

6.1.2 Low Samplerate Processing

The last section treat the part of the algorithm which run at low samplerate. These signals are all some representation of the change in the transfer function of the coil system in the metal detector. The frequencies in this signal are a function of the speed at which the conveyor belt is moving. The first part of this processing is the calculation of the features from the correlation values. The second part is the alignment and the last part comes in the calculation of the principal component analysis and the following classification.

Feature calculation

The feature calculation are composed of a mixture between summation/multiplication and some other operations which are more complex in implementation plus a large block containing logic operations which are used to determine the sign of the calculated phase. This can all be seen in figure 6.6

The features has now been extracted but there are still a DC offset coming from the off balance component. This component is removed with a highpass IIR filter. It could have been removed by an FIR filter but the cost of this filter is greater. The disadvantage of the IIR filter implementation is that it has a settling time measured in seconds due to the low cutoff frequency. This choice means that the system needs some time at startup before the filter has settled. However a startup time of up to a few minutes are not seen as a problem.

Figure 6.6: *This figure shows a diagram for the feature conversion algorithm. The figure does only show how to obtain the features represented as Real and Imaginary parts.*

6.2 Classification

In this section the classification is desribed. The raw signals for the real and imaginary parts of the signal are used to calculate the gain and the phase signals which are used in the alignment part. The amplitude and ph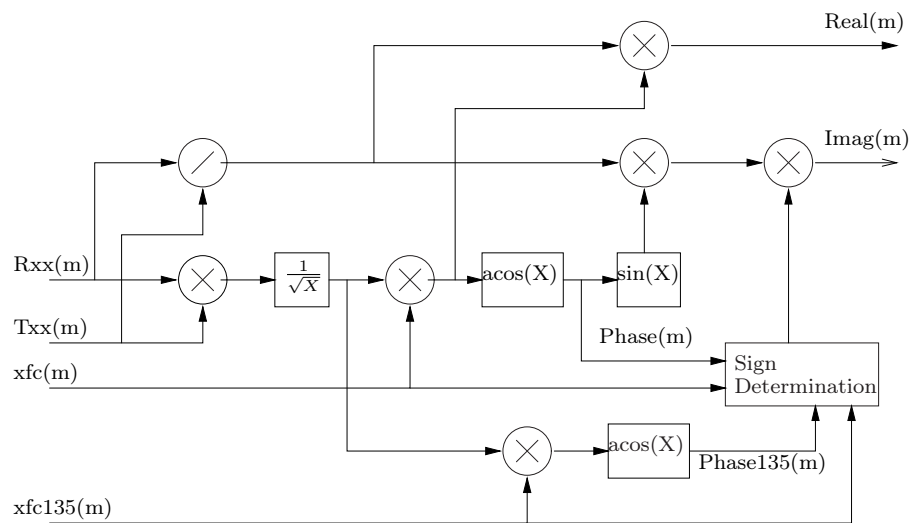ase representation are chosen for this part, because the step in phase and V shape of the signals are easy to find in the signals. The implementation of this are similar to much of the implementation of the feature extraction because it uses the same method to calculate a normalized cross correlation between a V shape signal for the gain feature and a step function for the phase feature. This does also involve an autocorrelation of the gain signal which are used to further enhance the ability to sort out the areas with noise because a simple level detection on this one can sort out the noise.

The align part gives a logical signal which tells whether an object is right at the alignment point or not. This logical signal are found by adding the normalized crosscorrelations from the gain and phase feature signals after they have been processed as shown in figure 6.7

The Principal component analysis which are basically a single input multiple output FIR filter is calculated when this logical signal indicate that the align point has been reached. The input signal for the principal component analysis consists of a signal composed of the real and imaginary feature signals in an interleaved fashion. The order which the data are put is not really that important as long as it is done the same way each time. The first part of this method is a little data preparation because the mean value needs to be subtracted. The mean values are calculated as seen in the figure 6.8

The next thing that follows is the calculation of the principal components. The algorithm for this calculation can be seen in figure 6.9

The training of the principal component analysis. As this is a prototype all data sets for the principal component analysis are saved and written to a file which both gives the opportunity to train the principal component analysis in matlab, and to create a scatter plot with new samples to see where they are placed in comparison to the classes formed by the training. This does have the disadvantage that it greatly limits the amount of time in which the system may be
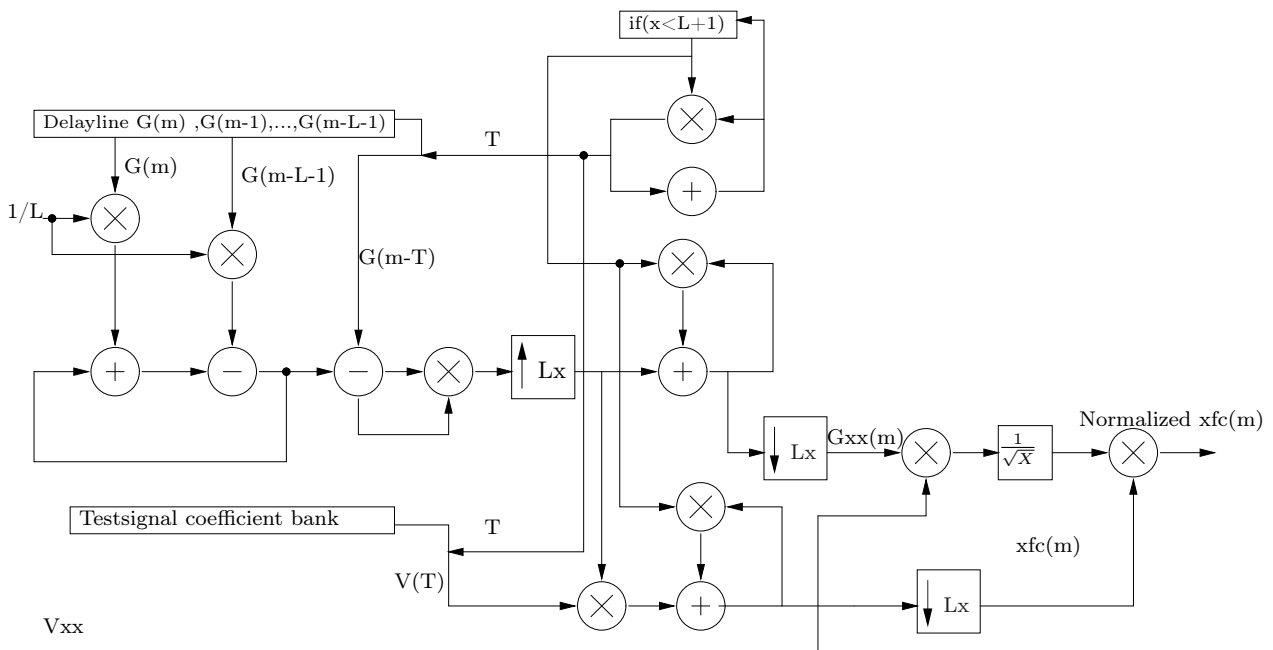
Figure 6.7: *This figure shows the calculations for one of the two crosscorrelations, where the V signal are the test signal and the G signal are the feature signal. Vxx are the autocorrelation of the test signal in lag 0. As the V signal is known there is no reason to calculate this each time*
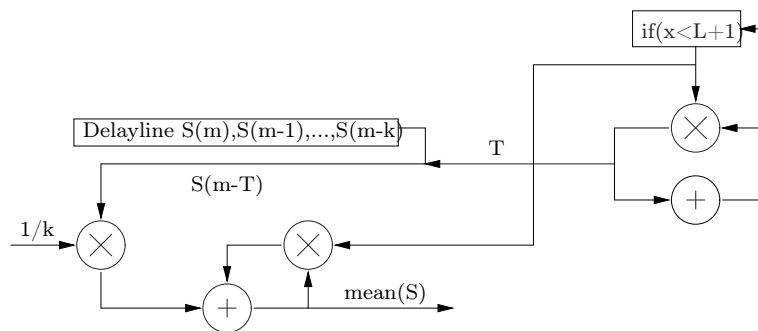
Figure 6.8: *This figure shows the calculation of the mean value of the interleaved data S used for the pca*

running before it is restarted because it uses up a lot of memory. An online training algorithm are to extensive for implementation in this project however a small change in the calculation when training can change the method from an eigenvalue problem to a singular value problem which can be calculated iteratively for each new data set.

The algorithm is now described, the different operation for the algorithm has been outlined and it was shown that the the algorithms run at two different samplerate. In the next chapter the overall system is setup and a processor platform is chosen for which the algorithm is mapped onto.
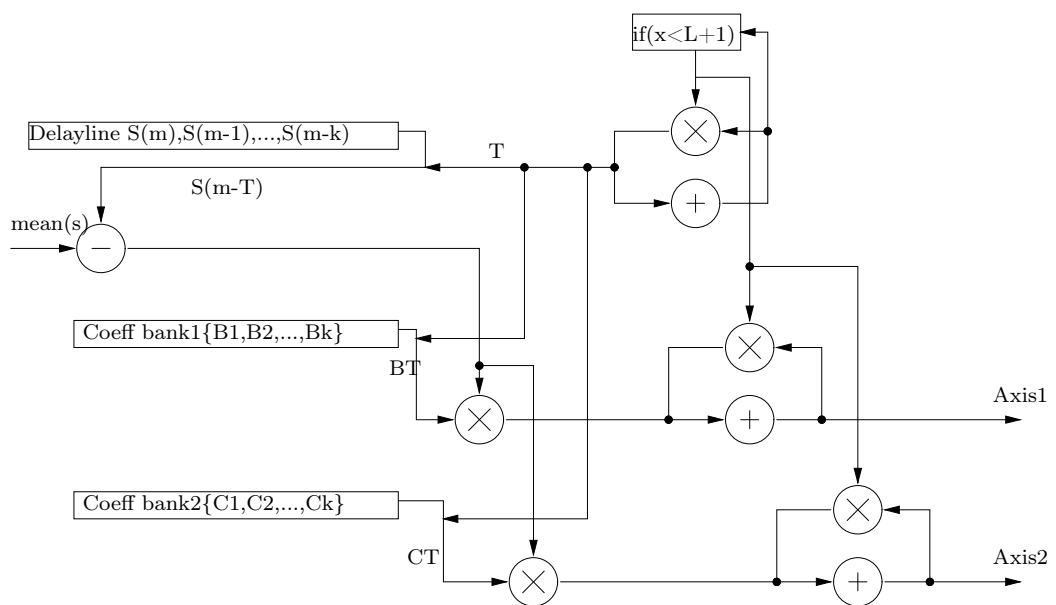
Figure 6.9: *This figure shows the calculation of the principal components, where the value an each axis is a part of the vector for the data point*

Chapter 7
System Design

This chapter presents the system design for the metal detection system. The overall system is first outlined. Then the processor platform for the feature and classifier algorithms is chosen. The Rugby model is then introduced which is used to design the implementation on the platform.

The overall system for the metal detector is shown in figure 7.1. The signal from the transmit coil Tx and receiver coil Rx is first amplified in instrumentation amplifiers. The signal on the receiver coil is also balanced to minimize the signal, caused by unbalance between the transmit coil and the two adjacent receiver coils, which was shown in chapter 4. The analog signals are then converted to digital signals and applied to the processor platform. In the processor features are extracted for the signals and a decision of whether metal is present in the detector is made.
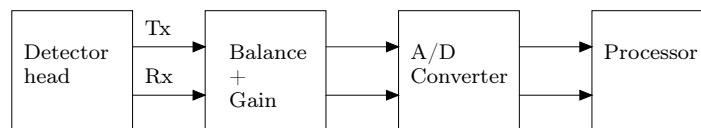
Figure 7.1: *The overall system for the metal detection*

7.1   Processor platform

The platform for the feature extraction and classifier is made in this section. It was shown in chapter 6 that the system is a multirate system, which processes data at the samplerate of the A/D converter and then down convert for feature conversion and classification. The amounts of operation for each sample at the high sample rate were estimated to 14 multiplications and 18 additions/subtractions, all basic operation. At the low sample rate the amount of operation per sample where higher and non basic operation is needed, such as arccosine and square root.

This setup is ideal for a HW/SW co implementation since the basic operation at high sample rate can be implemented in hardware and the operation running at slow sample rate, which included non basic operation, can be implemented in software. Based on this it is chosen to use a FPGA. It would also be possible to implement it on an DSP but it is desired to get some experience working with FPGA and hardware/software co-design.

The board used in this project is a DE2 development board based on the Cyclone-II FPGA. It has the option for integrating a soft-core processor, Nios II, which can communicatie with custom hardware blocks. The board does not have an A/D converter that are fast enough, so an external must be connected. It is chosen to use an AD9220 from Analog device C, which is setup by group 08gr1040. The A/D converter is connected to the DE2 board through the expansion header of the board. The board has 70 9 bit embedded multiplier and 33,216 logic elements which is sufficient for the implementation.

The platform for the algorithms is now determined and it is chosen to split the system into a hardware and software part. This demands some hardware/software co-design which is made based on the Rugby model.

7.2 Hardware/software co-design

The hardware and software boundary is setup in the section. First a short introduction is made to the Rugby model and then it is used to specify the hardware and software blocks.

7.2.1 Rugby model

The Rugby model is used for designing the Hardware/Software at different levels and combines the two domain. The model is an extension of the Y chart which primary was developed for hardware design. It has three domain: "Behavior", "Structural" and "Physical" and within each domain different level of abstraction exist. The design view see from the "behavior" domain regard the functionality of the system. The "structural" domain covers the subsystem of the system, which is the CPU, ALU etc. depending on the level of abstraction. The last domain "physical" also know a geometric, covers size, shape and placement of the implementation, what is feasible. The problem with the Y chart is that it does not cover, time, data and communication, and the mix of hardware and software.

This is possible in the Rugby model. The Rugby model has four domain: "Time", "Computation", "Communication" and "Data", see figure 7.2. The abstraction level within each domain varies from the idea phase to the physical system. At some point in the transition from high abstraction to low abstraction the domain line split into hardware and software part. The domain "computation" covers the behavior of the system, the relationship with input and output. The "communication" domain concerns the connection between the design elements at different level. The "data" domain concerns the data types, which means how the data are represented at different levels. The last domain "Time" control the time relation between events, this could be the propagation delay in hardware or the clock cycle for the software execution.
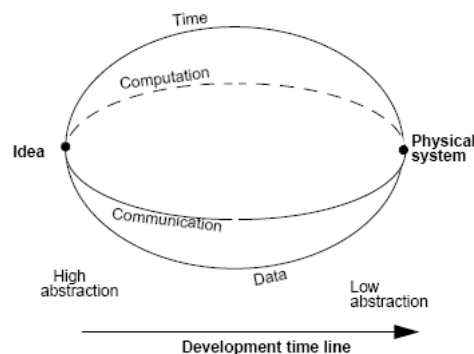
Figure 7.2: *The rugby model REFERENCE*

The model is used implicit throughout this project.

The "computation" domain starts at the high level abstraction where a box is desired which can estimate features that indicate if metal is present. Algorithms are then developed and tested in Matlab. The chosen algorithm is then examined at a lower abstraction level where all the operations are identified. The operation are then chosen if they should be in hardware or software , where the high sample rate in this project is chosen to be in hardware and the low sample rate in software. The block for the hardware and software are then designed at a lower abstraction.

In this project the implementation of hardware is mainly at the arithmetic block level where the arithmetic blocks are supplied by Altera is used.

The "communication" domain in this project regard the communication between the A/D converters and the FPGA, how do they interface with each other. Then there are the software and hardware communication, how are data exchanged between the domains.**FiXme**: (forstår ikke)

The "data" domain deals with the input format of the A/D converter and how the signals and coefficients in the hardware block is quantized. The data type for the software in the Nios II also concerns this domain.

The "time" concern for this project regards the critical paths for the hardware blocks which should be within the sampling time of A/D converter. For the low sample rate the cycles for the operation should not exceed the number of cycles available in the processor.

The overall specification for the hardware/software will now be set.

7.3   System specification

The system will be designed for transmit frequency of 30 kHz, since the performance of the analog hardware decrease as the frequencies increase 4. However the system will be made so it can operate at higher frequency only by changing the coefficients of the filter. In chapter 3 it was chosen to use the improved cross correlation method and simulations showed that the oversamplerate should be minimum 10 to make an accurate phase and amplitude estimate. The A/D converter used in this project support sample frequency up to 10 MHz. It has been chosen to use the full sample rate, which means the system can function up to 1 MHz, where the only change is the filter coefficients. The bit length of the A/D converter is 12 bit and the format is chosen two's complement. This means that the critical path of the hardware may not exceed 100 ns for the real time to be valid. In chapter 4 the frequency contend of the signal when object pass through the detector head is below 10 Hz, when the conveyor belt is running at 25 meter per minute. This requires a minimum sample frequency of 20 Hz but 100 Hz is chosen to be safe. In figure 7.3 the overall hardware/software system is shown.

Hardware implentation
Sample rate = 10 MHz

Software implentation
Sample rate = 100 Hz

Tx

Peak filter

Rx

Peak filter

Allpass filter
360°

Allpass filter
360°

Allpass filter
130°

Auto correlation

Auto correlation

Cross correlation

Cross correlation

ADC satuation

NiosII

Processor

Algorithms:
-Feature conversion
-Classifier
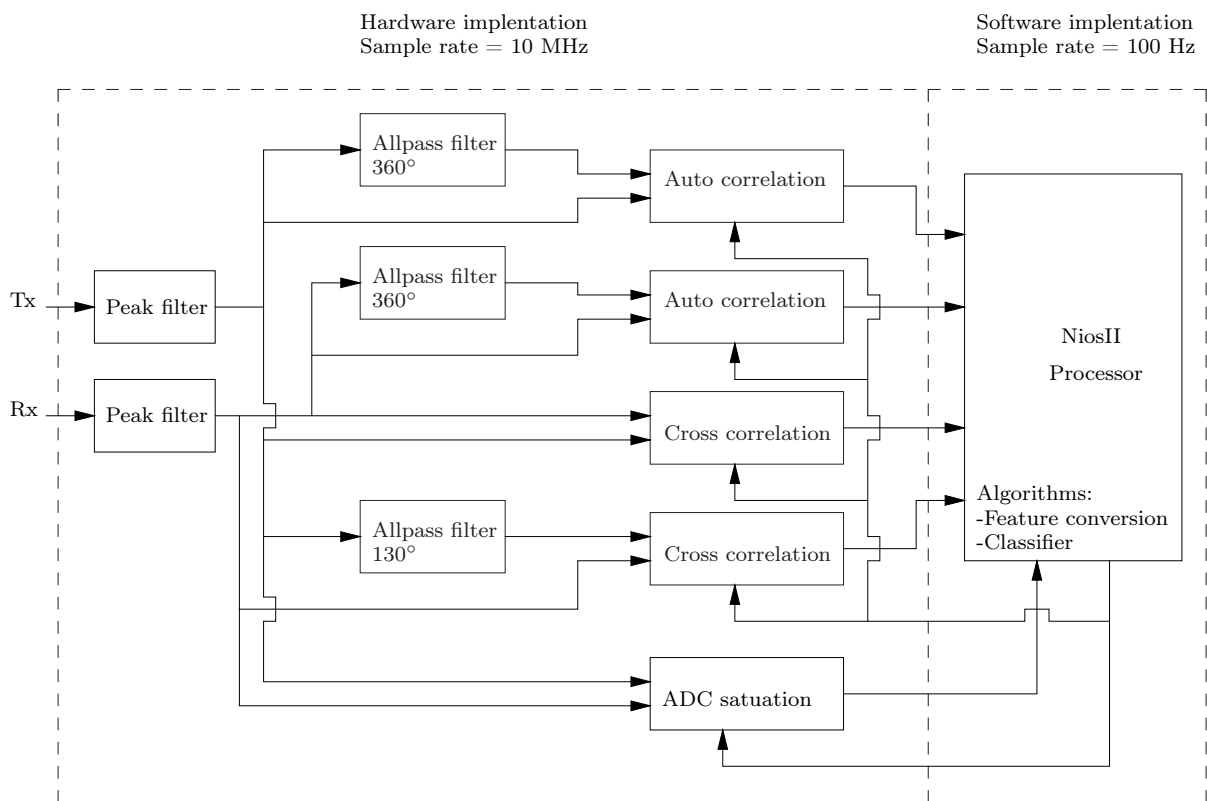
Figure 7.3: *Block diagram for the FPGA implementation*

Chapter 8
Implementation

8.1 FPGA design

In this chapter the implementation of the algorithms for feature extraction and classifier from section 6 is described. The algorithms will be implemented on the Altera DE2 development board chosen in section 7. The chapter is divided in two sections the hardware implementation and software implementation, according to figure 7.3. The design flow of the FPGA is shown in figure 8.1
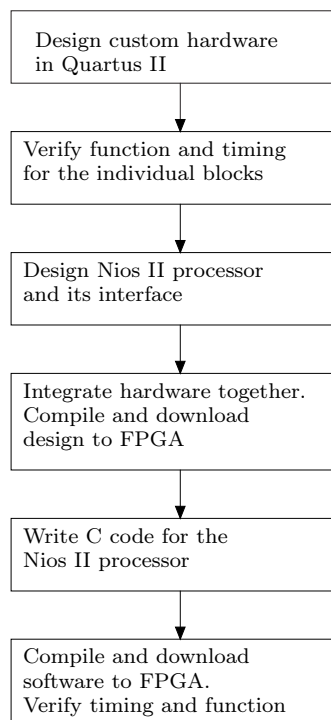
Figure 8.1: *Flow diagram for the FPGA implentation*

First the hardware blocks is designed and tested, which include the peak filter, allpass filter and MAC. Then the Nios II processor is designed and integrates with the custom hardware block and last software is written and tested.

8.2 Hardware implementation

The hardware implementation will now be described. First Quartus II is introduced which is the tool used for designing the FPGA. Then the three main blocks are implemented and tested for timing and functionality. With these block set the Nios II processor can be designed and interface for the custom hardware is setup. Last the hardware system is integrated together.

8.2.1 Quartus II

In this section the program for designing the FPGA is described, which is Quartus II. The description is based on how Quartus II has been used in this project.

An FPGA can be designed in two ways in Quartus II, the text based method where a descriptive language as VHDL is used or the schematic diagram method. In this project the schematic diagram method is used, since it gives a better overview of the system.

The design of the FPGA in the schematic diagram is made by inserting block with specific operations, add, multiplication etc., and then connect them with wires and possible clocks. The signal input and output for the block diagram is connected to pins. Most operation blocks can be found in library or they can be written in VHDL or Verilog. It has been decided to use the megafunction provided by Altera, since they are optimized for the Altera boards. The megafunctions which is used is add, subtract, multiply and DFF storage blocks. The shift operation, counter and other interface blocks is written in VHDL and transformed into blocks, so they can be inserted in the schematic diagram.

The design of the main system is made in sub blocks, where the allpass filters, peaks filters and MAC filters have their own sub block. Each sub block is designed with the arithmetic blocks, storage, etc. and then transformed into one block. The blocks can then be inserted in the main schematic diagram. This makes it easier to design the system since each block is designed and tested separately and it gives a better overview of the main system.

After the schematic diagram is designed, it is compiled in Quartus II. The compilation is made in four stages:

- Analysis and Synthesis - This stage checks the design files for error and perform synthesis to minimize the logic of the design. Then it integrates all the design files into a database.

- Fitter - This stage performs the place and route of the logic in the design, which means the placement of the logic, wire routing and pin assignment. Based on the database in the Analysis and Synthesis stage it fit the logic and timing requirement for the chosen FPGA.

- Assembler - It converts the logic, wire and pin assignments from the fitter to a programming image for the FPGA.

- Timing Analyzer - It analyses and validates the timing performance of all logic in the design, which means the propagation delay along the various paths, to give an indication of the timing performance.

After the compilation, status reports are provided with resource usage, propagation delays for each path, etc. The Assembler provides SRAM object files (.sof), which is used to program the FPGA board.

To verify that the system works before downloading the sof files to the FPGA, a simulator can be used. In Quartus II a vector waveform file can be made, where a vector of numbers for the input pins can be specified, and then the simulator calculate the output values. This form of test is used for testing the filters and MAC. It is also possible to test the system in running on the FPGA, which is done by Signal Tap II. Here it is possible to log the signal anywhere in the FPGA. This feature is used to test the A/D converter.
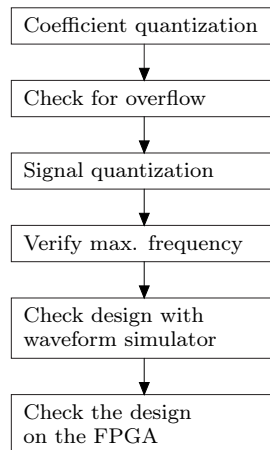
Figure 8.2: *Diagram for the FPGA implementation of the peak filter, allpass filter and MAC*

The implementation of the peak filter, allpass filter and MAC will now be implemented. The flow for the implementation is shown in figure 8.2.

First the coefficients quantization is examined, which is the effect of switching to finite word length. This causes the poles and zeros of a system to shift from the desired position, since only a limited pole and zero locations exist. The quantization effect can be minimized by increasing the word length or the structure of the filter can be chosen so the coefficients are insensitive to quantization. The quantization of coefficients is deterministic since the value which should be quantized is known. This makes it possible to state the effect of quantization. In this implementation the coefficient length will be chosen based on simulation.

After the coefficients are chosen the filter structure is examined for possible overflow. This can occur when values are subtracted and added together.

After overflow has been examined variable quantization is examined. This happens when analog signal are converted to digital signal and when the word length of a digital signal decrease. Quantization can be made by either truncation and rounding. For truncating the data value is represented with the highest quantization level that is less than or equal to the real value. For rounding the data value is represented with the nearest quantization level. The truncation error e(n) for two-complement is:

$$-2^{-LSB} < e(n) \leq 0 \tag{8.1}$$

and for rounding it is

$$-\frac{1}{2}2^{-LSB} < e(n) \leq \frac{1}{2}2^{-LSB} \tag{8.2}$$

This means that truncating gives a maximum error of the LSB, where the error for rounding is maximum 1/2 LSB. Based on this it is desired to use rounding, since the maximum error is only half of the error for truncating. The disadvantages are that it requires operations to perform rounding, where truncation is made by simply removing the bits. In this project all signal will be truncated. To modulate the effect of quantization a linear noise model can be used. Here the quantization error e(n) is thought of as additive noise, see figure 8.3. The input signal x(n) is being quantized to $\hat{x}(n)$ and the error due to the quantization process is model with an additive noise signal e(n). For this model to be accurate, the noise source e(n) and x(n) should not

correlate with each other. The input signal x(n) to the model is a sinusoid for the real system. If the amplitude of the input signal use most of the bit range, 12 bit, and the word length after quantization is above 4-5 bit the error can be assumed white [Oppenheim & Schafer, 1999].
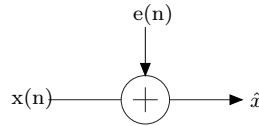

Figure 8.3: *Linear noise model for truncation*

For the implementation the possible truncation point will be outlined and the effect of truncation will be examined. Simulation will be made for the truncation point to see the effect of the truncation compared to the error in phase and amplitude estimation. For the truncation point chosen, a plot will be made for the word length after truncation (x-axis) and the amplitude of the signal (y-axis) given in bit, where 12 equal full range. Two plots are made, one for the phase error and one for the amplitude error. The error is estimated by calculating the phase and amplitude with truncation and without truncation and the calculated the percentage error. Based on the plot the level of truncation will be chosen. The simulation is made for a sinusoid of 30 kHz with sample frequency 10 MHz. Noise and the modulation of the signal is not included, so it do not given an exact answer, but it givens an overview of the truncation sensitivity at that point.

When truncation is determined the maximum operating frequency of the block is examined. It has been chosen to sample data at 10 MHz and so the system should also operate at this frequency. The parameters which determine the maximum frequency is the critical path between latches. Quartus II estimate the propagation delay though any path in the design when it compiles. Based on this the longest propagation delay between two latches is calculated, and converted to maximum frequency.

After the block is design it is tested with the vector waveform simulator in Quartus II. Here an input vector is applied and then the simulator compute the output. The result is compared with an implementation in Matlab, where truncation of coefficients and signal also is included. It is verified that the numbers for Matlab and Quartus II comply and that the signal in the design is available at the right times. The Matlab version has been tested with sinusoid to verify that the design work. The test of the design in Quartus II whas made with an impulse, which has the advantage that it is easy to create the test vector, while making a solid test.

The last step is to test the design on the FPGA. It is done by downloading an image, which sample data from the A/D converter and pass the signal through the block that is being tested. The output of the block and the input signal is passed to a Nios II processor which saves the signal into files. The files are then loaded into Matlab and it is verified that the signal comply with the expected. The input signal for the A/D converter is a sinusoid of 300 Hz sampled at 100 kHz. This is a factor 100 less than the actual system, which is because the Nios II cannot sample data at 10 MHz. The coefficients for the peak filter and allpass filter are the same, so the functionality can still be tested.

The flow for the implementation process has now been described and the three blocks will now be implemented.

8.2.2   Peak filter

In this section the peak filter is described. There are two peak filters in the system, one for the transmit signal and one for the receive signal, the peak filters are identical and therefore only one will be described.

The peak filter is going to have a peak at 30 kHz to remove noise outside the desired frequencies. The frequency of the modulated signal due to the object passing through the detector head is approximately 1 Hz and a minimum bandwidth of the peak is chosen 10 Hz.

The peak filter is characterized with zeros in -1 and 1 and poles lying on the unit circle. The last part makes them highly sensitive to coefficient quantization which can be seen in figure 8.4
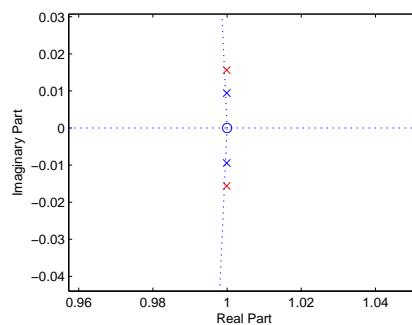

Figure 8.4: *This figure shows a zero pole plot of a peaking filter, where there are zoomed at the poles. The blue poles are of double precision, while the red poles are quantized to 12 bits*

The word length for the coefficients will now be chosen. The coefficients are calculated with the Matlab function `iirpeak`. Two factors which influence the sensitivity of the filter is the bandwidth and sample frequency. Since the sample frequency is fixed at 10 MHz, only the effect of bandwidth will be examined. When the bandwidth is decreased smaller variation in the peak will increase the attenuation at the desired peak. Increasing the bandwidth will decrease the attenuation for variation, but the attenuation of the adjacent noise is also decreased. To determine the bandwidth and word length for the coefficients, simulations are made for the A and B coefficients versus the bandwidth, see figure 8.5 and 8.6. The word length of the coefficients on the x-axis and the bandwidth of the peak is at the y-axis. The attenuation for a given bandwidth and word length is indicated with color. It is desired to find the point with the smallest word length and the smallest bandwidth, which has color indicate zero attenuation. It has been chosen to use bandwidth 100 Hz, see the ellipse on the figure, since the word length of the B coefficient are below 18 bit and therefore only require 2 9 bit multiplier. The word length for the A coefficient should be above 20 bit.

With the bandwidth fixed at 100 Hz a simulation is made for the attenuation at 30 kHz as a function of word length for the A and B coefficients, see figure 8.7. Based on the simulation 23 bit is chosen for the A coefficients and 18 bit is chosen for the B coefficients, this yields an attenuation of -0.02 and -0.25 respectively. Since one of the A coefficients is close to two, it has been chosen to divide all the coefficients with two, to move the fraction point. To compensate for the division of two, y(n) is multiplied with two.

In figure 8.8 the peak for the quantized coefficients is shown compared with the peak for the non quantized coefficients. It is shown that they are close to each other
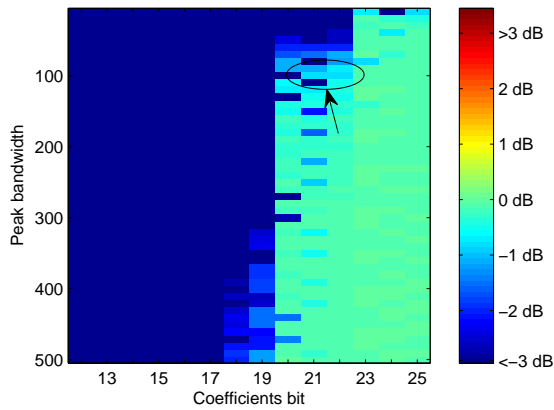
Figure 8.5: *Attenuation due to truncation of the A coefficient. The attenuation is a function of bandwidth and number of bit to represent the coefficients. The color indicates the attenuation.*
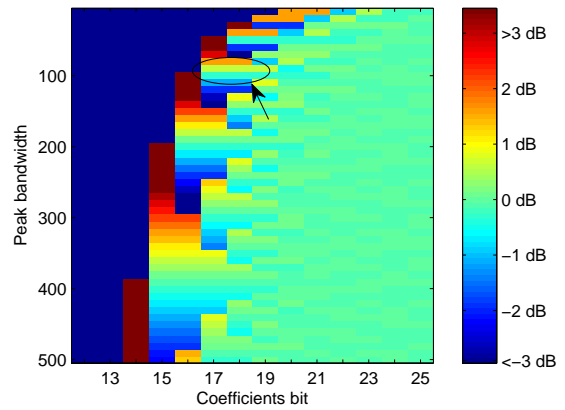
Figure 8.6: *Attenuation due to truncation of the A coefficient. The attenuation is a function of bandwidth and number of bit to represent the coefficients. The color indicates the attenuation.*
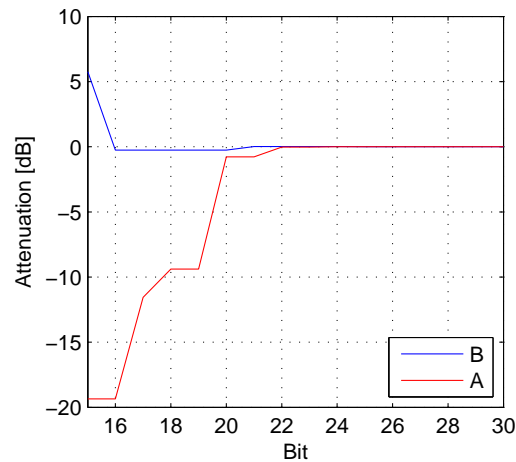
Figure 8.7: *Attenuation for the A and B coefficients as a function of bit representation for the coefficients*

The word lengths for the coefficients are now chosen and overflow for the block will be examined. In figure 8.9 the structure of the peak filter is shown. Overflow can occur after addition or subtraction which means that sub_x, add_y and sub_{xy} are possible overflow point. The other addition block e_x indicate possible signal quantization point and therefore should not be considered. At sub_x no overflow can occur since x(n) and x(n-2) are subtracted from each other and due to the high oversample the value are close to each other. At add_y no overflow will occur since y(n-1) is multiplied with approximately -1 and y(n-2) is multiplied with approximately 0.5. The last overflow point is sub_{xy} here overflow should not happen either, since the coefficient simulation showed that the output of the peak filter had little attenuation.

The overflow has now been examined and the last stage is the signal quantization. In figure 8.9 five quantization points is shown. The output of the peak filter will be truncated to 12 bit, which add the noise signal of e_{out}(n). The signal could also have been quantized after $mult_b$, but since the b coefficient is close to zero, it has been chosen not to. Since the input signal is 12 bit and the b coefficient is 18 bit, the input of sub_{xy} is 30 bit. No extra sign bit occur at the
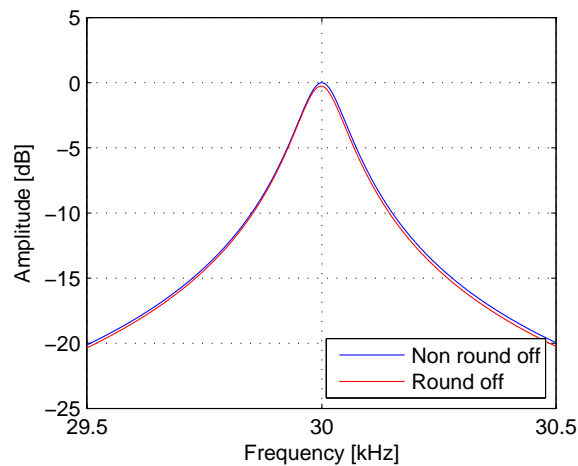
Figure 8.8: *Frequency response for non round off coefficients and round off coefficients*
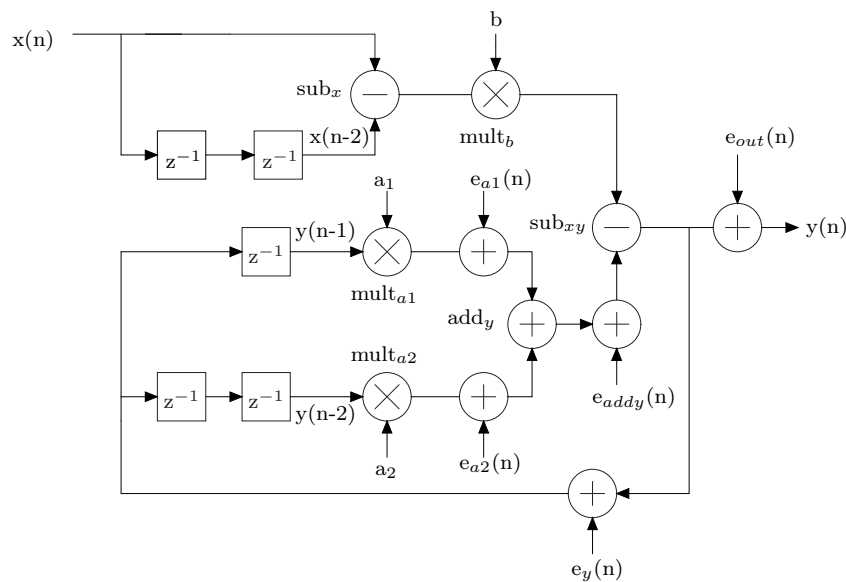
Figure 8.9: *Structure of the peak filter with quantization point indicated by* $e_x(n)$

output since the b coefficient is multiplied with two. The other input for sub_{xy} should also be 30 bit. A simulation is made where the feedback signal is quantized which add the quantization error $e_y(n)$. Quantization is also made after mult_{a1} and mult_{a1} adding the error e_{a1} and e_{a2}. Simulation show that the benefit is limited for quantizing after add_y, so hardware is saved. A sweep is made for the word length after quantization at e_y from 11 to 30 bit. The quantization at e_{a1} and e_{a2} is fixed to 30 bit since it should match the input of sub_{xy}. The simulation for the phase and amplitude error is shown in figure 8.10 and 8.11. The x-axis is the word length after truncating at e_y and the y-axis is the amplitude of the signal given in bits where 12 bits equal full range. The error in percentage is indicated with color where dark blue is approximately zero error. Based on the figure the word length is chosen to 26 bit, which yields phase and amplitude error below 1% down to an amplitude of 3 bit. When food product passes the detector head the amplitude will be higher than 3 bit, but to ensure that quantization noise do not drown signal from small metal objects 26 bit is chosen. The two LSB of the signal is controlled mostly by noise.
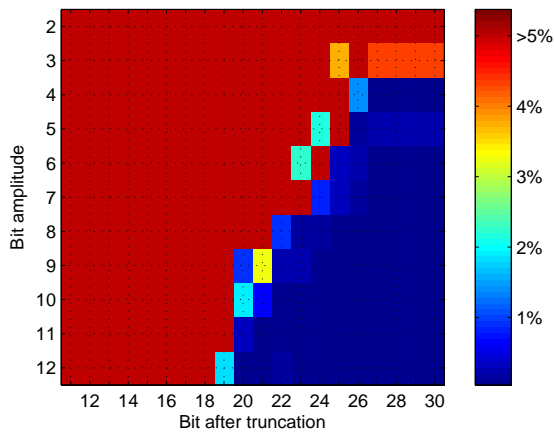
Figure 8.10: *Phase error indicated with color as a function of the signal amplitude given in bit and the number bit of after truncating in the peak filter.*
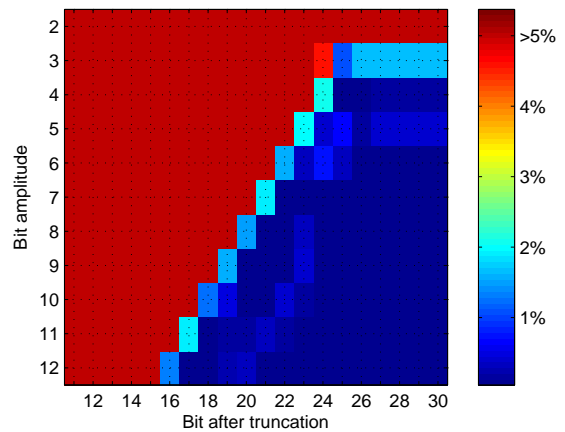
Figure 8.11: *Amplitude error indicated with color as a function of the signal amplitude given in bit and the number bit of after truncating in the peak filter.*

The peak filter is now designed, and the maximum frequency for the block will be examined. From figure 8.9 it can be seen that the critical path is from sub_x to sub_{xy} or from $mult_a1/mult_a2$ to sub_{xy}. The critical path contains, one multiplier and two addition/subtraction. The timing analyzer estimate the maximum frequency to 78 MHz and the critical path is from the output of the DFF for y(n-1) to the input of the DFF for y(n-1) which means the critical path is through the $mult_a1$ to sub_{xy}. Since the frequency is bigger than 10 MHz no further optimization is made.

To verify that the peak filter works an input vector of random values is applied to the simulation and the output values is compared with Matlab. The test shown that the number is identical and that the values are present at the right times. The second test is made on the FPGA board with a input sinusoid of 300 Hz as described. The measurement is shown in figure 8.12 and 8.13. In figure 8.12 the time signal for the peak filtered signal is shown compared to the non filtered signal. It is shown that the signals are close to each other, but the filtered signal is attenuated a bit **FiXme**: *?* and a small phaselag is introduced. In figure 8.13 the frequency response for the FPGA peak filter and the Matlab peak filter is compared, and they are almost identical.

In table 8.1 the resource for the peak filter is shown and the Quartus II block diagram can be seen in seen 8.14. It can be seen that the two multiplier $mult_a1$ and $mult_a2$ require lots of resource, this is because both the input exceed 18 bit. If the oversample rate were reduced the sensitivity of the coefficient will reduced and it would probably reduce the required word length.
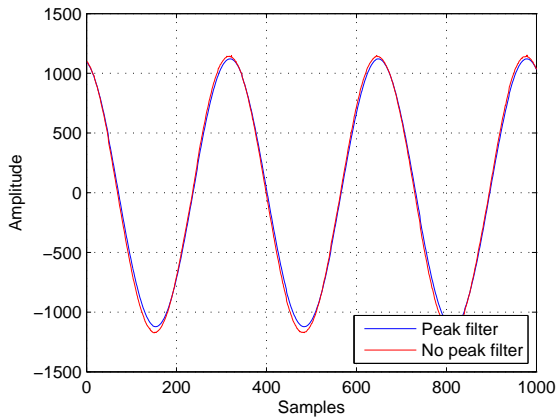
Figure 8.12: *Measurements on peak filtered signal and non filtered signal .*
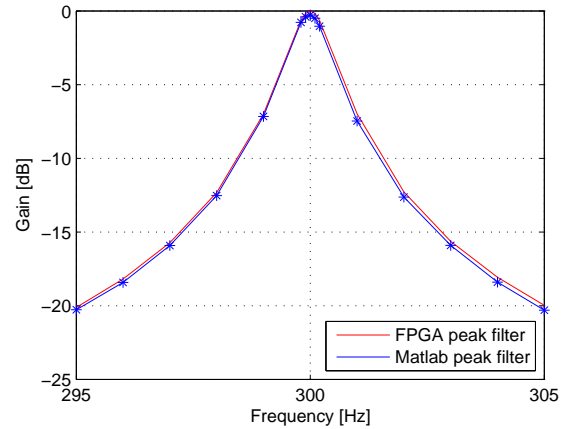
Figure 8.13: *Frequency response measured on the FPGA peak filter versus Matlab peak filter.*

Block	Units
sub$_{xx}$ (12 bit)	12 combinational Logic
mult$_b$ (18x18 bit)	2 X 9 bit embedded mult
mult$_{a_1}$ (27x23 bit)	7 X 9 bit embedded mult + 70 combinational Logic
mult$_{a_2}$ (27x23 bit)	7 X 9 bit embedded mult + 70 combinational Logic
add$_y$ (30 bit)	30 combinational Logic
sub$_{xy}$ (30 bit)	30 combinational Logic
DFF$_{in,out,x1,x2}$ (12 bit)	48 register
DFF$_{y1}$ (26 bit)	26 register
DFF$_{y2}$ (26 bit)	26 register
Total	16 X 9 bit embedded mult + 92 register + 229 Combinational Logic
2 x peakfilter	32 X 9 bit embedded mult + 184 register + 448 Combinational Logic

Table 8.1: *Resource used for peak filter*

8.2.3 Allpass filter

In this section the implementation of the allpass filter is described, which should make a phaselag of 360° and 130°.

First the coefficients are quantized. The phaselag of 360° and 130° is controlled by the coefficient λ and the equation which should be solved to find λ is [Karjalainen et. al., 2000]:

$$0 = (sin(\omega')cos(\omega) + sin(\omega)cos(\omega'))\lambda^2 - 2sin(\omega')\lambda + sin(\omega')cos(\omega) - sin(\omega)cos(\omega') \quad (8.3)$$

where ω' is the desired phaselag and $\omega = 2\pi f/f_s$. The solution of the equation above is found from the `root` function in Matlab.
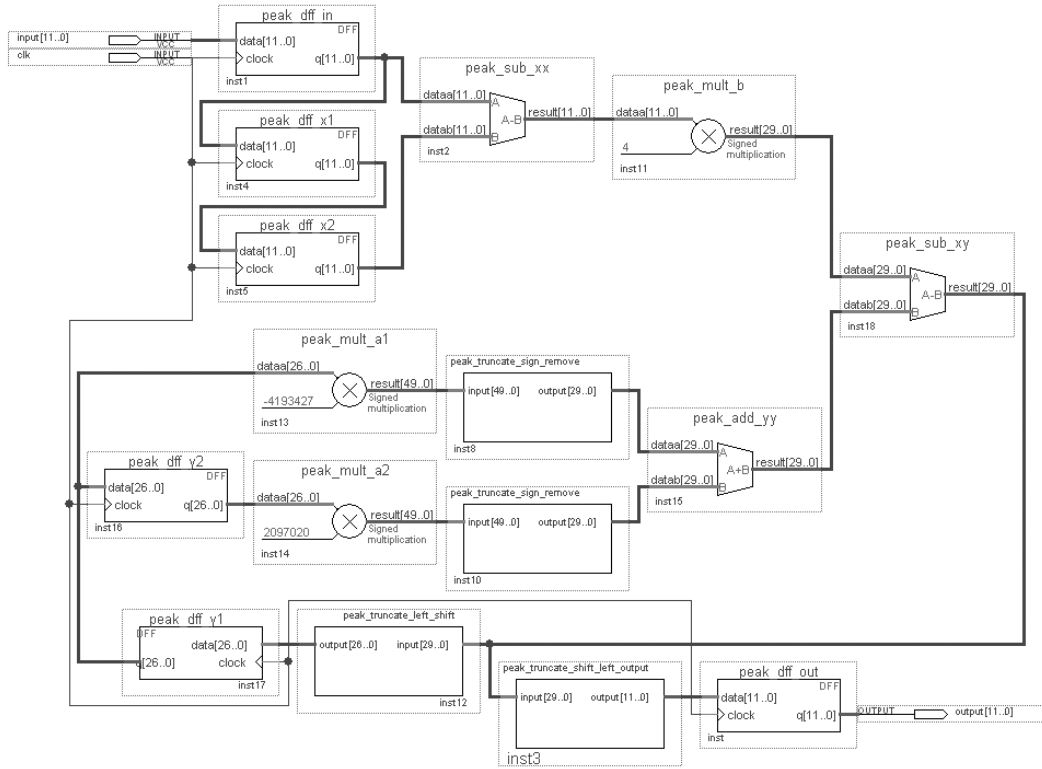
Figure 8.14: *Quartus II schematic block diagram for Peak filter*

Simulation has shown that one allpass filter can give a phaselag below 180°. This is sufficient for the 130°, but for the 360° three allpass filter is needed, each of 120°. The λ for 130° is 0.9912 and for 120° it is 0.9892.

Two simulation is made to find the word length for the two λ values. A sweep is made for the word length from 1 bit to 20 bit and the error is calculated based on: [Karjalainen et. al., 2000]:

$$\omega' = atan\frac{(1-\lambda^2)sin(\omega)}{(1+\lambda^2)cos(\omega) - 2\lambda} \tag{8.4}$$

The phaselag ω' is calculated for the truncated coefficients and non truncated coefficients and then the error is calculated as the difference. The result is shown in figure 8.17.

It is shown that the coefficients for 130° phaselag could be chosen 11 bit, which gives an phase error of -0.19°. The number of bit for 360° could be chosen to 15, which gives an error of -0.13. However since the embedded multiplier is used, no extra hardware is used when choosing 18 bit, so this is chosen for both coefficients. The phase error for 18 bit is -0.026 and 0.003 for 360° and 130° respectively. The phase error is bigger for 360° since three allpass filter is needed and therefore the error increase three times.

Possible overflow is checked for the block in figure 8.18 Overflow can occur after sub_{xy} and add_{out}. The output of sub_{xy} is the input signal x(n) subtracted with the output signal delayed one sample. Since the output signal is delayed more than 60°, simulation show that overflow can occur. For the add_{out} overflow should not occur since the gain though the allpass filter is one.
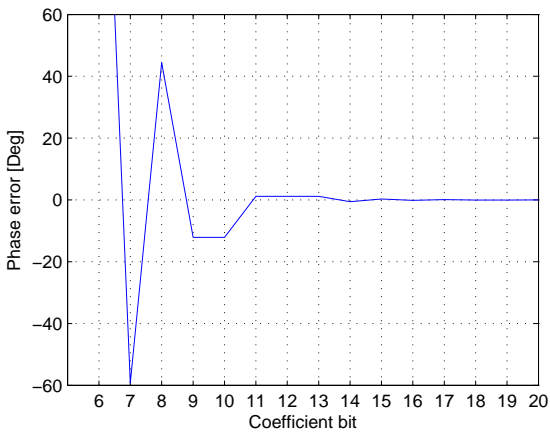
Figure 8.15: *Phase error for the 360° allpass filter as a function bit representation for the coefficients .*

Figure 8.16: *Phase error for the 130° allpass filter as a function bit representation for the coefficients.*

Figure 8.17: *Bit representation for allpass filter coefficient versus phase error*
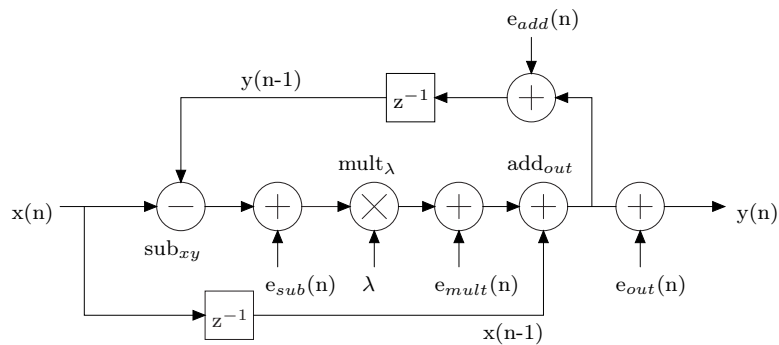
Figure 8.18: *Structure of the allpass filter with quantization point indicated by $e_x(n)$*

The overflow bit for sub_{xy} is added, which means the word length on the output is increased with one.

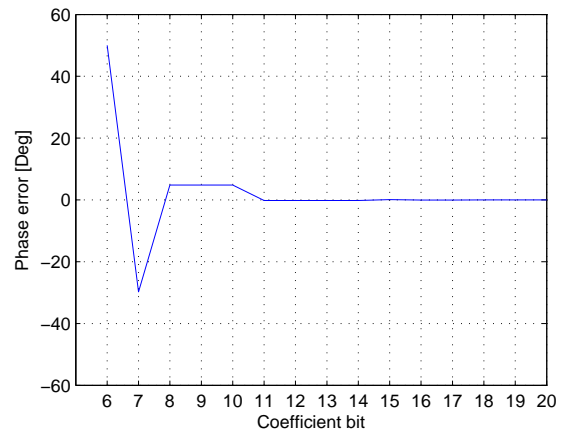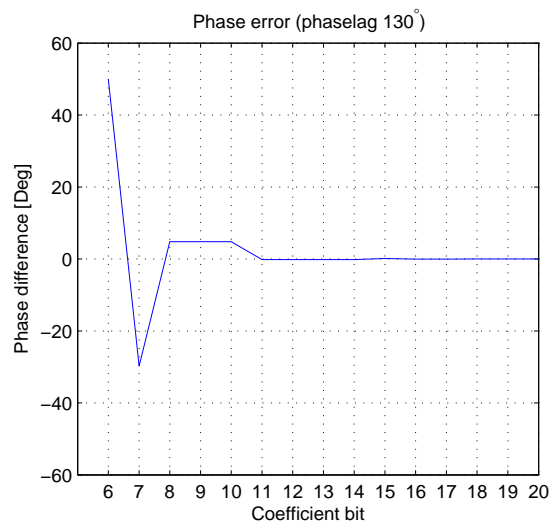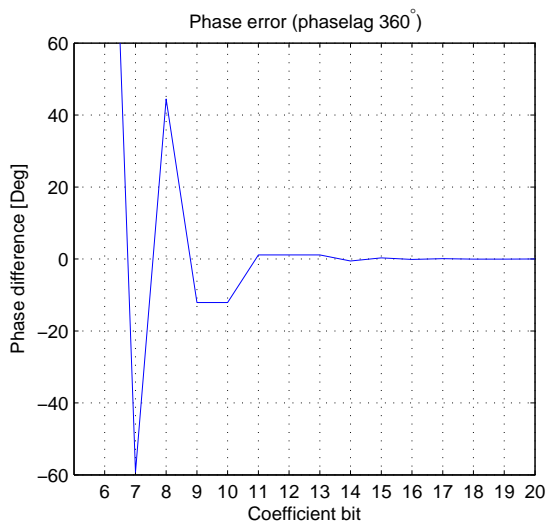The signal quantization is now examined. There are four point where the quantization can be performed marked with the noise addition $e_x(n)$. The output of the allpass filter is truncated to 12 bit which add the noise $e_{out}(n)$. Simulations have been made for the three other position, regarding phase and gain error. No significant difference was shown and so it has been chosen to quantize at $e_{mult}(n)$, to save hardware in the following blocks. The simulation for quantizing at $e_{mult}(n)$ is shown in figure 8.19 and 8.20 for respectively phase and amplitude error. The y axis is the amplitude level given in bit and the x axis is the word length after quantization. The percentage error for the phase and amplitude is shown as color, where dark blue indicates approximately 0% percent error and dark red indicates above 5 % error. The word length after quantization is chosen to 19 bits since it gives an error below 1 % down to an amplitude length of three bit. The bit length are reduced to 18 bit at y(n), since the fraction point is moved back down, from the overflow in sub_{xy}. The LSB is also removed after sub_{xy} to keep the word length below 18 bit, which reduce that hard in the multipliers significant.

Figure 8.19: *Phase error indicated with color as a function of the signal amplitude given in bit and the number bit of after truncating in the allpass filter.*

Figure 8.20: *Amplitude error indicated with color as a function of the signal amplitude given in bit and the number bit of after truncating in the peak filter.*

The design of the allpass filter is now made, the next stage is verifying that the maximum frequency for the block is above 10 MHz. From figure 8.18 it can be seen that the critical path is through sub_{xy} to add_{out}. The estimated maximum frequency in Quartus II is 117.6 MHz and it is controlled by the propagation delay from the output of DFF for y(n-1) to the input of the DFF. Since the requirements are kept no further timing analysis is performed.

To verify that the allpass filters work the design is simulated in Quarts II and test on the FPGA. The test in Quartus II is made with a random input vector and then the output vector is compared with Matlab, as described earlier. The test in the FPGA is made with the sinusoid of 300 Hz. The first test showed that the output number in Quartus II corresponded with the output in Matlab. The second test performed on the FPGA board is shown in figure 8.21 and 8.22. The signal for 360° is changed to make sure that it perform 360° and not just 0°. It can be seen that the signal is shifted as desired.

The units used for the allpass filter is shown in table 8.2 and the Quartus II block diagram can be in 8.23.

Block	Units
mult (18x18 bit)	2 X 9 bit embedded mult
sub (18 bit)	18 Combinational Logic
add_{xy} (19 bit)	19 Combinational Logic
$DFF_{in,out}$ (12 bit)	24 register
$DFF_{x1,y1}$ (18 bit)	36 register
Total	2 X 9 bit embedded mult + 60 register + 37 Combinational Logic
7 x allpass filter	14 X 9 bit embedded mult + 420 register + 259 Combinational Logic

Table 8.2: *Resource usage for allpass filter*

Based on the two tests the allpass filter is verified to work satisfactorily.
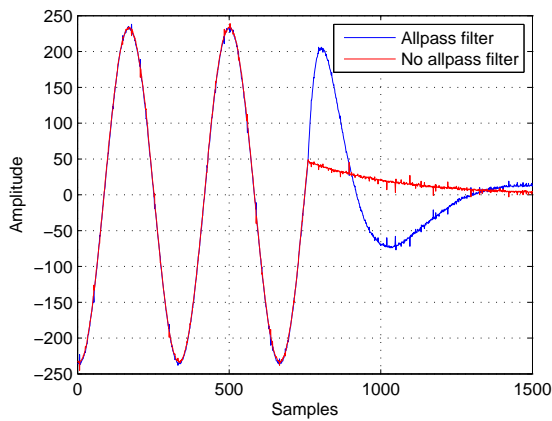
Figure 8.21: *Measurements on 360° allpass filtered signal compared to measurements on non filtered signal. The amplitude of the signal is changed to check that it is 360° and not 0°.*
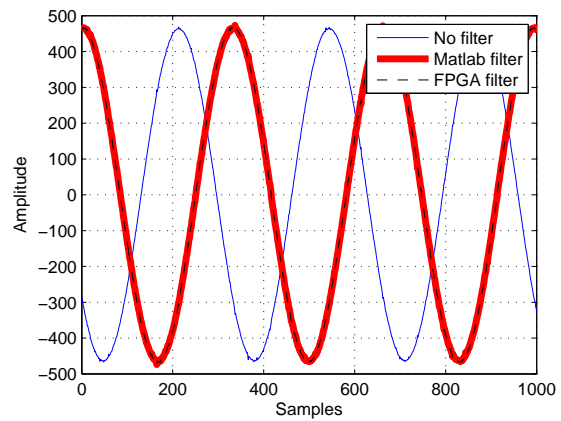
Figure 8.22: *Measurements on 360° allpass filtered signal compared to non filtered signal.*
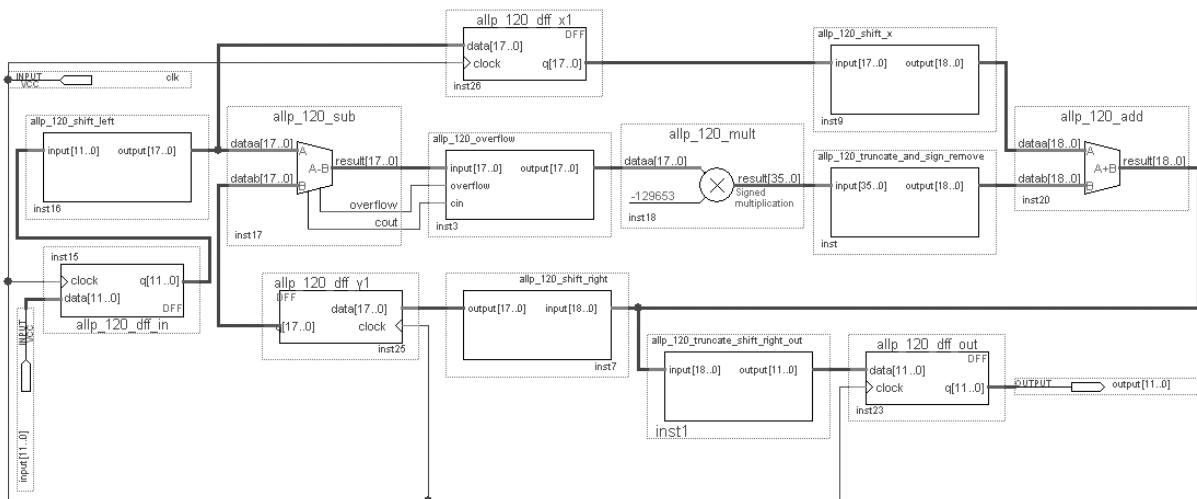
Figure 8.23: *Quartus II schematic block diagram for Allpass filter*

8.2.4 MAC

In this section the implentation of the four correlation function is described.

The truncation and overflow will be examined for this block. The correlation function is last verified if they work. In figure 8.24 the structure of the MAC is shown. No coefficients are needed for this block so overflow and truncation is described. The adder for this block will make overflow since the signals are being accumulated. It is this block where the sample rate is being reduced. The sample rate before and after is 10 MHz and 100 Hz, and based on this the block should accumulate 100000, before resetting the accumulator. Since 100000 values are being added together overflow will occur several times. To avoid overflow the maximum value of the 100000 addition should be estimated. The maximum value can be calculated by multiplying two identical sinusoid with amplitude one sample by sample and the sum all the product. The sinusoid in the system is 30 kHz with sample frequency of 10 MHz and the length is 100000. This yields a maximum result of 50000, which can be represented with 17 bit. In addition to the seventeen bit 24 bit should also be added, since it is the word length after multiplying the two input signal. This gives a maximum word length of 41 bit. The calculation is made for autocorrelation, which yields the highest value. The value for the two cross correlation will typically be smaller, but the maximum value is given by an exact correlation between the two signals, which means that the cross correlation is identical to the auto correlation. For that reason 41 bit is also used for the two cross correlation.
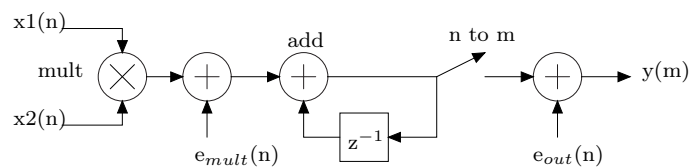
Figure 8.24: *Structure of the MAC with quantization point indicated by $e_x(n)$*

The next stage is the quantization of the signal. There are two quantization point in the block diagram $e_{mult}(n)$ and e_{out}. If quantization is made at $e_{mult}(n)$ the error will be accumulated 100000. In figure 8.25 and 8.26 the phase and amplitude error is shown. The x-axis is the word length after truncation and the y-axis is the amplitude range given in bit where 12 bit equal full range. Based on the figure it is possible to truncate a couple of bit and still get a low error for the phase and amplitude. It is however chosen not to truncate since the gain is only two 1 bit registers for the DFF and two logic blocks for the adder. It is chosen to truncate the output of the MAC to 32 bit, since it fits the data type of a double in the Nios II processor. Simulation is made to verify that error is not introduced when truncating at 32 bit, the result is shown in figure 8.27 and 8.28. It can be seen that there is approximately nothing lost in the phase and amplitude estimation because of the reduction to 32 bits

The MAC is now designed and the maximum frequency will be verified. The critical path is through the mult and add blocks. The maximum frequency is 136 MHz, this is the path for the output on the input DFF to the input of the accumulator DFF.

The MAC will now be tested. Two tests is made, one with Quartus II vector waveform file and one on the FPGA board as described earlier. The first test is made by applying two stimulus vectors to the MAC block, one for each input and then comparing the output with a Matlab
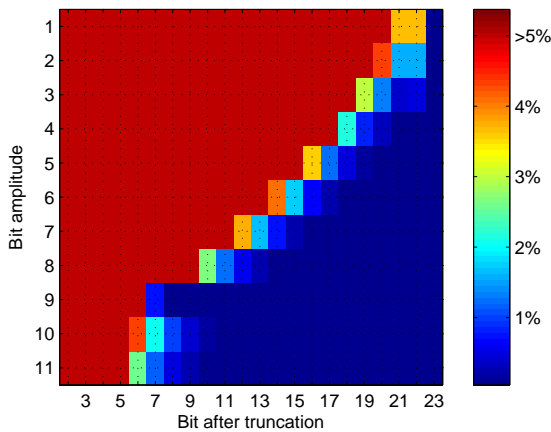
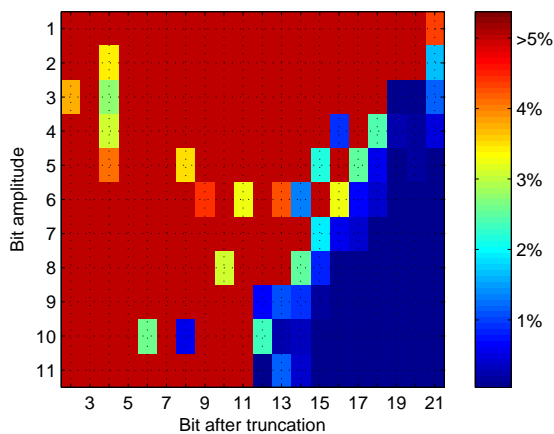**Figure 8.25:** *Phase error indicated with color as a function of the signal amplitude given in bit and the number bit of after truncating in the MAC.*
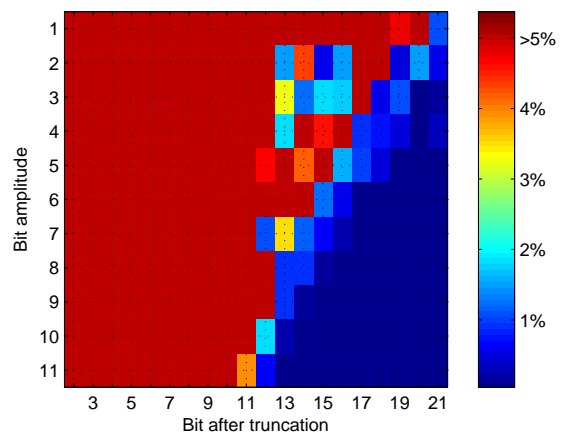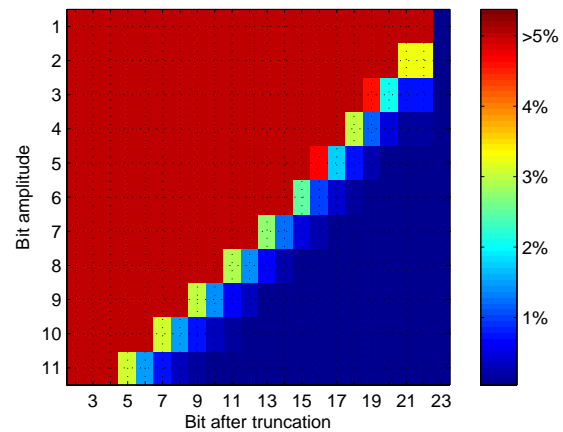

Figure 8.26: *Amplitude error indicated with color as a function of the signal amplitude given in bit and the number bit of after truncating in the MAC.*
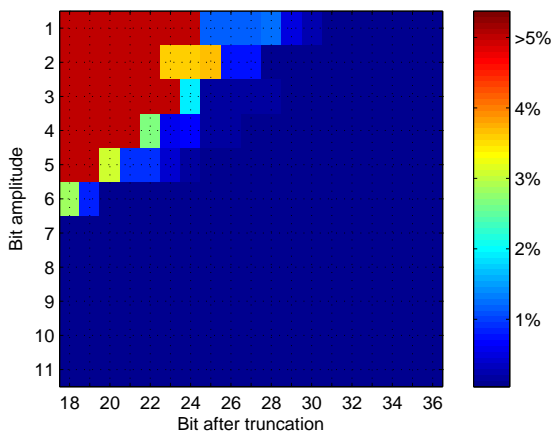
Figure 8.27: *Phase error indicated with color as a function of the signal amplitude given in bit and the number bit of after truncating the output of MAC.*
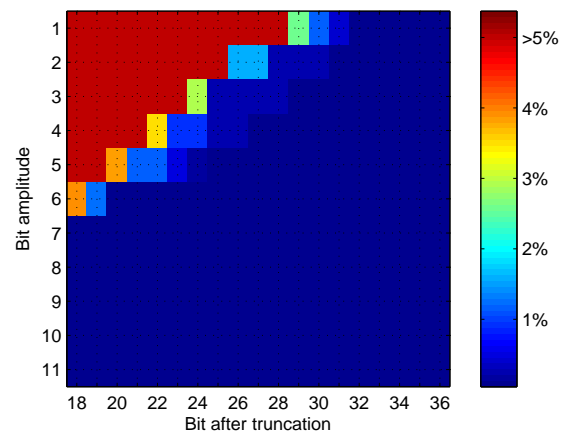
Figure 8.28: *Amplitude error indicated with color as a function of the signal amplitude given in bit and the number bit of after truncating the output of the MAC.*

simulation. A puls is also applied to the accumulator DFF to verify that it resets. The test on the FPGA with the sinus of 300 Hz and the MAC is reset for each 1000 samples.

The first test showed that the FPGA and Matlab implementation were identical. The result of the second test is shown in 8.30. It can be seen that the sequence of the FPGA and Matlab is approximately the same, there are a little deviation, but the FPGA is also compared with the true MAC implementation, which means no truncation is made for the Matlab implementation. It can be seen that the MAC is reset for each 1000 samples and there are six humps within each 1000 samples which correspond to the zero crossing area for the three sinusoids periods. The error of the output values before reset, which is the value used in the final implementation, was approximately 0.02 %. Based on the tests, the MAC block is working properly.

In table 8.3 the resource for the MAC block is shown and the Quartus II schematic file is shown

in 8.29.

Block	Units
mult (12x12 bit)	2 X 9 bit embedded mult
add (40 bit)	42 Combinational Logic
$DFF_{in1,in2}$ (12 bit)	24 register
DFF_{acc} (41 bit)	41 register
Total	2 X 9 bit embedded mult + 65 register + 42 Combinational Logic
4 x MAX	8 X 9 bit embedded mult + 260 register + 168 Combinational Logic

Table 8.3: *Resource usage for MAC*
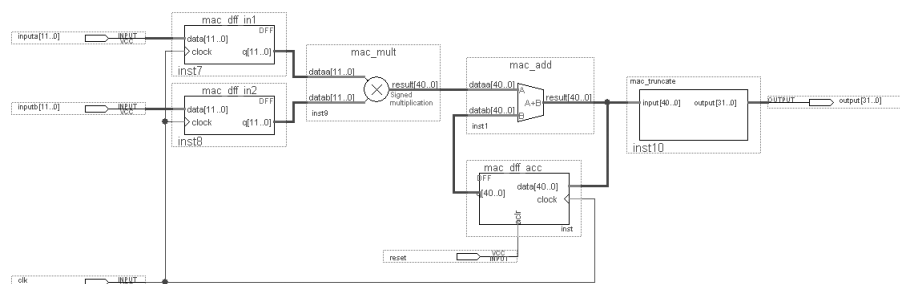
Figure 8.29: *Quartus II schematic block diagram for MAC*
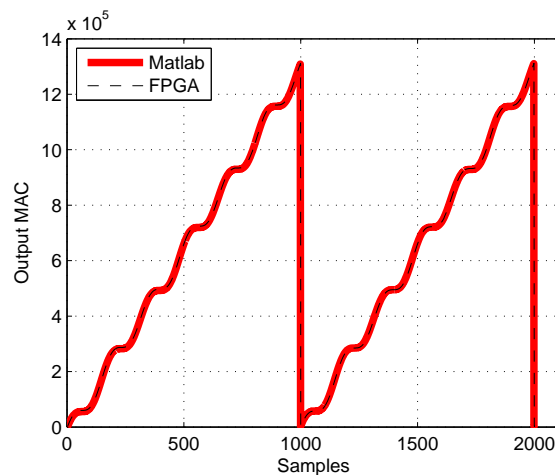
Figure 8.30: *Measurements performed on the FPGA MAC compared with Matlab implementation of the same signals.*

8.3 Nios II

In this section the NiosII processor is described, which is a general-purpose processor that can be implemented on the FPGA and communicate with hardware on the FPGA. It is desired to integrate a general-purpose processor on the FPGA, since some of the algorithm is run at low frequency and use non basic arithmetic. This will reduce the development time since the algorithm can be written in C.

The NiosII processor can be implemented in Quartus II with the SOPC (system-on-a-programmable-chip) builder. It as a graphical interface where the processor can be designed and the interface for peripherals can be connected.

There are three different Nios II processor: economy, standard and fast. In this project it chosen to use the fast processor to make sure it is fast enough for the algorithms. The main specification for this processor is:

- System clock 50 MHz

- Six stage pipeline

- Configurable data and instruction cache

- Branch predict

- Hardware divide

- Single cycle hardware multiply

To be able to debug the processor a JTAG debug module (Joint Test Action Group) needs to be added to the processor. There are four different debugger levels, where in this project level two is chosen. This gives the ability to download software, insert software/hardware breakpoint and trigger data. The higher level of debug the more logic elements is needed.

To optimize the processor for floating point operation, additional hardware can be added. Since all operation in the Nios II processes has been chosen to be floating point, this hardware is added for the processor.

After the processor is configured, interface for peripheral units should be added. First memory needs to be added for the program and data. Both on-board memory and SRAM is used in this system, since there was not sufficient on-board memory for the implementation.

To receive data from the custom hardware, which means the output of the MAC, four 32-bit parallel input is added. There are also added an input for data ready signal and for saturation indication. Two output ports are made for indicating that data has been received and to see how much of the processor time is used. The amount of processor time is done by setting the out high when entering an algorithm and then set it low again, when it exit.

To be able to write characters between the PC and FPGA board a JTAG UART is added.

In figure 8.31 the connection between the interface and Nios II is shown. The interconnection is made with the Avalon switch fabric which can be seen as a bus. The Avalon switch fabric allow for multiple master transaction, which means that more masters can use the Avalon switch fabric, as long as it is not for the same slave unit.

When the processor and interface is added, the program generates a hardware design and the Nios II processor can be inserted in the schematic diagram in Quartus II as a block.

When the Nios II block is connected, the design needs to be compiled and the image file should be downloaded to the FPGA. It is now possible to download a program, written in for example C, to the Nios II processor, this is done with the Nios II IDE program. This program works as an editor, C/C++ compiler, and debugger.
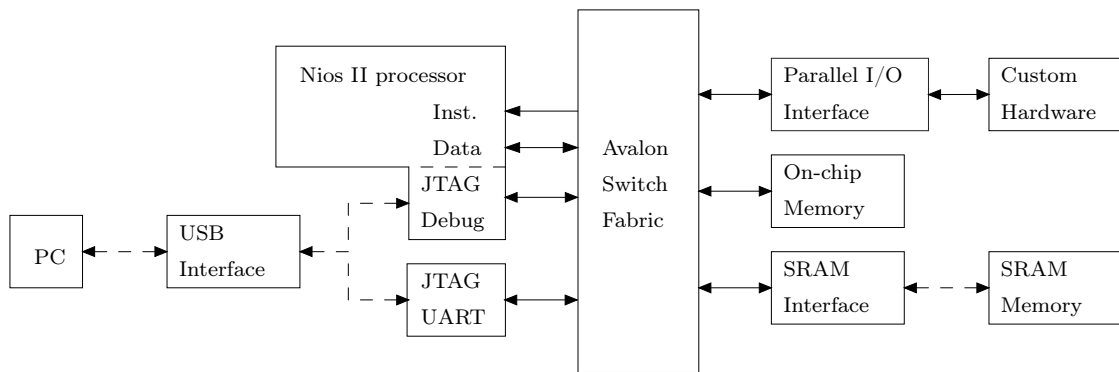
Figure 8.31: *Block diagram for the Nios II*

In the Nios II IDE a new project is first made where the SOPC system build file (ptf) for the Nios II processor is specified. This file contains all the information about the Nios II processor which has been designed. The program make three folder one for the C/C++ project, one for details about the specific NiosII system and one folder containing link to source code for all the Altera components, which is used during debug. When the code for the Nios II processor is written, the project can be build and the image file downloaded to the Nios II processor. Since there is not enough memory on the on-chip memory, the program and data memory needs to be relocated to the SRAM which is done in the system library. Since it is desired to save some of the data processed in the FPGA to a file, Altera Host based file system needs to be added. This allow one to read and write files to a PC in debug mode, which can be used for saving the phase and amplitude sequence and then plot them in Matlab.

8.3.1   System integration

In this section the connection of the blocks to the final hardware system is described. This includes the two peak filters, the three allpass filter and the four MAC described in the three previous subsection. There are also some control interfaces to make the block interact properly. An A/D saturation block is also described which alert the system if the input signal saturates the ADC.

After the signal from the transmit and receiver coil has been sampled with the A/D converter and passed through to the FPGA board the two signal enter the MSB converter as described in 7. When the MSB has been inverted, to make it two's complement, the signals are ready for processing. The system is using pipelining, which are made with DFF around the system. So for each input of the A/D converter, a new sum is produced at the MACs, which are the last blocks. The output value does however not correspond to the input, there are a delay depending on how many DFF is used. The DFF's are controlled by the same clock as the A/D converter. It has been chosen to use samplerate of 10 MHz. The FPGA has two onboard clocks one running at 50 MHz and the other 27 MHz. It is chosen to use the 50 MHz clock and then divide by five, which is done with one of the four integrated PLL. The implementation of the PLL is made with a megafunction provided by Altera. First the two signals enter the peak filter to remove signals outside 30 kHz plus the modulating signal. The next blocks are the three allpass filter for the two auto correlation function and the cross correlation function. The five other input signals for the correlation function must be delayed to compensate for the latches in the allpass filter.

The allpass filter with phaselag 360° has the most latches. It has two for each of the three 120° allpass filter, one for the input and one for the output, which yields a total delay of six samples. All of the signals from the peak filter to the four MAC needs to have a delay of six samples plus the desired phaselag in the allpass filter. The five signal without the allpass filter passes through a delay block, written in VHDL, which delay the signal six samples. The allpass filter with phaselag 130° has only two delay element and therefore the output of the allpass filter is delayed four samples before enter the MAC block. The four MAC blocks have in addition to the input signals and clock signal, a reset input, which reset the MAC function and thereby control the down conversion of the clock. The reset needs to be a short puls since the MAC is set to zero as long as the clock is high. The reset puls are made from the output of the PLL which has a frequency of 10 MHz. Since a frequency of 100 Hz is desired as input to the Nios II processor, the puls generator, which is written in VHDL, counts to 100000 and then set the output high. On the next rising edge of the input clock the output is set low again, which makes a short puls. The outputs of the MAC blocks are connected to four DFF which latches data on the rising edge of the puls. It has been checked that data are latched before the MAC reset. The puls is also latched in a DFF as it can been seen on the figure **FiXme**: *overordnet diagram from quartus i bilag.*. The output of the latch is connected to an input of the Nios II processor, which is used to indicate to the Nios II that new data are available. Then Nios II receive the data from the four DFF after the MAC and reset the data ready DFF, by setting an output of the Nios II high, which is connected to the DFF. As shown on the figure an OR gate is used for the puls and out of the Nios II processor, so when one of the signals is high the DFF is set.

To utilize the range of the A/D converter for small metal object, the signal from the receiver coil is adjusted so it almost utilizes the range when food product is passing though. This means that if the metal object is large, they will saturate the A/D converter and the system discards the product. To detect saturation a block is made in VHDL, which set the output high if one of the two signals from the A/D converter is maximum for 10 samples, which mean -2048 or 2047. The signal is passed to the Nios II processor and held high until the Nios II reset after reading it.

8.4 software

This section is about the software implementation. The section will not go deep into the implementation of the algorithms shown in algorithm design as they are quite simple in a software implementation. The main focus will instead be laid on the communication between the hardware and the software and the overall control of the software running on the system. The hardware/software communication will obviously have to be very hardware near and will explain the exchange signals used. The software control will look more into the handling of startup problems and how to handle the different algorithms used in the implementation.

8.4.1 Hardware/Software communication

The first part is to choose between the use of interrupt or polling to control when the software has to collect new data. Interrupt control has its great advantage when a system has non realtime processes which needs to be run when there are time to do so and let the realtime code run when an interrupt occurs. This may be an advantage if a online training algorithm are implemented

later on, however it is not necessary for the implementation of the prototype, where nothing else than the realtime algorithms are implemented. This is due to the fact that the system has to be able to calculate everything before the next sample occurs and therefore the system must have a some spare time where it can wait in a polling loop for the next sample time. The hardware has a dedicated one bit register which are set high when data are ready. The register are connected to the avalon interface and this register are read from the software in the polling algorithm. The results from the mac units in the calculations are put in a register and the mac units are reset, when the sampling clock goes high with the one bit register telling the system that data are ready. When this is seen the software breaks out of the polling loop and reads the data in the registers. When the software has read the data registers it will reset the control register indicating if data are ready and thereby ending the read cycle.

8.4.2   Software control

The software control are divided into three major parts. The first part is the setup of all the global constants and variables in the system. The next part is the initialization of the filters for ballancing. This part takes 15 seconds because the filters has a long settling time. The setup of these filters are simply done by running a loop similar to the one in the running mode but without calculation of alignment and pca, because these calculations are after the filter. This can be seen in figure:8.32

The functions implements the functions described in the algorithm design. The control of the data in the data buffer for the alignment function are controlled by the function itself, which means that it is only necessary to give it the pointer to the array and it will handle the rest. This is done to enable a the same interface even though the function are changed in a new revision. The pca function does calculate the small linear transformation for each of the classes and checks if a given data point belongs to one of the classes, which is indicated in figure:8.32
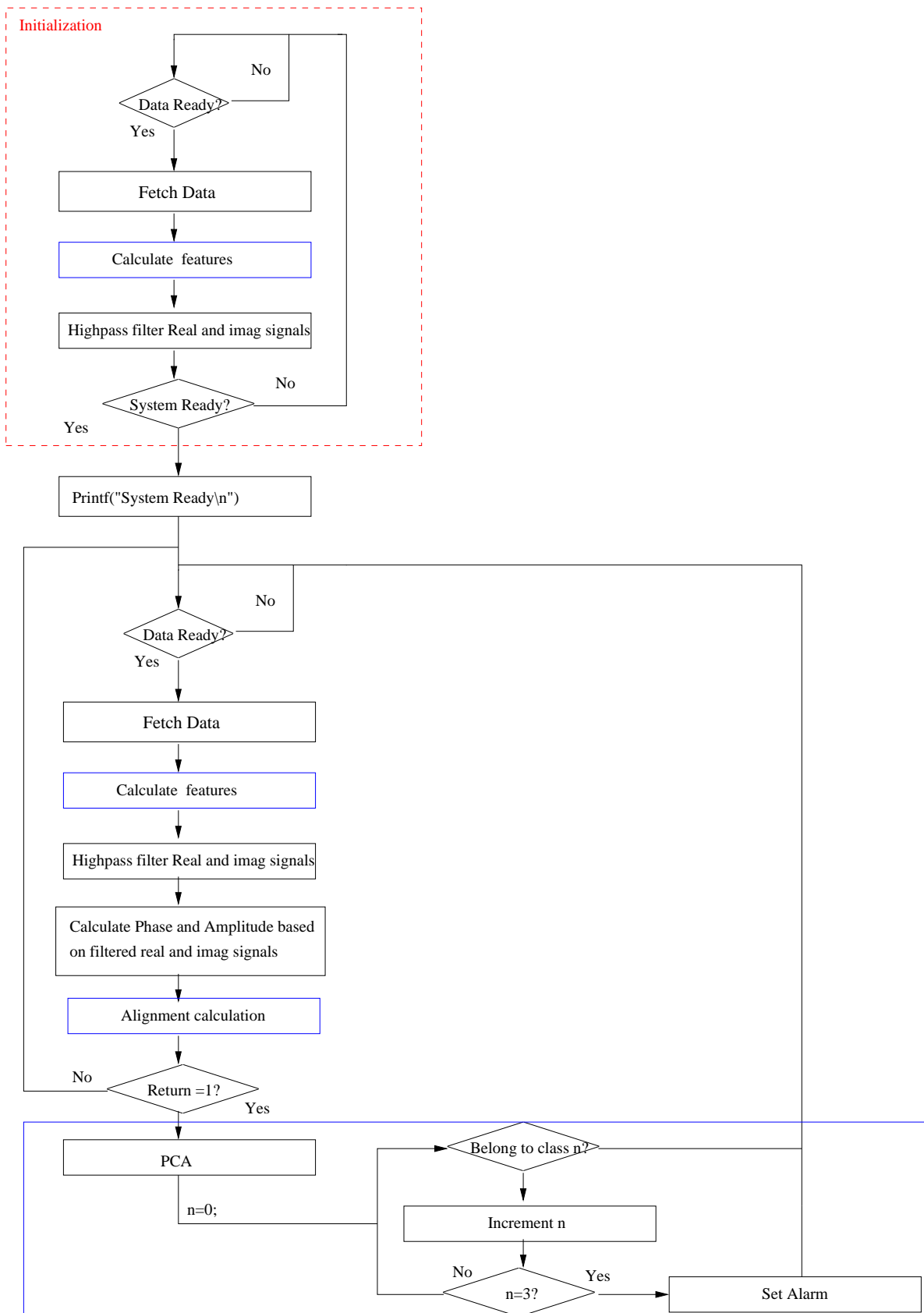
Figure 8.32: *This figure shows the software flow of the system. Everything inside a blue box are handled as a function*

Chapter 9
System test

The purpose of this test is to examine and document the systems ability to make a correct detection. This means that it has to make a correct detection in the case where there are nothing on the conveyor belt and in the case where there are either a product, a metal object or both on the conveyor belt. A classification are seen as succesfull if it classifies that a metal object has passed, when and only when a metal object passes. This means that regardless of products inside the system it should classify correctly. During this test there will be distinguished between the classification by the pca and the classification given by the overflow control on the system. This is done to reduce the number of tests, because there are no doubt that the system will catch the situations where an object gives an overflow. The reduction are made as follows. A metal object that has passed through the metal detector 5 times in a row placed at the middle of the conveyor belt and given a warning of overflow will not be tested any further and larger objects of the same metal will not be tested as they will also give an overflow and thereby be detected. The testing of the rest of the objects are made by letting 25 pass the system and count the number of correct and the number of faulty classifications. The placement of the objects on the conveyor belt should be made random or at least as random as possible, when they are placed on the conveyor belt by a person. The test results for the tests where the objects are not mixed, are listed in table:9.1. The results for the mix between popcorn and the metal objects are listed in table:9.2

9.1   Systemtest Conclusion

The result of the tests are that the system are able to find metal pieces over a certain size. When the sizes decreases it becomes a problem it first becomes a problem to see the objects when they are mixed with the product. The only difference for this whas the 3.5mm bronze piece which mapped clossely into the same region as the popcorn, but whas clearly visible when it was mixed with the popcorn because the mixing made the difference. The tests did not reveal anything surprising as the early analysis with the classifier stated that it would be impossible to see the smaller objects. The test results did show that the feature signals from the 2mm Bronze and AISI 304 was hidden in noise. It may be possible to find these signals with a slight improvement of the feature extraction, however it is quite clear that it will not be possible to find them inside the product unless the variance on the products are reduced.

Test Object	Correct	Faulty	Overflow	Nothing detected
Nothing	25	0	-	25
Popcorn	24	1	-	0
Iron 1mm	25	0	-	0
Iron 2mm	25	0	-	0
Iron 5mm	-	-	X	0
Iron 10mm	-	-	X	0
AISI 304 2mm	0	25	-	25
AISI 304 3mm	25	0	-	0
AISI 304 5mm	25	0	-	0
AISI 304 10mm	-	-	X	0
Bronze 2mm	0	25	-	25
Bronze 3.5mm	?	?	-	0
Bronze 5mm	-		X	0
Bronze 10mm	-		X	0
Alu 2mm	25	0	-	0
Alu 3mm	25	0	-	0
Alu 5mm	-	-	x	0
Alu 10mm	-	-	x	0

Table 9.1: *The table shows the results from the tests where the product was not mixed with the metal objects. Row with nothing detected indicates if a faulty classification happened because the object was not detected in the alignment algorithm.*

Test Object	Correct	Faulty	Overflow
Iron 1mm	9	16	-
Iron 2mm	25	0	-
Iron 5mm	-	-	X
Iron 10mm	-	-	X
AISI 304 2mm	20	5	-
AISI 304 3mm	25	0	-
AISI 304 5mm	25	0	-
AISI 304 10mm	-	-	X
Bronze 2mm	0	25	-
Bronze 3.5mm	22	3	-
Bronze 5mm	-		X
Bronze 10mm	-		X
Alu 2mm	25	0	-
Alu 3mm	25	0	-
Alu 5mm	-	-	x
Alu 10mm	-	-	x

Table 9.2

Chapter 10
Conclusion

The first major part of the project was to understand the mechanisms of the transducer in the detector head. This was done with a thorough analysis the parameters, which affects the signal strength in the transmit coil of the transducer and the parameters affecting the receiver coils ability to obtain the signals. Most of the parameters, for which it is possible to make adjustments has been shown to give a benefit in one place, while they reduce the performance in another. This means that the transducer ends up being a compromise on the parameters, which has an effect. A great improvement was made on the transmit coil and the receiver coils with a resonance circuit.

The next part has been an analysis on different types of material and how the different types of materials will behave inside the transducer. A model from a similar system used for mine detection was found, as this model was made for a different setup it needed to be tested with real measurements. These tests showed that the model did not differ significantly from the reality. The inputs to this model is the parameters of a given material and the output is a transfer function for the link between the transmit and receiver coils. The model does show that materials with magnetic properties are easy to see at low frequencies while materials that are able to conduct an electric current gives a stronger signal at high frequencies. As the product are the only known material it will be an advantage to choose the frequency where the product gives a small signal so it becomes less significant. The size of the object that needs to be found has a high significance on the amplitude of the signals obtained from the transducer, as it increases with the square of the radius on the object. What was more surprising was that the size of the object may affect the phase as well.

The next major phase of the project was to create the analog hardware which were needed to obtain the signals from the coils. This included a power amplifier on the transmit side to cope with the high currents for the transmit coil. On the receiver end it was necessary to build a voltage amplifier system with a high gain as the signals measured on the receiver coils was in millivolts. This amplifier needed to be an instrumentation amplifier because it gives a high gain with a small introduction of noise. The early model of this system used a PC sampling card for which a small program was created to obtain some measurements for analysis in the application part of the project. The construction of the analog hardware and the software for the sample board were not the scope of this project, but it proved necessary to create it, in order to obtain some signals for analysis. The analog hardware does prove to be a limitation for the choice of frequency, even though it did take some time to create. The first measurements which were made with this system proved to be time consuming because it took a great amount of time to adjust some small metal pieces inside the transducer to make up for the unbalance between the receiver coils.

The next part of the project was the application part which are divided into two parts. The first part was the feature extraction of the gain and phase from the transducer head. Several different methods were examined and tested. The variety of these methods spanned both time and frequency based estimation methods, where some methods where known methods and some

was created from scratch. One of these methods was the adaptive allpass filtering which was not as good as all the other methods when it came to feature extraction, but it did give the idea for the electronic balancing system for the transducer. The methods were thoroughly tested with respect to varies design parameters to span a multidimensional space which had the different feature extraction methods as one dimension and the design parameters to be the rest of the dimensions. The tests did generally prove that the best method, was an improved version of a the cross correlation method. The second part of the application design phase was the classification based on the features. Two methods were attempted where the first method tried to filter the features from the product out of the signals, by using that the feature vector should point in a constant direction for the product. The second method was a classic principal component analysis. The principal component analysis method was chosen, as it proved to give fairly good results and it proved difficult to make the filtering work. This problem occurred because the product did not follow the rule of the feature vector pointing in the same direction. The exact course of this was not discovered, but it is believed that the product consisted of several different materials, where they gave a different response. The choice of classification method concluded the application design phase of the project.

The next phase of the project was to map the chosen application to an algorithm. The operations for each algorithm are identified, and a flow for different algorithms are shown. The abstraction level are taken to a lower level in the algorithms, but as the algorithms has a low complexity there are no need to spend a lot of time on different ways to calculate them. The training of the classifier will need some work at this level as a eigenvalue problem has a high complexity, but this was not done as an online training of the classifier was not made. The lower abstraction level of the algorithms has the advantage that it is easy to identify the different samplerates throughout the system and thereby identify which part of the system that are heavy on calculations. This is useful in a hardware/software co-design where it is necessary to choose if a certain part of the algorithm has to be implemented in hardware or software. The choice of an implementation on a FPGA rather than a DSP was made mainly to gain some experience on this kind of platform. This may prove to be a great advantage if an implementation of an online training algorithm is to be made, because this enables the opportunity to create a hardware accelerator to solve the eigenvalue problem.

The last phase in the design was the architecture level. It was chosen to use the standard building blocks from the quartus environment as much as possible. This choice was made because these blocks were already made and optimized for the platform, making it difficult to create a better design. This made it possible to put the focus on the quantization of internal variables and filter coefficients, which are equally important because it gives the possibility to optimize the system to use as few bits as possible and thereby reduce the costs. Simulations with the possibility to adjust the wordlength of the variables for each of the filters in the system were created. These simulations were used as a basis for the choice of wordlength on the internal variables of each of the filters. The main focus on the software implementation were made on the communication link between hardware and software and on the communication between the software and the functions implementing the algorithms shown in algorithm design. Each of the blocks in the implementation has been tested individually to see if it performed the operation it was required to before it was integrated with the rest of the system.

The final integration test has been made as a system test were it is tested if the system is able to identify metals and to find the minimum size of these metals for a sure identification. The system does not give a good improvement when it comes to the identification of metal objects that are not mixed with the food. However the place where the system excels is when the metals are mixed with the product, because it does not have a significant loss in performance when they are mixed.

10.1 Perspectives

This section will be divided into two parts. The first part handles the future work that may be done on the system and the second part debates the possibilities of expanding the use of the principles in other applications.

The things that which may or should be improved for before the system are ready for implementation are listed below.

- The current version of the system uses a development FPGA board and several smaller analog extension boards which are all connected with long wires. A print layout of this should be made for the final system were it only includes the parts of the FPGA board which are used in the current implementation. It is believed that the reduction of interconnection wires will give a significant increase in the systems signal to noise ratio.

- Analog hardware which are able to cope with significant higher frequencies could be made to increase the system frequency.

- As the bandwidth of the signal are significantly lower than the carrier frequency it could be examined if it is possible to obtain similar good results if the signals are mixed down to a lower frequency before they are sampled.

- A mechanical solution could be made to ensure that the product lies in a similar fashion on the conveyor belt and thereby reduces the variance from the positioning of the product.

- Automated balance and online training should be made to decrease the amount of maintenance on the final product, which eventually will reduce the cost.

- The detector head may be improved as it has been shown that a change in impedance due to a change in the coils may be cancelled by a resonance circuit.

As the system has the ability to classify material properties of an object it may be possible to use the system as a test system which has to verify if a product lies within specification limits on their material properties.

Bibliography

[ad844, 2003] Analog Devices. Opamp ad844.
    URL: `http://www.analog.com/UploadedFiles/Data_Sheets/AD844.pdf`. January, 2008.

[AD9220, 2003] Analog Device. Datasheet ad9220.
    URL: `http://www.analog.com/UploadedFiles/Data_Sheets/AD9221_9223_9220.pdf`.
    April, 2008.

[ASSDA, 2007] Australian Stainless Steel Development Association. Assda.
    URL: `http://www.assda.asn.au/`. November 2007.

[BC547, 2003] Philips. Npn transistor bc547.
    URL: `http://komponenten.es.aau.dk/fileadmin/komponenten/Data_Sheet/`
    `Transistor/BC547.pdf`. January, 2008.

[BDX33-34B, 1998] SGS-Thomson Microelectronic. Darlington power transistor bdx33-34b.
    URL: `http://komponenten.es.aau.dk/fileadmin/komponenten/Data_Sheet/`
    `Transistor/BDX33-34.pdf`. January, 2008.

[Bruschini et. al., 2000] Claudio Bruschini and Hichem Sahli. *Phase angle based EMI object discrimination and analysis of data from a commercial two frequency system. SPIE AeroSense 2000, Detection and Remediation Techologies for Mines and Minelike Targets.* 2000.

[Demarest, 1998] Kenneth R. Demarest. *Engineering Electromagnetics.* Prentice Hall, 1998.
    ISBN: 0-13-889783-2.

[Duda, Hart & Stork, 2001] C. Britton Rorabaugh. *Pattern Classification.* John Wiley & Sons,
    2001, second edition.
    ISBN: 0-471-05669-3.

[ECT, 2007] Eddy Current Technology Incorporated. Ect.
    URL: `http://www.eddy-current.com/condres.htm`. November 2007.

[Ida, 2004] Nathan Ida. *Engineering Electromagnetics.* Springer-Verlag, 2004, second edition.
    ISBN: 0-387-20156-4.

[ina111, 2000] Texas Instruments. Instrumentation amplifier ina211.
    URL: `http://www.focus.ti.com/lit/ds/symlink/ina111.pdf`. January, 2008.

[ina217, 2005] Texas Instruments. Instrumentation amplifier ina217.
    URL: `http://focus.ti.com/lit/ds/symlink/ina217.pdf`. January, 2008.

[Johnson & Johnson, 1997] John L. Hilbrun David E. Johnson, Johnny R. Johnson and Peter D. Scott. *Electric Circuit Analysis*. Prentice Hall, 1997, third edition.
ISBN: 0-13-252479-1.

[Karjalainen et. al., 2000] Aki Härmä & Matti Karjalainen & Lauri Savioja & Vesa Välimäki & Unto K. Laine & Jyri Huopaniemi. *Frequency-Warped Signal Processing for Audio Applications. J. Audio Eng. Soc., Vol. 48, No. 11.* 2000.

[Kitchin & Counts, 2004] Charles Kitchin and Lew Counts. A designerzs guide to instrumentation amplifiers.
URL: `http://www.analog.com/UploadedFiles/Associated_Docs/404380967COMPLETE_IN_AMP_GUIDE.pdf`. January, 2008.

[Kraus & Fleisch, 1999] John D. Kraus & Daniels A. Fleisch. *Electromagnetics with applications*. McGraw-Hill companies, 1999, fithe edition edition.
ISBN: 0-07-289969-7.

[linkwitzlab Aktive Filters , 2008] linkwitzlab. Aktive filters.
URL: `http://www.linkwitzlab.com/filters.htm#4`. June 2008.

[Oppenheim & Schafer, 1999] Alan V. Oppenheim & Ronald W. Schafer. *Discrete-Time Signal Processing*. Prentice-Hall, Inc., 1999, second edition.
ISBN: 0-13-083443-2.

[PCI-DAS4020/12, 2006] Measurement Computing. Specification pci-das4020/12.
URL: `http://www.measurementcomputing.com/pdfs/pci-das4020_12.pdf`. January, 2008.

[Schwarz, 1999] Steven E. Schwarz. *Electromagnetics for Engineers*. Saunders College Publishing, 1990, international edition edition.
ISBN: 0-03-006517-8.

[Sedra, 2003] Adel S. Sedra and Kenneth C. Smith. *Microelectronic Circuits*. Oxford University Press, Inc., 2003, fifth edition.
ISBN: 0-19-514252-7.

[Ulaby, 2005] Fawwaz T. Ulaby. *Electromagnetics for Engineers*. Pearson Education, 2005.
ISBN: 0-13-197064-X.

AALBORG UNIVERSITY
INSTITUTE OF ELECTRONIC SYSTEMS

New Generation Metal Detector for Food

APPENDIX REPORT

Frank Thornemann Hansen
Lars Vinding

APPLIED SIGNAL PROCESSING AND IMPLEMENTATION

MASTER THESIS

GROUP 1041

JUNE 2008

Appendix A
Measurement system

In this appendix the setup for the measurement system is described. A system consisting of a conveyor belt with appurtenant motor and detectorhead is put at our disposal from Detectronic. The detectorhead is made for 30 kHz and it contains seven windings for the transmitter coil and 14 windings for the receiver. The receiver coil is divided into seven windings on each side of the transmitter, and the two sections are coiled opposite. To operate the system a signal generator is needed for the transmit coil and two amplifiers is desired to fit the input range of the sample board which is ±1 V or ±5 V. In section 2 it was showed that magnetic flux is proportional to the current. A high magnetic field is desired so one is able to detect small object. The signal generators at AAU are not able to supply sufficient current, so an amplifier is needed.

A.1 Power amplifier for signal generator

The power amplifier which is used to supply the sufficient current to the transmitter is shown in figure A.1. It is a class AB which is biased with a V_{BE}, the circuit is from [Sedra, 2003]. The input of the circuit is couple with a capacitor to remove possible DC offset. The opamp work as a voltage amplifier and adjust the signal on the output through the feedback. The opamp is coupled as an inverting amplifier and the gain is controlled by G=-R_2/R_1. An AD844 is chosen for the opamp, since it has a wide bandwidth [ad844, 2003]. The resistors R_3-R_5 plus R_v and the Q1 transistor make up the V_{BE} multiplier. It maintain a voltage equal the V_{BE} voltage for the Q_2 and Q_3 transistor, so to minimize the zero crossing distortion. A variable resistor is used R_V, so one can adjust the voltage. The two transistor Q_2 and Q_3 are working as the current amplifier, and resistor R_6-R_7 reduce the thermal runaway.

An BC547 is chosen for Q_1 since no hard requirement are need [BC547, 2003]. The transistors chosen for Q_2 and Q_3 is BDX33B and BDX34B, since they can supply high current, handle high voltage and they have high current gain at high frequency [BDX33-34B, 1998]. The component used for the current amplifier is listed in table A.1, and they are calculated based on [Sedra, 2003].

R_1	R_2	R_3	R_4	R_5	R_6	R_7	R_V	Opamp	Q_1	Q_2	Q_3
2.49k	10.2k	324	200	1k	1	1	1k	AD844	BC547	BDX33B	BDX34B

Table A.1: *Resistor value for power amplifier*

A.2 Interface for sample board

An interface circuit for the sample board is made so one can control the amplitude of the input signal and to secure the board from high voltage. It is desired to measure the current on the transmitter coil and the voltage on the receiver. The voltage on the receiver coil is a difference and so an instrumentation amplifiers is chosen. The interface circuit is shown in figure A.2. The input for the instrumentation amplifier is coupled with a capacitor (C_1 and C_2) to remove
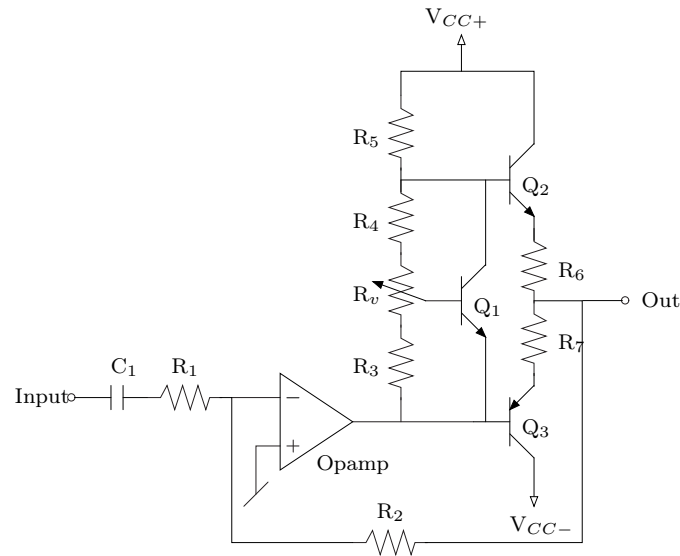
Figure A.1: *Amplifiere for signal generator*

possible DC offset. To avoid the input bias current for the instrumentation amplifiers to charge up the capacitors, a high value resistance (R_1 and R_2) is connected to ground, which enables a small current to flow to ground [Kitchin & Counts, 2004]. The variable resistor (R_V) controls the gain in the instrumentation amplifier. Two different instrumentation amplifier has been used for the project that is the INA111 and INA217. The reason why two different instrumentation amplifiers has been used is that the INA111 was first used to make measurement at 30 kHz, it was however not optimal at 300 kHz, so INA217 was chosen instead, which has a bigger bandwidth. It is desired to have an instrumentation with high gain and high common mode reject, so the received signal can be amplified much. The gain for INA111 and INA217 is respectively chosen as: $G=1+50k\Omega/R_G$ and $G=1+10k\Omega/R_G$ [ina111, 2000][ina217, 2005]. A 10 kΩ logarithmic resistor is chosen. The opamp operates as a non-inverting amplifier with gain given as $G=1+R_2/R_1$. Note that the opamp is only present for the receiver interface, since the signal needs to be amplified much more. A fixed gain of 10 is chosen.

A.2.1 Sample board

It is desired to use a sample board so measurement can be made on the system and one can work the measurement on a computer. Detectronic has set a sample board at our disposal, it is a PCI-DAS4020/12 [PCI-DAS4020/12, 2006]. It has 4 channels and can sample continuous at 20 MHz in two channels and 10 MHz in four channel. We need two channels for the transmit and receive signal and with an operating frequency of 30 kHz and 300 kHz we get an oversample rate of 666.67 and 66.67 respectively, which is sufficient. The resolution is 12 bit and it can measure in two ranges ±1V and ±5V. It yield voltage step of 488 μV and 2.4 mV for respectively ±1V and ±5V, and a min-max ratio of 66 dB. Note however the number of efficient bit is less due to noise.

There was no software included for the sample board, so this has to be made. It is chosen to use Linux and driver from comedy lib, since it is free and should do the job.
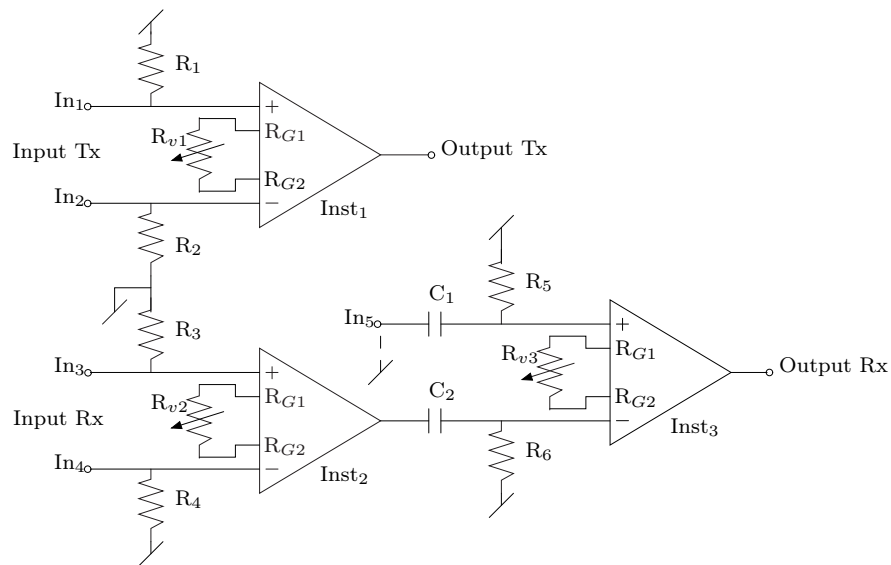
Figure A.2: *Amplifiere for signal generator*

A.3   Measurement program

In this section the program for sampling data is described. The sample board is pci-das4020/12. Two channels are used on the sample board to measure the current on the transmit coil and voltage on the receiver coil. The operating system for which the program run is Linux version 2.6.22-2-686 (Debian 2.6.22-4) and the driver for the sample board is from comedi version 0.7.74.

To get knowledge on how diferent objects behave in the metaldetector and to make qualified tests for the classifier, it is desired to have many measurements. For that reason a menu system has been made to speed up the measurement process and to keep track of the many measurement with expressive names. The program contain two menu, the main menu and the settings menu see figure A.3 and A.4. The structure and features in the menus will now be described.

A.3.1   Main menu

The main menu is shown in figure A.3. In the main menu the measurement to be performed is chossen. The name can be choosen from the predefined names which is for number 7 and above. The predefined measurements name are loaded from a file, which is selected in settings. If the measurement name is not included in the predefined measurement name, an user defined name can type, which is option 3. It is also possible to combine two measument name, which is used when food and metal are mixed, option 4. Option 5 "Multiple measurements" choose from one measurement when off, to multiple measurement when on. This means that when "Multiple measurements" are on, one can performe multiple measurements of the same measurement name. An extention is added to the name, #x, where x is the number of the measurements for that name. The number of measurement for each name is writed to the right of the name, as shown in the menu. This is useful when many measurement are desired for the same measurement type, for example to see if the signal is the same for a given type of obejct. When "Multiple measurements" is off only one measurement can be made for that name. If a measurement is choosen and already performed, a warning apear where one can overwrite or choose antother

measurement. This is useful when only one measurement are are desired for a given type and that measurement should be right. When a measurement of a given name is performed a # is shown, where that numbers are for multiple measurments. The last option, 6, add text to a measurement name in the beginning. The text is shown in the [ ], in figure A.3 "position_" is added in the beginning of the measurement name. This option can be used to indicate the postion of the object on the conveyour belt, how balancing is performed, etc. The measurement data are divided into two files one for the transmit coil and one for receiver coil, tx and rx is added to the measurement name at last of the names. The operating frequency is also added to the file names, which is spicified in the settings menu. The name of the files look like:

```
position_measurement_name_frequency_tx.dat
position_measurement_name_frequency_tx.dat
```

where "`position_`" originate from option 6 "Add to measurement", see figure A.3. It could also be empty.

Figure A.3: *Main menu for measurement program*

A.3.2 Settings menu

To enter the settings menu, option 2 should choosen in the main menu. The settings menu is shown in figure A.4. In the header the current value for the settings is choosen. The option 2-4 control the sample freqeuncy of the sample board, the operating freqeuncy for the transmit coil and the sample time for the sample board. Option 5-7 control the settings of the channels, where option 5 choose between the four avaible channel, the channels should be of pair 0-1 or 2-3. Option 6-7 control the range of the two selected channels, which can be either ± 5 V or $\pm$ 1 V. In option 8 the directory where measurement is saved can changed. A list of current directories is shown from which one can choosen and new directory can also be made. In the last option "Change measurements" the predefined measurements name in the main menu can be changed. A list of files with extension .mes is shown for which one can select. The files contain measurement name which can be choosen from in the main menu. If for example measurements for different kind of meat should be performed, a measurement file named `meat.mes` can be made. In this files the meat to be measured should be listed, one name on each line, and then saved in the main directory. When option 9 is choosen `meat.mes` will be listed, and one can choose this file. When one return to the main menu the name from the `meat.mes` files will be listed under predefined measurements. This feature help to plan the measurements before one start

to meaure and it also makes the measurement names more consistent, and of cource it makes the mesurements easier. When the settings menu is quit the settings is save in a file named `settings`. Each times the program started the settings is loaded, so one keeps the same settings as last time the program was run.

Figure A.4: *Settings menu for measurement program*

A.3.3 Program flow

In this section the program flow will be described. A flowchart for the program flow is shown in figure A.5 and based on this, the program flow will be described in more detail.

When the program starts variable are initialised and settings are loaded from the settings file, which was mentioned in the settigs menu. The program enters the main menu, which run in an infinite loop that can only be quit with option 1 in the main menu. For all selection in the main menu and settings menu the input is verified to be within the valied numbers. If numbers or characters outside the valid range is choosen, the input is ignored and new input can be choosen. When user defiend measurement are defined, the user can input the name desired and the program start to measure. The user can also type b to go back. When multiple measurement are choosen, option 4, the main menu is updated, and the user can only select between the predefined measurements or select option 4 to go back. When a predefined measurment are selected the main menu update, and the user can selct the second predefined measurement. After the second measurment is selected the program start to measure. The two predefiend measurements are combined with a "+" between the names.

When measurement names are selected from either option 3,4 or options above 6, the program starts the measuring process. First information are printed with about the sample freqeuncy, sample time, the size of the data files and what channels are used. Then an array for the data is initilized, where the data from the sample board is stored. The samples from the two channels on the board are placed interleaved. The first eight entries in the array are used as header to store: samples freqeuncy, sample time, range for channel and the operating frequency for the two channels.

Afterwards the board is also initlized with the selected sample frequency, the amount of data to sample, channels and the range for the channels. Then the measurement board is opened and
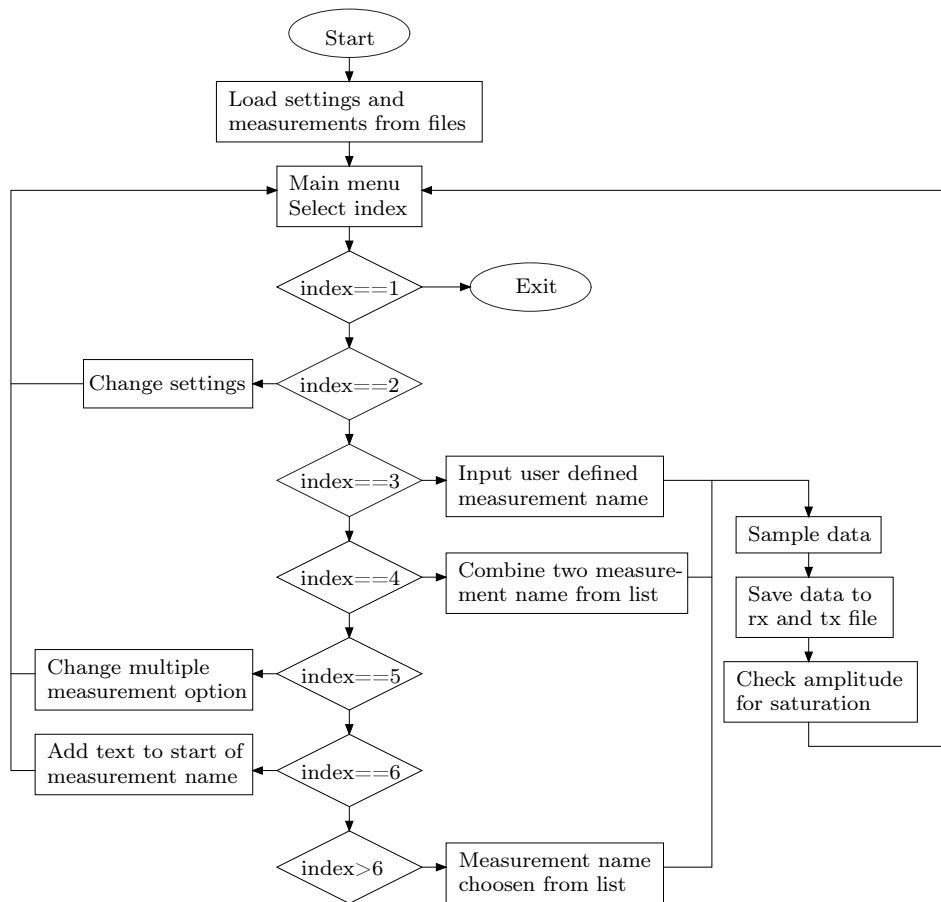
Figure A.5: *Flowdiagram for measurement program*

data are sampled continus to the data array until the data received correspond to the samples freqeuncy times the sample time times the number of channels. The sampling process is run in a while loop which run untill the data received execced the data size. Each times the while loop runs data are receiver from the board and if no data are received from the board the measureing stop since data are not sampled fast enough by the sample board. If for example the mouse is moved while sampling the sample board often can sample data fast enough. To minimize this effect the program should be run with a higher prioty then other process in linux, in this project the pritoy is set to -10 by the command `nice`.

When data acquisition is finish, the data are stored in the two files for transmit and receive, with that names selected in the main menu.

Last a test is made to see if the input signal satuate according to the range of the board. The signal is divied into 5 segments and then minimum and maximum value are found. The minimum and maximum value are converted to voltage and printed to the screen, and the percentages of the amplitude according to the range are also printed to the screen. From these information one can see if the signal satuarete and if it involes the hole signal. The program stop after this test and wait for the user to hit enter to return to main menu.

The interface and flow in the measurement program has now been described. A menu system has been used to ease the performance of the measurement and to ensure a good structure of the measurement files. The code for the program is included on the CD **FiXme**: *Fil skal på CD*.

Figure A.6: *Information when performing measurement*

Appendix B

Measurement report

B.1 Measurement on metal detector

This measurement report describe the measurements performed a metal detector model, which was made to get an idea of how the metal detector work. The purpose of this measurement report is to measure the phase between the transmit coil and receiver coil when metal object is present in the detector. A frequency sweep will be made to see the response o the phase when changing the frequency. The measurement will be compared to the simulation made on the theoretical model in section 2.4

B.1.1 Setup

The setup for the measurements are shown in figure B.1. A sinusoidal generator is applied through an amplifier to the transmit coil with a resistor in series. The amplifier has a voltage gain of 4 and supply current to the transmit coil, see section A.1. The resistor is inserted to measure the current in the transmit coil, the reason for this is that the current is proportional with the magnetic field generated. The resistor is chosen 1 Ω. The voltage is measured on the receiver coils.
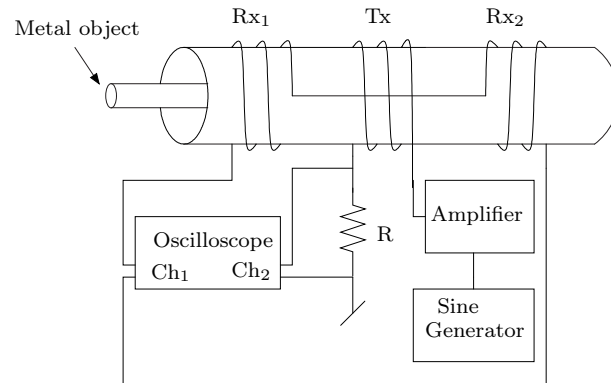
Figure B.1: *Setup for measurement on metal detector model*

The specification for the model is:

- Number of turns for each of the three coils: 25

- Diameter of the cross section area: 5 cm

- Length of each coils: 2cm

- Distance between the receiver coils and the transmit coil: 2 cm

B.1.2 Equipment

The instruments used to perform the measurements on the metal detector model is shown in table B.1

Name	Type	Placement	AAU nr.
Power supply	Hameg HM7042	B1-101-P-8	33888
Function generator	Philips 08559	B1-101-L-5	08559

Table B.1: *Instruments used for measurements on metal detector model*

B.1.3 Procedure

The procedure for the measurements is described in this section. There are made measurements for five different metal rods:

1. Ferrite (1 cm)

2. Aluminum (2 x 1.5 cm)

3. Stainless steel (2 cm)

4. Brass (2.5 cm)

5. Iron (2.5 cm)

Note that the values in the bracket equal the diameter of the rods. Aluminum is a rectangular rods and the values in the bracket are the length of sides.

When measurement are performed the metal rod is placed in one of the receiver coil where the amplitude of the receiver signal is maximized. The rods are placed in the middle of the cross section of the metal detector.

The frequency for the signal generator is adjusted to the lowest frequency where the signal can be seen. The voltage is also adjusted to the maximum amplitude where no distortion is notable.

When the signal generator is tuned, the delay between the transmit and receive signal is measure med. The cursor on the scope is adjust to where the transmit and receive signal intersect origo on the falling edge. The delay is then read from the scope.

The frequency is then increased and the new delay is measured. The process is repeated until 1 MHz. The voltage is adjusted regularly to ensure a good signal.

B.1.4 Results

In this section the result for the measurements are presented. The delay versus the frequency for Brass, Aluminum, Stainless Steel, Iron and Ferrite are listed in tables B.2, B.3, B.4, B.5 and B.6 respectively. The phase ϕ can be calculated based on the delay T_d and frequency f as:

$$\phi = (1 - f \cdot T_d) \cdot 360 - 180 \tag{B.1}$$

The reason why 1 is subtracted with $f \cdot T_d$, is that the delay is measured on the wrong side. The phase is also subtracted with 180 to move it down to $\pm 90°$. The phase versus the frequency for the five metal is shown in figure B.2.

Freq [kHz]	0.3	0.5	0.8	1	2	3	4	5	6	7
Delay [μs]	2080	1300	850	690	352	238	180	144	119	104
Freq [kHz]	8	9	10	15	20	25	30	35	40	45
Delay [μs]	91.0	81.6	73.6	49.2	37.4	29.6	24.6	21.0	18.4	17.0
Freq [kHz]	50	55	60	65	70	75	80	85	90	95
Delay [μs]	15.2	13.8	12.6	11.6	10.6	10.1	9.3	8.8	8.3	7.9
Freq [kHz]	100	150	200	250	300	350	400	450	500	550
Delay [μs]	7.5	5.0	3.8	3.1	2.6	2.2	1.9	1.7	1.5	1.4
Freq [kHz]	600	650	700	750	800	850	900	950	1000	
Delay [μs]	1.2	1.17	1.10	1.01	0.96	0.91	0.85	0.79	0.75	

Table B.2: *Measurements for Brass*

Freq [kHz]	0.5	0.8	1	2	3	4	5	6	7	8
Delay [μs]	1350	860	700	356	240	182	146	122	104	92.0
Freq [kHz]	9	10	15	20	25	30	35	40	45	50
Delay [μs]	81.0	73.2	50.0	37.6	30.0	25.4	21.6	19.0	16.7	15.0
Freq [kHz]	55	60	65	70	75	80	85	90	95	100
Delay [μs]	13.7	12.6	11.7	10.8	10.2	9.6	9.0	8.6	8.1	7.6
Freq [kHz]	150	200	250	300	350	400	450	500	550	600
Delay [μs]	5.0	3.8	3.0	2.5	2.2	1.9	1.7	1.5	1.4	1.3
Freq [kHz]	650	700	750	800	850	900	950	1000		
Delay [μs]	1.18	1.1	1	0.96	0.89	0.85	0.81	0.76		

Table B.3: *Measurements for Aluminium*

Freq [kHz]	1	1.5	2	3	4	5	6	7	8	9
Delay [μs]	490	336	268	190	148	121	106	91.0	83.0	73.2
Freq [kHz]	10	15	20	25	30	35	40	45	50	55
Delay [μs]	66.4	46.0	35.6	28.4	23.6	20.2	18.4	16.2	14.5	13.1
Freq [kHz]	60	65	70	75	80	85	90	95	100	150
Delay [μs]	12.0	11.0	10.6	9.9	9.3	8.7	8.2	7.8	7.4	4.9
Freq [kHz]	200	250	300	350	400	450	500	550	600	650
Delay [μs]	3.7	3.0	2.5	2.2	1.9	1.6	1.5	1.4	1.3	1.2
Freq [kHz]	700	750	800	850	900	950	1000			
Delay [μs]	1.08	1.02	0.95	0.91	0.84	0.81	0.76			

Table B.4: *Measurements for Stainless steel*

Freq [kHz]	0.3	0.5	0.8	1	2	3	4	5	6	7
Delay [μs]	900	540	330	260	132	84.0	65.0	51.0	43.0	35.0
Freq [kHz]	8	9	10	15	20	25	30	35	40	45
Delay [μs]	32.0	28.6	25.2	17.2	12.4	10.0	8.6	7.4	6.0	5.5
Freq [kHz]	50	55	60	65	70	75	80	85	90	95
Delay [μs]	4.9	4.7	4.2	3.7	3.5	3.3	3.2	3.0	2.8	2.6
Freq [kHz]	100	150	200	250	300	350	400	450	500	550
Delay [μs]	2.4	1.7	1.2	1.0	0.8	0.72	0.64	0.58	0.52	0.5
Freq [kHz]	600	650	700	750	800	850	900	950	1000	
Delay [μs]	0.46	0.4	0.34	0.3	0.3	0.3	0.3	0.28	0.26	

Table B.5: *Measurements for Ferrite*

Freq [Hz]	10	20	30	40	50	60	70	80	90	100
Delay [ms]	28	14.4	9.8	7.4	5.8	5	4.4	4	3.4	3.2
Freq [Hz]	150	200	250	300	350	400	450	500	550	600
Delay [μs]	2100	1600	1280	1080	960	850	760	690	630	590
Freq [kHz]	0.65	0.70	0.75	0.80	0.85	0.90	0.95	1	2	3
Delay [μs]	550	492	468	436	412	392	376	356	188	130
Freq [kHz]	4	5	6	7	8	9	10	20	30	40
Delay [μs]	101	84	70	60	54	48.8	44.4	24.4	17.8	13.9
Freq [kHz]	50	60	70	80	90	100	200	300	400	500
Delay [μs]	11.6	10.0	8.7	7.9	7.1	6.4	3.4	2.4	1.8	1.4
Freq [kHz]	600	700	800	900	1000					
Delay [μs]	1.22	1.04	0.92	0.78	0.72					

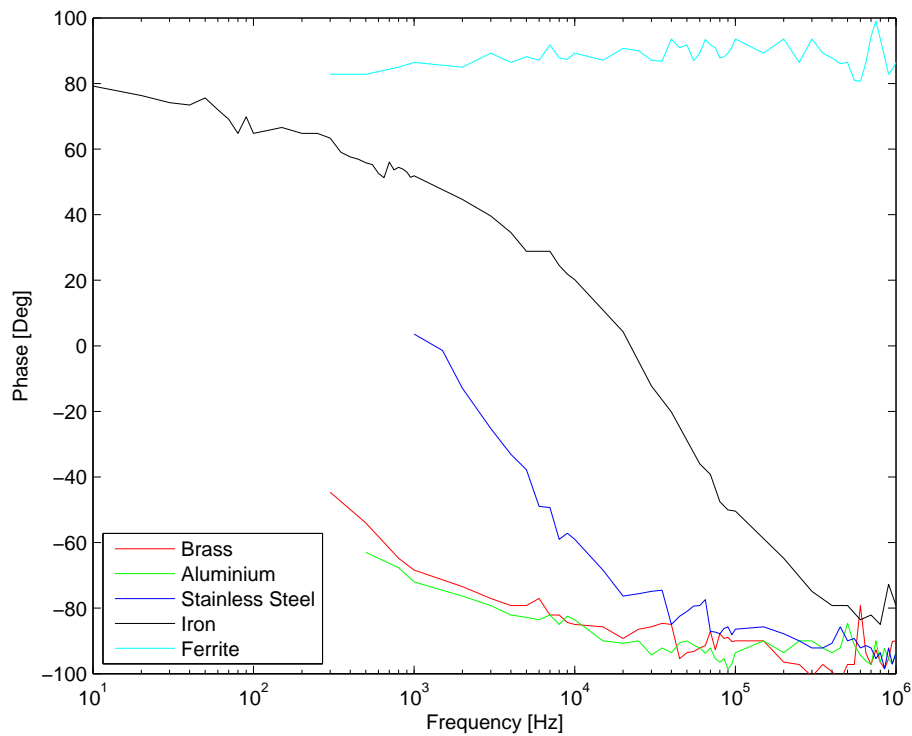**Table B.6:** *Measurements for iron*

Figure B.2: *Phase versus frequency for five different metal*

B.1.5   Conclusion

The measurement show that the phase decrease when the frequency increase, and the phase saturate at -90°, except from ferrite, this comply with the theory in section 2. It can be seen from figure B.2 that there are some scattering on the measurements. This is due to the uncertainty when measuring the delay with the cursor on the scope. The signal also becomes weaker when increasing the frequency. This is due to the impedance of the transmit coil increase and the current therefore decrease. It is also not possible to supply the same amount of current at high frequency. A capacitor could be inserted in series with the coil to make up a series resonance circuit to decrease the impedance. This however require change in capacitor when the frequency increase for the resonance frequency to fit. It is therefore not chosen to use the capacitor.

B.2 Measurement on metal detector

This measurement report describe the measurements performed on the metal detector from Detectronic. Measurements are made with two frequencies for the transmit coil, that is 30 kHz and 300 kHz. For each transmit frequency varies measurement are performed with metal, food and a mix of food and metal. The purpose of the measurements is to compare the response of the object passing through the detectorhead to see at what frequency it is easiest to detect metal object.

B.2.1 Setup

The setup for the measurements performed on the metal detector is shown in figure B.3. A sine generator is connected to an amplifier which amplify the voltage 4 times and ensure sufficient current to the transmit coil. A capacitor C_1 and resistor R_1 is connected in series with the transmit coil. The capacitor is placed in series with the coil to make a series resonance circuit and thereby minimize the impedance and the resonance frequency. The capacitor C for the resonance circuit can be calculated as:

$$C = \frac{1}{(2 \cdot \pi \cdot f)^2 \cdot L}$$

(B.2)

Where f is the resonance frequency and L is the inductance of the coil. The transmit coil is measured to 47.9 μH

The resistor R_1 is used to measure the current in the transmit coil, by measuring the voltage across it. The voltage is applied to an instrumentation amplifier and from that connected to the sample board.

The receiver coils Rx_1 and Rx_2 is connected to an instrumentation amplifier with a capacitor in parallel C_2. The capacitor make up a parallel resonant circuit, which yields a high impedance in the resonance frequency and work as a peak filter. The resonant frequency is calculated the same way as for the series resonant circuit, see equation B.2. The inductance of the receiver coil is 27.3 μH.
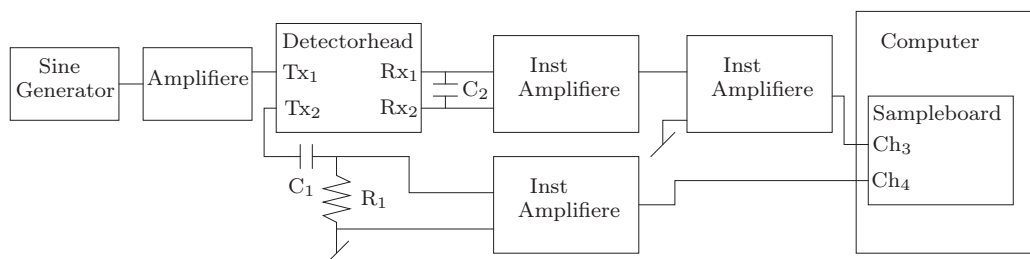

Figure B.3: *Setup for metal detector measurements*

There are used two instrumentation amplifier to ensure sufficient gain to the receive signal. An Opamp amplifier could also be used instead of the last instrumentation amplifier, but the reason for the instrumentation amplifiers is due to the option for electronic balancing.

B.2.2   Equipment

The instruments used to perform the measurements on the metal detector is shown in table B.7

Name	Type	Placement	AAU nr.
Power supply	Hameg HM7042	B1-101-P-8	33888
Power supply	Hameg HM7042	B1-101-N-5	33891
Function generator	Philips 08559	B1-101-L-5	08559
Multimeter	Fluke 189 True RMS	B1-101-B-3	52832
Computer	2.13 GHz Intel Core 2 Duo, 3 GB RAM		
Sampleboard	PCI-DAS4020/12		

Table B.7: *Instruments used for metal detector measurement*

The measurements are made on metal sphere, food and mix of sphere and food. 15 different metal sphere has been used, which are shown in table B.8.

Type	size (mm)	size (mm)	size (mm)	size(mm)
AISI 304	2	3	5	10
Aluminium	2	3	5	10
Iron	1	2	5	10
Bronze	2	3.5	5	

Table B.8: *Metal sphere used in measurements*

The food which are used for the measurements are listed in table B.9.

Type	Name
Rusk 250 g	Bakkegårdens kammerjunker
Raisin 250 g	Sultanien Ungeschwefelt
Crackling 200 g	Snackstreet No 1 flæskesvær
Candy 200 g	Malaco famielie mix

Table B.9: *Food used in measurements*

B.2.3   Procedure

In this section the procedure for measurements is described.

The measurements are sampled with the program described in section A.3. Sample frequency is set to 20 MHz and sample time is 2 seconds.

Before the measurements are carried out four step is performed:

1. Calculated capacitor C_1 and C_2 with equation B.2 according to the desired transmit frequency.

2. Adjust the signal generator to the desired frequency and verify if the transmit and receive signal approximately hits the resonance frequency.

3. Adjust the signal generator to maximum voltage without notable distortion. The signal is measured over R_1. Note that the signal from the signal generator is amplified 4 times in the amplifier.

4. Balance the detectorhead with various metal pieces to ensure more gain for the received signal. The gain is adjusted to fit either ± 1 V or ± 5 V, which is the range supported by the board.

When the system is initialized measurements are performed. The object is placed on the conveyor belt and the signal on the transmit and receive coil are sampled when the object passes through the detectorhead.

30 kHz measurement

The capacitor C_1 is calculated according to equation B.2, with resonance frequency 30 kHz and inductance 27.3 μH. The capacitor is calculated to 1.03 μF where 1 μF is chosen. The capacitor for the receive signal C_2 is calculated with the same equation and resonance frequency, but with inductance 47.9 μH. The capacitor is calculated to 587 nF, which is made with two capacitor of 100 nF and 470 nF connected in parallel which equal 570 nF. The resistor R_1 where the current is measured is chosen to 1 Ω. The signal generator is tuned to 28 kHz since it yields a higher signal. The resonance frequency is calculated to 30 kHz but it can be due to inaccuracy in the components. The capacitor could have been fitted, to yield a resonance frequency in approximately 30 kHz, but for the purpose of this test it make no difference if it is 28 kHz or 30 kHz. The voltage of the signal generator is set to 1.1 V. The detectorhead is balanced and the gain for the first instrumentation amplifier is approximately 250 times and approximately 10 times for the last. This yields a total of 2500 times or 68 dB. The signal from the transmit and receive coil are 1.22 V and 0.65 V respectively, when no object is present in the detectorhead. The range of the sample board is set to $\pm$ 5 V for the transmit signal and $\pm$ 1 V for the receive signal except for all 10 mm spheres and iron 5 mm where the range is set to $\pm$ 5 V, since the signal exceed the range of $\pm$ 1 V.

300 kHz measurement

The capacitor C_1 is calculated according to equation B.2, with resonance frequency 300 kHz and inductance 27.3 μH. The capacitor is calculated to 10.3 nF where 10 nF is chosen. The capacitor for the receive signal C_2 is calculated with the same equation and resonance frequency, but with inductance 47.9 μH. The capacitor is calculated to 5.87 nF, which is made with two capacitor of 10 nF and 15 nF connected in parallel which equal 6 nF. The resistor R_1 is chosen 0.33 Ω, since it made a better signal than 1 Ω. The signal generator is set to 300 kHz and the voltage of the signal generator is set to 0.5 V. The detectorhead is balanced and the gain for the first instrumentation amplifier is approximately 30 times and approximately 5 times for the last. This yields a total of 150 times or 43 dB. It was difficult to balance the detectorhead, since the hand which implement the metal yields a response in the receiver. The signal from the transmit and receive coil are 0.25 V and 0.88 V respectively, when no object is present. The range of the sample board is set to $\pm$ 1 V for both channel.

B.2.4 Result

The result of the measurement will be described in this section.

In figure B.4 an example for iron 5mm at 28 KHz is shown. It can be seen that the coils are not balanced completely since the sinusoid are present in the receiver when no object is present. The response from the iron sphere is high and the overall signal-to-noise ratio is good.
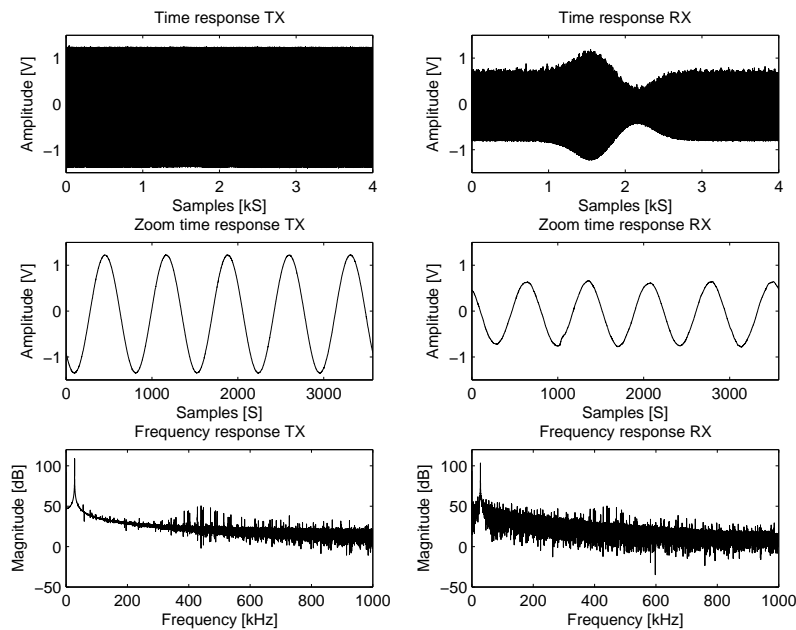

Figure B.4: *Transmit and receive signal for iron 5mm at 28 kHz*

In figure B.5 an example for iron 5mm at 300 kHz is shown. The response for the iron sphere is greatly reduced in the receiver coil. This is due to the current reduction in the transmit coil and the lack of gain in the receiver coil. The lack of gain is a consequence of missing balance and the ability for the instrumentation amplifiers to amplify the signal sufficient. The SNR ratio is high.

B.2.5 Conclusion

The measurement for both 28 kHz and 300 kHz have a high SNR. The current in the transmit coil is approximately two times higher for 30 kHz, this is due to the amplifier cannot supply sufficient current, when the frequency increase to 300 kHz. The response from the iron sphere is also greatly reduced, which is due to the reduced magnetic field in the coil and lack of amplification, which is reduced 17 times. The reduced gain is because of lack in balancing at 300 kHz. It is difficult to balance at high frequency because the hand which implant the metal yields a response in the receiver coil.
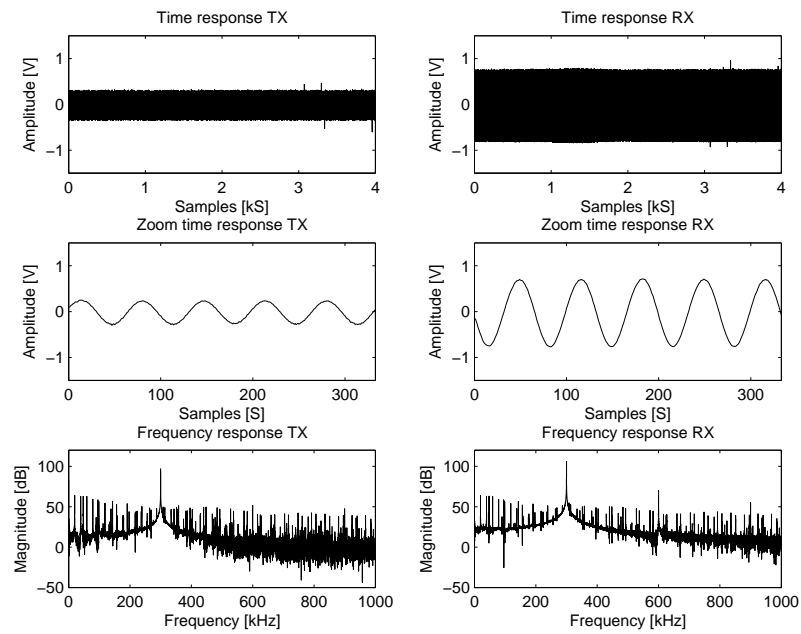
Figure B.5: *Transmit and receive signal for iron 5mm at 300 kHz*

Appendix C
A/D converter

In this section the A/D converter is described, which should be connected to the expansion header of the FPGA board.

In this project an A/D converter from Analog Device is used AD9920 [AD9220, 2003]. It is a 12 bit A/D converter with a maximum sample rate of 10 MHz. The required power supply for the A/D converter is 5 V DC and the input range is 5V peak-peak. The hardware setup of the AD9220 is provide by group 08gr1041 AAU.

The basic operation of the A/D converter is that an clock is provided and then on the rising edge the value of the analog signal is sampled. In figure C.1 the timing diagram of the AD9220 is shown. The t_C is the clock period, t_{CH} is the clock high period, t_{CL} is the clock low period and t_{OD} is output delay of the data. The clock time depends on the provided clock signal and the output delay t_{OD} is stated to be minimum 9 ns and maximum 19 ns. In addition to the output delay a pipeline of 3 samples is made.
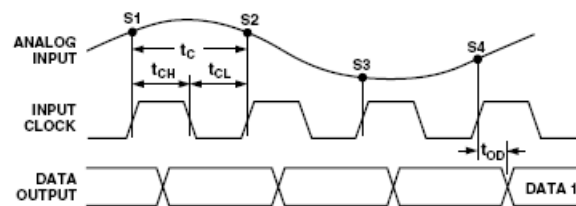

Figure C.1: *Timing diagram for the AD9220 [AD9220, 2003]*

The communication between the A/D converter and the FPGA is made with the expansion header provided by the DE2 board. The expansion header consist of 36 I/O pins, one 5 V supply, one 3 V supply and two ground. The 5 V supply pin and ground is connected to the A/D converter to supply the power. The first 12 I/O pins is used for the output of first A/D converter and the last 12 I/O pins, 24-35, is used for the second A/D converter. The clock to control the sampling of the analog signal is providing by the 50 MHz frequency which is available on the FPGA board. The clock is connected to pin 19 on the expansion header. In the previous section the minimum sample rate for the cross correlation was stated to 300 kHz, it is chosen to use the full speed of the A/D converter which means 10 MHz. This will increase the accuracy of the phase and amplitude a bit and it will make the system able to work at higher transmit frequency up to 1 MHz by only changing the confidents of the filters. The disadvantage is that the peak filter will be more difficult to design . When the 12 bit input is passed to the FPGA, the MSB of the data should be inverted to convert the data format to two's complement.

Since the range of the A/D converter is optimized so food product almost use the range, the A/D converter will saturate when large metal object enter the detector. This will probably be detected in the classifier, but to be certain an saturation block is inserter to monitor saturation of the input signals.

To verify that the A/D converters works, an image of a FPGA design, which read data from the expansion head, is download to the FPGA. To watch the value of the input from the A/D

converter, a real-time debugger interface in Quartus II is used, called Signal Tap II. It allows the user to specify what signals in the FPGA design that should be logged. In this test the signal after the MSB has been inverted is logged. The analog test signal on the input of the A/D converter is a DC value, made as a variable voltage divider on the supply voltage. Two test will be made the first is a sweep from 0 V to 5 V to check that the sequence of the binary value which should be -2048 to 2047. The second test is made for checking the signal to noise ratio, and it is made by adjusting the voltage to random values and then check how stable the binary value is.

The first test showed that the A/D converters could change from -2048 to 2000 and -2040 to 1980. The reason why the values are not -2048 and 2047 is due to limitation in the voltage divider. The second test showed that the value for both A/D converters were unstable within approximately four value, which means the last two bit is controlled with noise. The maximum signal-to-noise ratio of the A/D converts is approximately 54 dB.

List of Corrections